MICROCOPY RESOLUTION TEST CHART
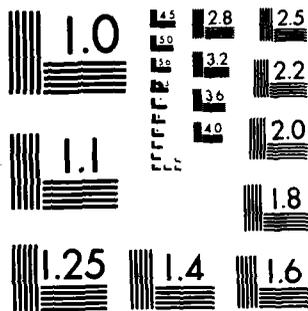NATIONAL BUREAU OF STANDARDS-1963-A

XEROX WEBSTER RESEARCH CENTER

CHEMICAL BONDING, INTERDIFFUSION AND ELECTRONIC
STRUCTURE AT InP, GaAs, and Si-METAL INTERFACES:
INTERIM SUMMARY REPORT

L.J. Brillson, Principal Investigator
Xerox Webster Research Center
Webster, NY 14580
Telephone (716) 422-6468

January 15, 1984

AD-A141 809

DTIC FILE COPY

DTIC
SELECTED
JUN 4 1984

A

84 05 30 022

I. Overview

Over the past two years, we have carried out an experimental program to investigate the interface electronic states and its relation to the chemical structure formed at InP, GaAs, and Si-metal interfaces as a result of interface chemical reaction and diffusion. We have used soft x-ray photoemission spectroscopy to characterize interfacial bonding and diffusion on an atomic scale. We have used surface photovoltage spectroscopy to identify interface electronic states within the semiconductor band gap. We have also used Auger electron spectroscopy coupled wth ion sputtering to profile the interface chemical structure after the Schottky barrier is formed and have identified spatial changes in stoichiometry normal to the interface plane which are dependent on chemical bond strength between metal and semiconductor. These measurements provide new, more detailed relationships between the surface and interface chemical structure on a microscopic scale and the Schottky barrier formation. This interim report summarizes the bulk of this research and includes papers published as a result of this effort. A list of the papers published under Navy contract # N00014-80-C-07789 (NR # 372-098) during the past two years appears at the end of this section.

II. Background

We have used a number of complementary experimental techniques to probe the electronic structure of semiconductor surfaces and interfaces and its relation to the chemical nature (i.e., new atomic bonding, atomic rearrangement, added chemical species) of these surfaces and interfaces. Our work has concentrated primarily on InP surfaces and interfaces since unlike the relatively well-studied semiconductor GaAs, it exhibits Fermi level movements over a significant part of the band gap and

Schottky barriers which are significantly different for junctions with different metals. Furthermore, the InP surface exhibits recombination velocities which are strongly dependent on conditions of preparation. This electronic behavior is not due to any intrinsic states at the InP surface but is related to substantial chemical effects at processed surfaces and metal-InP interfaces which have been uncovered by surface science techniques.[1] For example, we have previously shown that the stoichiometry of In and P outdiffusion[2] into metal overlayers can be correlated with the magnitude of the Schottky barrier for that metal-InP junction,[3,4] that the outdiffusing anions can react with the metal overlayers to form metal-anion complexes of finite and variable widths,[5,6] and that the Fermi level movements with the deposition of monolayers of metal depend in detail upon the particular interfacial chemical reaction or diffusion.[7] We have made use of such chemical effects to modify InP-metal Schottky barrier heights by introducing interlayers of different reactivities and thicknesses between the InP (or, for that matter, GaAs, CdS, and CdSe) and the metal overlayer.[4,8-11] These results demonstrate that a wide range of Schottky barrier heights can be achieved with a III-V compound semiconductor by different chemical interactions at the interface.

We have extended our studies from III-V semiconductors to Si in order to investigate the nature of chemical reaction and interdiffusion in various metal-Si systems. Here the issue of anion/cation stoichiometry does not exist. However, the initial steps of interdiffusion - whether metal indiffusion or Si outdiffusion - and their ultimate effect on chemical and electronic structure is far from being understood. Such interdiffusion can now be studied on a monolayer scale via surface science and marker techniques, in analogy to experiments already performed for metals on compound semiconductors.[9-12] Such studies can provide new avenues

for characterizing kinetics and thermodynamics of metal-Si systems on a monolayer scale and their relation to the macroscopic metal-Si junction chemistry, which has been more extensively studied.[14] These microscopic phenomena may then be extended back to compound semiconductors, for which the kinetics and thermodynamics at bulk metal interfaces is less well understood.

We have carried out soft x-ray photoemission spectroscopy (SXPS) experiments on these metal-semiconductor systems at the Tantalus Storage Ring at the Synchrotron Radiation Center of the University of Wisconsin-Madison. We used high quality InP single crystals obtained from the Naval Research Laboratory (courtesy of R. Henry and H. Lossoff), Lincoln Laboratories (courtesy of J. Iseler), and MCP Industries, England. We obtained single crystal Si bars and wafers from a number of commercial vendors. The single crystal InP and Si bars were cleaved and successively deposited with submonolayer and monolayer amounts of evaporated metal. At each step, we monitored the energies of core level and valence band features as well as the core level intensities for each element at the interface. These spectral features yield information on the detailed chemical bonding and spatial distribution of atoms near the metal-semiconductor interface. Chemical and electronic effects can be analyzed on an atomic scale by selecting synchrotron radiation energies such that the resultant kinetic energies of the photoemitted electrons fall in the range corresponding to the minimum electron escape depth (i.e., 50-100 eV).

We have carried out Auger electron spectroscopy (AES) measurements coupled with sputter-profiling with an Ar^+ ion beam in order to determine the rearrangement of metal and semiconductor atoms near the interface after a bulk metal film has been deposited on the semiconductor surface. These measurements were performed at

the Xerox Webster Research Center using a multitechnique ultrahigh vacuum (UHV) chamber. We used low energy (500 eV) Ar^+ ion beams to analyze the chemical composition as a function of depth, normal to the surface, thereby minimizing the bombardment-induced atomic disorder and permitting detection of features localized to within 10 or 20 Å.

In addition we performed surace photovoltage spectroscopy (SPS) measurements on InP single crystals under UHV conditions. SPS is a relatively unconventional technique[15,16] which involves direct optical transitions to and from states within the band gap with optical precision ($\ll$ 0.1 eV). The high sensitivity of SPS relative to photoemission, electron loss, and reflectance techniques is based on the strong dependence of semiconductor band bending on small changes in surface charge density. Population or depopulation of states within the band gap alters the surface charge, the band bending, and the surface work function as measured by a vibrating kelvin probe in UHV chamber. We studied the surface states present on InP (100) surfaces after a variety of surface chemical treatments and after deposition of different metals. InP (100) wafer specimens were provided by Bell Telephone Laboratories through Dr. Adam Heller, one of our collaborators. Both n- and p-type (100) surfaces were investigated. For metal-deposited surfaces we compared the (100) wafer surfaces with (110) surfaces obtained by UHV cleavage. With the SPS technique, we were able to study the role of surface states on metal-treated InP surfaces known to exhibit dramatically reduced surface recombination velocity (SRV). Correlating the SPS results with AES analysis of the chemically-treated surfaces, we were able to idenfity a chemical factor responsible for the reduced SRV.

III. Results

The work performed under this contract within the past two years falls into four areas: 1) the relationship between chemical structure and Schottky barrier formation at metal interfaces with InP and with other compound semiconductors, 2) the chemical structure of InP-metal interfaces after bulk metal formation, the influence of chemical interlayers on that chemical structure, and the relation between chemical structure and Schottky barrier formation, 3) the surface states on InP surfaces after metal deposition and a variety of wet-chemical treatments and their relation to Schottky barrier formation and to reduced surface recombination velocity, and 4) the interdiffusion and chemical bonding which occurs at the initial stages of interface formation between Si and simple metals and its relation to bulk thermodynamic predictions and to observed interfacial behavior of "conventional" metal-Si junctions.

Soft x-ray photoemission measurements of InP, GaAs, and other III-V compound semiconductors reveals that significant differences exist between the interface chemistry of III-V and II-VI compound semiconductors with metals.[13,17-19] These differences include a reversal in stoichiometry of semiconductor outdiffusion for III-V compounds which is absent for II-VI compounds, a Schottky barrier lowering due to effective doping of II-VI but not III-V/metal interfaces by dissociated cations, and II-VI compound semiconductors which are more spatially extended than those of their III-V counterparts. The chemical differences between these two classes of semiconductors can account for the wider range of II-VI vs. III-V/metal Schottky barriers. II-VI compound semiconductors interfaces with metals exhibit a wide range of diffusion behavior which resembles that of III-V compounds with decreasing semiconductor ionicity, further emphasizing the link between chemical and electrical trends.

We have used AES sputter-profile experiments to provide new information on atomic redistribution at the metal-InP interface.[20] Complementing SXPS measurements, our AES results demonstrate that qualitative differences in interdiffusion and segregation occur over many tens of Å for reactive vs. unreactive[5] metals on the InP (110) surface. Unreactive metals such as Au, Cu, and Ag permit diffusion of both In and P through the metal film and segregation at the free metal surface. Reactive metals attenuate P outdiffusion, producing an accumulation of P at the intimate metal-InP interface. These effects depend monotonically on the thickness of the reactive metal layer. These observations clearly confirm the phenomenon of interface "chemical trapping".[8] We can associate low Schottky barriers of reactive metals with a P excess at the metal-InP interface and within the InP bulk and high Schottky barriers with a P deficiency near the interface. The results for reactive metals are not consistent with Fermi level pinning by simple native defects and suggest that more complex defects may dominate the metal-InP Schottky barrier formation.

We used SPS to determine the surface states present on n- and p-type InP (110) surfaces which were cleaved in UHV as well as n- and p-type InP (110) surfaces which were chemically-treated in a variety of ways.[21-23] No intrinsic surface states were found on UHV-cleaved or Ar+-bombarded surfaces. Wet-chemical etching, metal deposition, and oxidation produced a wide variety of extrinsic surface states with discrete energies ranging across the semiconductor band gap. These extrinsic states are highly sensitive to surface chemical treatment. Even UHV-cleaved surfaces exhibit extrinsic states associated with the creation of P-rich surface layers for the particular InP crystals which we used. The direct optical transitions to and from surface states in the band gap which SPS is sensitive to correlate with reported

Fermi level pinning behavior. However, surface states can not account for the unique reduction in surface recombination velocity (SRV) at $KAg(CN)_2{}^-$-treated InP surfaces.[24] From a comparison of SPS and AES features obtained from the same surfaces, we conclude that this reduction in SRV results from the formation of a surface layer which excludes ambient-induced recombination states.

We have used SXPS to characterize the rearrangement of Si and metal atoms during the initial stages of Au and Al interface formation with UHV-cleaved (111) or (100) Si surfaces.[25] From AES depth-profiling measurements, we were able to monitor the nature and extent of metal-Si interdiffusion after deposition of thick Au and/or Al overlayers.[26] From Si 2p core level spectra as a function of metal overlayer thickness and as a function of incident photon energy, we obtain evidence for strong Si bond changes at submonolayer Au coverages but only weak interactions between Al and Si. Marker experiments show that Au diffuses into Si with the first few deposited Au monolayers, followed by outdiffusion of Si into Au. In contrast Si diffuses into Al initially. We find no evidence for Au diffusion into the Si lattice. Only when annealed at 600°C or higher does the Al-Si interface exhibit extensive interdiffusion. These SXPS results are all consistent with the bulk phase diagram for the Al-Si system.[27] This correspondence is an encouraging sign that macroscopic thermodynamic behavior is relevant to microscopic interface interface phenomena. Conversely, the pronounced interdiffusion of Au and Si at temperatures well below the Au-Si eutectic emphasizes the need to take into account particular atomic processes - e.g., formation of rapidly diffusing dissociated species via lattice description.

The experimental results for the Al-Si interfaces indicate that junctions formed by Al deposition on clean, highly ordered Si surfaces are orders-of-magnitude more abrupt

than previously believed, even when annealed under typical processing conditions.[26] Rather than extending tens of microns, the Al-Si diffusion at temperatures of 400-450°C, we observed characteristic interdiffused widths of only a few hundred Å or less (tens of Å at room temperature). Ar^+ bombardment and disordering of the Si surfaces prior to Al deposition results in a massive increase in Al-Si interdiffusion, demonstrating that surface disorder plays a critical role in promoting Si diffusion into the Al overlayer.

We have also used pulsed laser techniques to grow high-quality SiO_2 on Si in a new, very fast, and relatively low temperature technique.[28] This process involves SiO_2 growth up to thicknesses of one micron in an oxygen environment using a XeCl excimer laser. From such nonequilibrium thermal treatment, one obtains growth rates 30 times larger than those for conventional oxidation processes with acceptable interface state densities. Applications of these Si-SiO_2 and Si-metal findings to corresponding device interfaces could have useful implications.

In summary, we are continuing to frame the detailed relationships between the macroscopic electronic properties and microscopic chemical structure of metal interfaces with InP and other compound semiconductors. These analytical techniques have been extended to interfaces with Si, the results of which suggest new methods of controlling chemical and electronic structure at semiconductor interfaces in general.

Publications of Work Sponsored by the Office of Naval Research - March 1982 to January 1984

1. "Systematics of Chemical Structure and Schottky Barriers at Compound Semiconductor-Metal Interfaces", L.J. Brillson, C.F. Brucker, N.G. Stoffel, A.D. Katnani, R. Daniels and G. Margaritondo, Proceedings of the Second IUPAP Semiconductor Symposium on Surfaces and Interfaces, Surface Science 132, 212 (1983). Invited

2. "Photoemission Studies of Reactive Diffusion and Localized Doping at II-VI Compound Semiconductor Interfaces", L.J. Brillson, C.F. Brucker, N.G. Stoffel, A.D. Katnani, R. Daniels, and G. Margaritondo, Proceedings of the 16th International Conference on the Physics of Semiconductors, Physica Scripta 117B&C, 848 (1983).

3. "Contact Technology in 3-5 Device Analysis and Modification of Metal-Semiconductor Contact Interface in 3-5 Devices", L.J. Brillson, IEEE Technical Digest of the International Electron Devices Meeting. Invited.

4. "Soft X-Ray Photoemission Techniques for Characterizing Metal-Semiconductor Interfaces", L.J. Brillson, Proceedings of the Brookhaven Conference on Advances in Soft X-Ray Science and Technology. Invited.

5. "InP Surface States and Reduced Surface Recombination Velocity", L.J. Brillson, Y. Shapira, and A. Heller, Applied Physics Letters 43, 174 (1983).

6. "Investigation of InP Surface and Metal Interfaces by Surface Photovoltage and Auger Electron Spectroscopies", Y. Shapira, L. Brillson, and A. Heller, Journal of Vacuum Science and Technology A1, 766 (1983).

7. "Studies of Surface Recombination Velocity Reduction of InP Photoelectrochemical Solar Cells, Y. Shapira, L.J. Brillson, and A. Heller, Proceedings of the Fifth EC Photovoltaic Solar Energy Conference, Athens, Greece, in press.

8. "Origin of Surface and Metal-Induced Surface States on InP", Y. Shapira, L.J. Brillson, and A. Heller, Physical Review B, in press.

9. "Auger Depth Profiling Studies of Interdiffusion and Chemical Trapping at Metal-InP Interfaces", Y. Shapira and L.J. Brillson, Journal of Vacuum Scienc ad Technology $\underline{B1}$, 618 (1983).

10. "Reduction of Silicon-Aluminum Interdiffusion by Improved Semicoi ,u   r Ordering", L.J. Brillson, M.L. Slade, A.D. Katnani, M. Kelly and G. Margaritondo, Applied Physics Letters, in press.

11. "Photoemission Studies of Atomic Redistribution at Gold-Silicon and Aluminum-Silicon Interfaces", L.J. Brillson, A.D. Katnani. M. Kelly, and G. Margaritondo, Journal of Vacuum Science and Technology, in press.

12. "Ultrafast UV-Laser Induced Oxidation of Silicon", T.E. Orlowski and H. Richter, Proceedings of the Materials Research Society (North-Holland, NY, 1984), in press.

References

1. See, for example, L.J. Brillson, Surf. Sci. Reports 2, 123 (1982); L.J. Brillson, J. Phys. Chem. Solids 44, 703 (1983).

2. P.W. Chye, I. Lindau, P. Pianetta, C.M. Garner, C.Y. Su, and W.E. Spicer, Phys. Rev. B18, 5545 (1978).

3. L.J. Brillson, C.F. Brucker, A.D. Katnani, N.G. Stoffel, and G. Margaritondo, J. Vac. Sci. Technol. 19, 661 (1981).

4. L.J. Brillson, C.F. Brucker, A.D. Katnani, N.G. Stoffel, and G. Margaritondo, Appl. Phys. Lett. 38, 384 (1981).

5. L.J. Brillson, Phys. Rev. Lett. 40, 260 (1978).

6. L.J. Brillson, C.F. Brucker, A.D. Katnani, N.G. Stoffel, R. Daniels and G. Margaritondo, Phys. Rev. Lett. 46, 838 (1981).

7. L.J. Brillson, C.F. Brucker, A.D. Katnani, N.G. Stoffel, R. Daniels, and G. Margaritondo, J. Vac. Sci. Technol. 21, 564 (1982).

8. L.J. Brillson, G. Margaritondo, and N.G. Stoffel, Phys. Rev. Lett. 44, 667 (1980).

9. L.J. Brillson, G. Margaritondo, N.G. Stoffel, R.S. Bauer, R.Z. Bachrach, and G. Hansson, J. Vac. Sci. Technol. 17, 880 (1980).

10. C.F. Brucker and L.J. Brillson, Appl. Phys. Lett. 39, 67 (1981).

11. C.F. Brucker, L.J. Brillson, A.D. Katnani, N.G. Stoffel, and G. Margaritondo, J. Vac. Sci. Technol. 21, 590 (1982).

12. L.J. Brillson, R.S. Bauer, R.Z. Bachrach, and G. Hansson, Appl. Phys. Lett. 36, 326 (1980).

13. L.J. Brillson, C.F. Brucker, N.G. Stoffel, A.D. Katnani, R. Daniels, and G. Margaritondo, Surf. Sci. 132, 212 (1983). (See attached paper.)

14. K.N. Tu and J.W. Mayer, in Thin Films - Interdiffusion and Reactions, edited by J.M. Poate, K.N. Tu and J.W. Mayer, (Wiley-Interscience, New York, 1978) p. 359, and references therein.

15. H.C. Gatos and J. Lagowski, J. Vac. Sci. Technol. 10, 130 (1973).

16. L.J. Brillson, Surf. Sci. 51, 45 (1975).

17. L.J. Brillson, C.F. Brucker, N.G. Stoffel, A.D. Katnani, R. Daniels, and G. Margaritondo, Physica Scripta 117B&C, 848 (1973). (See attached paper.)

18. L.J. Brillson, IEEE Technical Digest of the International Electron Devices Meeting, in press. (See attached paper.)

19. L.J. Brillson, Proc. Brookhaven Conference on Advances in Soft X-Ray Science and Technology, in press. (See attached paper.)

20. Y. Shapira and L.J. Brillson, J. Vac. Sci. Technol. B1, 618 (1983). (See attached paper.)

21. L.J. Brillson, Y. Shapira, and A. Heller, Appl. Phys. Lett. 43, 174 (1983). (See attached paper.)

22. Y. Shapira, L.J. Brillson, and A. Heller, J. Vac. Sci. Technol. A1, 766 (1983). (See attached paper.)

23. Y. Shapira, L.J. Brillson, and A. Heller, Phys. Rev. B15, in press. (See attached paper.)

24. A. Heller, R.G. Vadimsky, W.D. Johnson, Jr., K.E. Strege, H.J. Learny, and B. Miller, Proc. 15th IEEE PHotovoltaic Spec. Conf. (June 1981), p. 1422.

25. L.J. Brillson, A.D. Katnani, M. Kelly, and G. Margaritondo, J. Vac. Sci. Technol., in press. (See attached paper.)

26. L.J. Brillson, M.L. Slade, A.D. Katnani, M. Kelly, and G. Margaritondo, Appl. Phys. Lett., in press. (See attached paper.)

27. M. Hansen and K. Anderko, Constitution of Binary Alloys (McGraw-Hill, New York, 1958).

28. T.E. Orlowski and H. Richter, Mat. Res. Soc. Symp. Proc. (North-Holland, NY, 1984), in press. (See attached paper.)

Systematics of Chemical Structure and Schottky Barriers at Compound
Semiconductor-Metal Interfaces

L.J. Brillson and C.F. Brucker
Xerox Webster Research Center, 800 Phillips Road, Webster, NY 14580

and

A.D. Katnani, N.G. Stoffel, R. Daniels and G. Margaritondo
Dept. of Physics, University of Wisconsin-Madison, Madison, WI 53706

Abstract

Surface science techniques reveal a variety of chemical behavior at compound
semiconductor-metal interfaces. Strong differences in chemical reaction and
diffusion are observed between III-V and II-VI compound semiconductor-metal
interfaces which can account for the qualitative difference in their ranges of Schottky
barriers formed.

I. Introduction

The phenomenon of Schottky barrier formation at semiconductor-metal
interfaces has been studied intensively for over three decades, yet remains one of the
most active areas of solid state physics today. This fact can be ascribed not only to
the technological importance of Schottky barrier junctions in electronic devices but
also to the new phenomena being uncovered on an atomic scale by surface science
techniques. A central aim of this research has been to understand the formation of
Schottky barriers sufficiently well that electronic barrier heights can be predicted for
a given interface and perhaps even modified.

Of major significance has been the difference in Schottky barrier behavior between covalent and ionic semiconductors - i.e., covalent compounds exhibit relatively narrow ranges of barrier heights for contact metals with a wide range of work functions, whereas ionic compounds exhibit more classical behavior [1]. Therefore, an important feature of any physical model for the electronic structure of semiconductor-metal interfaces is the prediction of the variation of interface behavior with semiconductor ionicity.

Kurtin, McGill, and Mead [2] viewed differences in interface behavior with ionicity in terms of differences in density of intrinsic surface states. Over the past decade, experiments carried out under ultrahigh-vacuum (UHV) conditions have shown that intrinsic surface states are not present in the band gap of most compound semiconductors for clean, well-cleaved surfaces and therefore play no role in the Schottky barrier process [3,4]. Instead chemical reaction and interdiffusion between the metal and the semiconductor are found to play a dominant role. Such chemical phenomena lead to a new picture of the Schottky barrier junction. In contrast to the sharp boundary between metal and semiconductor portrayed in most solid-state texts, the interface in general encompasses an extended region such as that indicated in Fig. 1 and which may involve 1) a reacted region with new dielectric properties and chemical composition (as indicated by the varying vacuum-to-Fermi-level energy as well as built-in potential gradients and 2) an interdiffused region below the semiconductor surface in which the band bending is not necessarily parabolic [5,6]. Within this interdiffused region, the band curvature depends on the distributions of electrically-active sites due to semiconductor vacancies, interstitials, metal impurities, and their complexes. The type and distribution of such electrically-active sites depends on the detailed movements of interface atomic species which in turn

depends sensitively on the interfacial chemical bonding. The extent of the reacted and/or interdiffused regions in Fig. 1 is only tens to hundreds of Å, in contrast to the surface space charge region, which is typically larger than hundreds or thousands of Å. Nevertheless, it is the interfacial region which dominates the Schottky barrier formed. In turn, all of the features portrayed in the extended interface of Fig. 1 are determined by the strength and nature of interfacial bonding at a given temperature of formation.

II. Chemical Dependence of Schottky Barrier Heights

Although covalent and ionic compound semiconductors appear to have qualitative differences in interface behavior, nevertheless they exhibit a common variation in Schottky barrier height when parametrized by an interface-specific variable - e.g., interface chemical reactivity. Figure 2 illustrates this relationship between φ_{SB} and the interface heat of reaction ΔH_R for a variety of metals on four compound semiconductors [7]. ΔH_R values were calculated per metal atom for the reaction

$$M + (1/x) CA \rightarrow (1/x) [M_x A + C] \qquad (1)$$

so that

$$\Delta H_R = (1/x) [H_F(CA) - H_F (M_x A)]. \qquad (2)$$

ΔH_R is the difference in heat of formation [8-10] H_F for a compound semiconductor CA and the most stable metal-anion product $M_x A$, normalized per metal atom. Barrier heights were measured primarily by internal photoemission for

semiconductors cleaved in vacuum [1]. Each curve describes the data at least as well as linear plots of φ_{SB} vs. metal work function φ_M or electronegativity X_M.

The Ref. 1 data was obtained from semiconductors cleaved in a stream of evaporating metal at $\sim 10^{-7}$ torr so that the amount of interface contamination was probably relatively low. The more ionic semiconductors should have particularly low contamination levels since their sticking coefficients for common ambients are extremely small. Indeed, φ_{SB} values for both covalent and ionic semiconductors have stood up remarkably well over the past two decades in comparison with UHV results.

In all four graphs of Fig. 2, the solid curves exhibit sharp changes in φ_{SB} at a common transition value of ΔH_R. The arrow in the CdS panel marks a critical heat of reaction ΔH_R^C between reactive and unreactive CdS-metal and CdSe-metal interfaces, which has been determined experimentally by low energy electron loss spectroscopy (LELS) [7]. All of these four plots are qualitative similar even though they represent a wide range of ionicity and interface behavior. The same dependence of barrier height on ΔH_R also occurs for other semiconductors such as InP, a representative III-V compound semiconductor [12,13], Zn_3P_2, a p-type semiconductor [14], and PbTe, a narrow-gap II-VI compound semiconductor [15]. The transition in φ_{SB} occurs at approximately the same ΔH_R in each case. ΔH_R^C for ZnO, ZnS, and CdS [Fig. 2] as well as InP (see Fig. 4 insert) is $0.38 \pm .4$ eV. Even the few scattered GaP data points suggest $-1 < \Delta H_R^C < 0.5$ eV. Considering that the ΔH_R are calculated from Eq. 2 using H_F rather than free energy G values, that bulk rather than surface enthalpies are of necessity used, and that the ΔH_R scale extends over 9 eV, the observation of a common φ_{SB} transition over this relatively narrow energy range is all the more remarkable. Data for metal-

compound semiconductor systems such as ZnSe suggest analogous behavior [1]. Even data for GaAs. for which many metal-arsenide H_F (and thereby ΔH_R) values are not available suggest a similar break between reactive and unreactive metals [1] - where metal reactivity is guaged by ΔH_R calculated for the same metal with other III-phosphides and III-antimonides. The extension of reactivity plots to other semiconductor systems appears to be limited only by the availability of electronic and thermodynamic data. Thus the success of φ_{SB} vs. ΔH_R plots such as those in Fig. 2 demonstrates the importance of interface-specific chemcial processes in forming Schottky barriers.

Another correlation which emphasized the role of the anion in determining barrier heights was proposed by McCaldin et al. [16.17] and involved φ_{SB}^P for Au on p-type compound semiconductors versus the anion electronegativity [18]. Figure 3a illustrates the energy of the valence maximum relative to the Au Fermi level (i.e.. φ_{SB}^P) plotted as a function of anion electronegativity χ. using φ_{SB} data of Mead [1]. A similar correlation is obtained using the Phillips [19] rather than the Pauling [18] x scale. Implicit in each data point of this plot is that semiconductors with a common anion have approximately the same φ_{SB}^P regardless of the difference in band gap. It applies to both III-V and II-VI compounds, with the exceptions of AlSb. AlAs. and ZnO. Similar correlations but with more scatter exist for Ag and Cu replacing Au [20]. No such correlations obtain for the semiconductor cations and the respective Au Fermi levels in the band gap [16,17]. Swank [21] found a roughly linear correlation between ionization potential (i.e., $E_{vacuum} - E_{VBM}$) and anion electronegativity, indicating the strong anion character of the valence band. McCaldin et al. viewed their result in terms of bond-producing, p-like atomic states of the anion [22-26] which are capable of fixing the Au Fermi level and whose

position should scale with anion electronegativity. McCaldin's "common-anion rule" has been verified experimentally for mixed-cation MBE layers of InGaAs [27], InGaSb [28], and $Ga_xAl_{1-x}As$ (x<0.3) [29]. On the other hand, Brillson [30] has found a similar correlation between Au $\varphi_{SB}{}^p$ values and the same semiconductor anions using ΔH_R as a variable. The results given in Figs. 3b, 3c, and 3d correspond to $\varphi_{SB}{}^p$ for Au, Ag, and Cu, respectively, on the same semiconductors as in 3a. They exhibit at least as good a fit as that in Fig. 3a and, in contrast to Fig. 3a, can accommodate data for ZnO as well. Figures 3b, 3c, and 3d plus Fig. 2 provide systematic correlations of barrier height for the same semiconductor and different metals as well as the same metal and different semiconductors. Figure 3c suggests that different mechanisms of barrier formation apply to III-V vs. II-VI compounds with Ag, but not necessarily with Au and Cu.

III. **III-V Compound Semiconductor-Metal Interfaces: Barrier Heights and Chemical Structure**

For III-V compound semiconductor-metal interfaces, the φ_{SB} values tend to fall into two energy categories. For the case of InP, as shown in the Fig. 4 inset compiled by Williams *et al.* [12], the high and low energy ranges are well separated. For the GaP plot of φ_{SB} vs. ΔH_R in Fig. 2 as well as GaAs and narrower gap semiconductors, the energy separation is smaller but nevertheless recognizable. The presence of two "plateau" values of φ_{SB} with few if any intermediate values for different metals suggests that the semiconductor Fermi level E_F is "pinned" at either of two levels within the band gap. A number of semiconductor defect models have been proposed to account for the formation of similar φ_{SB} with different adsorbates on III-V compounds [31-36], although emphasizing a single pinning position for all

adsorbates on the same n-type or the same p-type surface [35,36]. In fact. the separation of φ_{SB} values into reactive and unreactive regimes in Figs. 2 and 4 leads to a chemical basis for the two levels.

A variety of UHV techniques have shown that diffusion of anions and cations can occur at room temperature from the semiconductor into the metal overlayer [32,37]. Figure 4 shows that the stoichiometry of this outdiffusion varies from anion-rich to cation-rich with increasing metal-anion reactivity ΔH_R [38]. Here the stoichiometry was measured as the ratio of integrated P2p to In 4d core level intensities, as determined from soft x-ray photoemission spectroscopy (SXPS). The difference in stoichiometry becomes more apparent with increasing thickness of deposited metal. Figure 4 demonstrates that anion (cation)-rich outdiffusion corresponds to high (low) φ_{SB} [12]. This correlation indicates that electrically-active sites associated with excess anion (cation) vacancies can be associated with E_F pinning at 0.5 eV ($\approx$ 0 eV) below the conduction band edge.

Recent Auger depth profiling results [Y. Shapira and L.J. Brillson. unpublished] show that segregation of anion and cation to the free metal surface are not significant at the metallic coverages reported here and do not affect our conclusions of stoichiometry, relative diffusion. and interface width based on the SXPS data.

The importance of interface chemical bonding in determining stoichiometry of outdiffusion can be established from the effect of different metal interlayers at the interfaces of otherwise identical metal-semiconductor contacts. Fig. 5 demonstrates the very high sensitivity to a reactive metal (Al) interlayer of semiconductor (GaAs) outdiffusion into a relatively unreactive metal (Au) [39,40]. Here the ratio of

integrated Ga 3d to As 3d core level intensities diffused through a Au overlayer increases dramatically with increasing Al interlayer thickness. Only a few monolayers of interlayer metal are needed to convert the outdiffusion from anion-rich to cation-rich. Furthermore, for a given Au coverage, the Ga/As ratio exhibits the same monotonic dependence on Al coverage, demonstrating that the changes in Fig. 5 are characteristic of bulk rather than any grain boundary diffusion [39]. Similar effects occur at semiconductor heterojunction interfaces [41]. The effect of increasing cation/anion ratios with increasing chemical reactivity derives primarily from "chemical trapping" of the anion by the interlayer metal [5,39]. SXPS measurements reveal steep declines in anion intensity over the thicknesses of reactive interlayers. Indeed, it has been shown that the effective interface width - the characteristic attenuation length of semiconductor anion with metal overlayer - decreases monotonically with increasing ΔH_R [5].

The use of reactive metal interlayers and other adsorbates to alter III-V compound semiconductor surfaces can produce electrical changes as well. For example, a 10Å Al interlayer between Au dots and UHV-cleaved n-type InP (110) yields a 0.1 eV φ_{SB} decrease relative to Au-InP diodes without interlayers on the same semiconductor surface [6,38]. We have also used monolayer thicknesses of various interlayers to obtain 0.1 - 0.2 eV φ_{SB} shifts at n-type GaAs (110) Au interfaces [5,42]. Montgomery et al. [43] has described substantial decreases of InP-Au and Ag barriers with exposure of InP to H_2S, and Massies et al. [44,45] have reported a 0.4 eV modulation of the Al-GaAs (110) φ_{SB} by H_2S exposure. They also find a reversal of surface stoichiometry with φ_{SB} change.

The fact that outdiffusion stoichiometry reverses between reactive and unreactive metal overlayers has been observed for several bulk III-V compounds - GaAs, GaSb, InAs, and InP [6,42]. This is because the semiconductor outdiffusion through unreactive metals such as Au is in general anion-rich and, as noted above, reactive metals strongly reduce anion outdiffusion.

Exceptions to the correlation of unreactive metals with high n-type φ_{SB} are metals which diffuse into the semiconductor and form electrically-active sites. In such cases, the energy levels of the impurity alone or of the impurity complex with native defects [46,47] will dominate the Schottky barrier formation. Such levels will pin E_F at new positions in the band gap and change the doping of the semiconductor. At high enough doping levels, the surface space region will narrow sufficiently to permit tunneling between metal and semiconductor through the barrier so that the contact appears "ohmic". III-V/metal interfaces for which semiconductor is believed to lower the Schottky barrier include Au on GaAs [48] and Sn and In on InP [49].

That metals diffuse into semiconductors near room temperature has been established by marker techniques coupled with SXPS [40,50,51]. Figure 6 illustrates the changes in integrated SXPS peak ratio of anion and cation to metal interlayers with Au overlayer thickness for three different semiconductors. Because only one-half monolayer coverages of interlayer metal are used, their presence at the interfaces has only a secondary effect on the interdiffusion. Figure 6a shows that both Ga/Ti and As/Ti ratios decrease with initial Au coverage, consistent only with Au diffusion into the outermost layers of the GaAs (110) surface. Above approximately 8Å Au coverage, both ratios increase, corresponding to more

semiconductor outdiffusion than Au indiffusion. Similar results are obtained with an Al interlayer [50,51]. The arrows indicate from top to bottom the order of atomic motion observed which can account for the formation of metal-induced surface states. Figure 6b illustrates the analogous behavior for Au on InP (110). In this case. In and P outdiffusion is observed before Au indiffusion. Figure 6c demonstrates that Au diffusion into II-VI compound semiconductors such as CdS occurs as well.

Evidence for metal indiffusion can be inferred from the relatively slow electronic changes which occur with metal deposition on a UHV-cleaved semiconductor surface. For example. Fermi level position [52,53] and band bending [30] changes occur over many monolayers for Au on GaAs (110) but occur much more rapidly for Al on GaAs (110) [30,54]. Likewise SXPS spectra of Au on GaAs (110) exhibit valence band features characteristic of dispersed atoms for coverages of several monolayers [32]. Electrical and Rutherford backscattering spectrometry (RBS) studies of Au-GaAs interfaces as a function of heat treatment show φ_{SB} decreases and extended Au indiffusion with annealing as well [48,55].

The chemical and electrical behavior described here for III-V semiconductors indicate that interface chemical reactions and diffusion contribute to φ_{SB} behavior in a number of ways. The outdiffusion of anions and cations as well as the indiffusion of metal atoms can produce new electrically-active sites within the surface space charge region. In general the strength and nature of chemical bonding near the interface will determine the spatial distribution of such electrically-active sites and thus the electric field gradients within the surface space charge region. Metal-anion bonding can also give rise to new dielectric layers with their own field gradients as

well as trapped charge which induces additional band bending within the semiconductor. Furthermore, free cations released by metal-anion bonding at the interface can change the effective work function difference between "metal" and "semiconductor" so that the charge transfer may in fact obey a classical relation [56,57]. For metals on the GaAs (110) surface, defect complexes induced by metal chemisorption provide the simplest explanation of the two φ_{SB} regimes observed. For the GaAs (100) surface, Grant *et al.* [58] have used different surface treatments to produce at least four different pinning levels ranging in energy over half the band gap. Recent SXPS measurements for different metals on InP (110) surfaces [59] suggest that more than two pinning positions are possible, so that metal induffusion, reacted dielectric layers, and/or cation phases may play a role. Indeed, the SXPS core level features provide evidence for a metal-cation phase within a few monolayers of many of the metal-InP interfaces [59].

IV. II-VI Compound Semiconductor-Metal Interfaces

As shown in Fig. 2, the II-VI compounds exhibit a much larger range of φ_{SB} for different metal contacts. Considerably more of the φ_{SB} values for ZnO, ZnS, and CdS as well as other II-VI compounds lie in the transition region between high and low φ_{SB} limits [1]. Furthermore, the lower "plateau" is less well-defined for II-VI than for III-V semiconductors. Thus a pair of defect levels are not likely to account for Schottky barrier formation in general at II-VI compound semiconductor-metal interfaces. (Of course, one can always rationalize any E_F pinning position within the semiconductor band gap in terms of varying densities of two or more gap states near each band edge [60]).

Consistent with the importance of interface chemical reactions in determining φ_{SB} values, we have now found from SXPS data that, for a large set of II-VI compounds, there exists a qualitative difference in interface chemical behavior between II-VI and III-V compound semiconductors [61]. Furthermore, this chemical behavior for II-VI compounds varies with compound ionicity, resembling III-V behavior with decreasing ionicity [18,19].

A major difference between chemical behavior of these two classes of semiconductor compounds is that the stoichiometry of outdiffusion does not appear to reverse with reactive vs. unreactive metals on the II-VI's as it does on the III-V's. Both semiconductor classes exhibit anion-rich outdiffusion into unreactive metal overlayers, but reactive metals appear to enhance anion outdiffusion and retard cation outdiffusion for many II-VI compounds instead of "chemical trapping" the anion as for III-V compounds. Even those II-VI compounds which do not enhance anion outdiffusion fail to exhibit a stoichiometry reversal. Figure 7 illustrates the attenuation of SXPS integrated Cd 4d and Se 3d core level intensities as a function of Al overlayer thicknesses on a UHV-cleaved CdSe (1010) surface [62]. Since Al forms uniform overlayers on the cleaved CdSe surface [63,64], the high level of Se detected at Al thicknesses many times the photoelectron escape depth [65] indicates that the reactive metal draws the anion toward the free metal surface, rather than trapping it at the semiconductor interface. This is in marked contrast to the Cd intensity, which decreases rapidly with the first 10Å of deposited metal.

Figure 8 illustrates the anion-rich outdiffusion behavior observed by XPS for all metals studied thus far on UHV-cleaved CdSe and CdS [66]. Unreactive metals such as Au and In yield cation/anion XPS intensity ratios which are always less than

unity. Highly reactive metal overlayers or interlayers of Al or Ti reduce these ratios even further. Therefore, if E_F pinning is due to defects associated with semiconductor outdiffusion, then only one type of defect should dominate for both reactive and unreactive metals on II-VI compounds and E_F should not be restricted by levels within the band gap associated with anion and cation deficiencies, as proposed for the III-V compounds [36]. This is consistent with the wider range of φ_{SB} for metals on II-VI vs. III-V compounds [1].

Figures 9 and 10 demonstrate that chemical behavior at II-VI/metal interfaces can vary, depending on the semiconductor. Here SXPS anion and cation core level intensities have been normalized to their cleaved surface values. For Al interlayers between UHV-cleaved CdS (10$\bar{1}$0) surface and Au overlayers (Fig. 9), the level of cation (Cd) outdiffusion $I_C(1-M)$ decreases with interlayer thickness 1 at a given overlayer thickness M while the anion levels $I_A(1-M)$ increase, analogous to the behavior of Fig. 7. Cu interlayers produce a similar enhancement for CdS and CdSe [66]. For the same overlayer (Au) - interlayer (Al) depositions on UHV-cleaved ZnSe (110) (Fig. 10), the level of cation (Zn) again decreases. However, the anion (Se) intensity decreases, in contrast to the Se behavior in Fig. 7. The behavior of all other II-VI compounds studied resembles that of either Fig. 9 or 10. Furthermore, the effect of the reactive metal interlayer on the anion outdiffusion varies monotonically with the semiconductor ionicity [61]. Table 1 exhibits the SXPS integrated peak ratio $I_A(M+1)/I_A(M)$ of semiconductor anion diffused through a 40 Å Al (=I) interlayer. $R = I_A(M+1)/I_A(M)$ in column 4 decreases with decreasing ionicity, whether defined according to Phillips (column 2) [19] or Pauling (column 3) [18] scale. For CdS, ZnS, and CdSe, the interlayer acts to increase R by enhancing anion outdiffusion while for ZnSe, CdTe, and CdTe, the same interlayer acts to

decrease R [61]. Column 5 reveals no regular dependence on ionicity of cation diffusion with interlayers on the same semiconductors. Thus, the more ionic the semiconductor, the more pronounced are its differences in anion outdiffusion relative to III-V compounds. That such a trend exists is significant since the more ionic II-VI compounds exhibit a larger range of φ_{SB} values [2].

Interfaces between metals and II-VI vs. III-V compounds also differ in their spatial extent. Whereas metal-anion phases between metal and semiconductor are less than 25Å thick for III-V compounds [5], Figs. 7 through 10 show that such phases can extend to 100Å or more for II-VI compounds. Low energy electron loss spectroscopy (LELS) measurements have shown that reacted interfacial layers can have new dielectric properties [63]. The metal-anion complexes can form a semiconducting or insulating film between metal and semiconductor and as such can contribute to the measured φ_{SB}. Depending upon the charge transfer during the initial formation of such interface layers, they can contribute to an increase or decrease in effective barrier height. Indeed, interface dipole and band bending voltages extracted from Kelvin probe measurements yield good agreement with observed φ_{SB} values for many metal-semiconductor interfaces [30,67]. Since the II-VI interface layers are significantly wider than those of II-V compounds, one expects less tunneling and thus greater effective contributions to φ_{SB}.

An additional factor in the wider range of metal/III-V barrier height is a doping of the interface by localized cations [66,68,69]. As Figs. 7, 9, and 10 show, the anion diffusion promoted by reactive metals leaves a preferentially cation-rich region near the metal-semiconductor interface. Dissociated cation features have been detected in photoemission spectra for Al on CdS [64], CdSe [66], CdTe and the

Zn chalcogenides [61], and Cu on CdS [66,70] and CdSe [66]. Since a cation excess with the semiconductor surface results in an increase in doping density, reactive metal overlayers and interlayers can give rise to a high doping and sharp band bending near the semiconductor surface. If this band bending reduces the surface space charge width to the point where tunneling occurs, then it can reduce the effective Schottky barrier height.

Brucker and Brillson [71,72] have shown from SXPS measurements that such sharp band bending does occur in fact for reactive interlayers between Au and UHV-cleaved CdSe (10$\bar{1}$0). Figure 11a illustrates the anomalous broadening of the Se 3d core level which is attributed to sharp band bending at the CdSe surface for $h\nu = 70$ eV and minimum surface sensitivity. For this photon energy, the escape depth for Se 3d photoelectrons is 90-100 Å below the semiconductor surface according to Fig. 11c. The lower panel in Fig. 12 illustrates this core level broadening schematically. Such broadening is absent for the $h\nu = 130$ eV spectra and maximum surface sensitivity (6-10Å), as shown by Figs. 11b and c. No such broadening occurs for Au-CdSe or Al-CdSe junctions without an interlayer. Capacitance-voltage (C-V) measurements of the interfaces with Al interlayers reveal a narrowing of the surface space charge region and an increase in doping density [68,71]. Figure 12 illustrates these three cases schematically - a reactive metal (e.g., Al), an unreactive metal (e.g., Au) and a thin reactive interlayer plus metal overlayer on CdS or CdSe. To the right of each schematic energy band diagram are schematic current-voltage (J-V) characteristics measured *in situ* for each case. The dashed energy bands of the interlayer case correspond to narrowing of the surface space charge region by localized cation doping. The dashed J-V characteristic for this case represent a "softening" of the rectifying characteristic.

The extent of the doping can be controlled by the thickness of the reactive interlayer, leading to dramatic effects on the measured Schottky barrier height. For example, one can effect a transition from a highly rectifying contact with $\varphi_{SB} = 0.8$ eV (middle panel) to "ohmic" behavior (upper panel) with increasing thickness of Al interlayer at Au-CdS and CdSe interfaces [68]. The entire transition requires only 2A Al for the Au-CdS (10$\bar{1}$0) case. Presumably, thicker layers of Al narrow the width of the surface space charge region to zero, leading to the band diagram for Al on CdS in the upper panel of Fig. 12.

Because excess cations at the metal/II-VI compound semiconductor interface can effectively dope the semiconductor surface, reactive metals on II-VI compounds can produce low barrier heights by narrowing of the surface space charge region. SXPS core level and electrical measurements appear to rule out similar phenomena at metal/III-V compound semiconductor interfaces. Thus the localized cation doping provides an additional mechanism which extends the range of II-VI but not III-V φ_{SB} values.

Conclusions

Significant differences exist between the interface chemistry of II-VI and III-V compound semiconductors with metals. These differences include a reversal in stoichiometry of semiconductor outdiffusion for III-V compounds which is absent for II-VI semiconductors, a Schottky barrier lowering due to effective doping of II-VI/metal interfaces by dissociated cations, and II-VI compound semiconductor-metal interfaces with new dielectric properties which are more spatially extended than their III-V counterparts. The chemical differences between these two

semiconductor classes can account for the wider range of II-VI/ vs. III-V/metal Schottky barriers. II-VI compound interfaces with metals exhibit a wide range of diffusion behavior which resemble that of III-V compounds with decreasing semiconductor ionicity, further emphasizing the link between chemical and electrical trends. The chemical structure of all of these interfaces can be modified by new atomic species at the intimate metal-semconductor junction, giving rise to contacts with new electrical behavior. Thus the dependence of interface chemical structure on the strength and nature of metal-semiconductor bonding on an atomic scale provides exciting new possibilities for the chemical modification of interface electronic structure.

Acknowledgements

Table Caption

1. II-VI compound semiconductors tabulated with their ionicities (either on a Phillips [19] or Pauling [18] scale) and the relative changes in anion and cation intensities due to a 10Å Al interlayer between the semiconductor and a 40Å Au overlayer. $I_A(T)$ and $I_C(T)$ are anion and cation SXPS core level intensities respectively at thickness T of interlayer plus metal overlayer (T = I + M) or metal overlayer alone (T = M). For example. $I_A(I+M)/I_A(M)$ for CdS is the ratio of I_{Cd}^{4d} (55 eV) with a 10 Å Al interlayer and a 40 Å Au overlayer to I_{Cd}^{4d} (55 eV) with a 0 Å Al interlayer and a 40 Å overlayer in Fig. 9. Arrows denote trend in anion outdiffusion as a function of ionicity. No obvious trend appears for cation outdiffusion (after Brillson et al. [61]).

Figure Captions

1. Schematic diagram of the extended metal-semiconductor interface. The reacted and/or interdiffused regions are determined by the strength and nature of interfacial bonding. The reacted region can have new dielectric properties and built-in potential gradients. The interdiffused region can have nonparabolic band bending determined by the distributions of electrically-active sites due to the movements of the various atomic constituents (after Brillson et al. [5,6]).

2. Barrier heights from Mead [1] correlated with heats of interface chemical reaction ΔH_R for metals on ZnO, ZnS, CdS, and GaP. ΔH_R is calculated according to Eq. 2. All of the semiconductors display the same qualitative behavior regardless of ionicity, although their ranges of $\varnothing_{SB}$ vary. A critical heat of reaction $\Delta H_R^C \sim$ 0.5 eV per metal atom, determined experimentally, marks the transition region between reactive and unreactive interfaces (after Brillson [7]).

3.   (a) Energy of the valence band maximum relative to the Fermi level of a Au contact (i.e. $\emptyset_{SB}^{p}$) plotted vs anion electronegativity [e.g., Refs. 18 and 19]. Semiconductor-Au barriers compiled by Mead [1] for each anion are averaged (after McCaldin et al. [16,17]). Same data $\emptyset_{SB}^{p}$ plotted vs heat of reaction $\triangle H_R$ [7] for (b) Au. (c) Cu, and (d) Ag.

4.   SXPS ratio of surface anion/cation core level intensities I_P^{2P}/I_{In}^{4d} vs Ag. Pd. Cu. Au. Al. Ti. or Ni coverages on InP (110) relative to the UHV-cleaved surface ratio. $\emptyset_{SB}$ vs $\triangle H_R$ is plotted in the inset (after Williams [12]). This plot illustrates the correspondence between $\emptyset_{SB}$ and the stoichiometry of outdiffusion (after Brillson et al. [38]).

5.   SXPS ratio of surface cation/anion core level intensities at $h\nu$ = 130 eV. $Ga^{3d}_{130}/As^{3d}_{130}$, relative to the UHV-cleaved GaAs surface and vs Au overlayer thickness T.   Each curve corresponds to a different Al coverage.   Inset shows interlayer configuration schematically (after Brillson et al. [39]).

6.   SXPS ratio of surface cation/marker and anion/marker core level intensities vs Au overlayer thicknesses on (a) GaAs. (b) InP, and (c) CdS. The decrease (increase) of these ratios relative to the ratios of surfaces without Au signifies metal (semiconductor) indiffusion past the marker into the semiconductor (metal).

7.   SXPS integrated Al 2p($h\nu$ = 130 eV), Se 3d($h\nu$ = 130ev) and Cd 4d($h\nu$ = 90ev) core level intensities as a function of Al overlayer thickness on a UHV-cleaved CdSe $(10\bar{1}0)$ surface (after Brucker and Brillson [62]).

8.   Ratio of cation/anion XPS (hν = 1487 eV) integrated core level intensities as a function of metal overlayer coverage on CdSe (solid lines) or CdS (dashed lines). Ratios are normalized to unity for the cleaved surface (after Brucker and Brillson [66]).

9.   Integrated SXPS peak areas for (a) Cd 4d and (b) S 2P core levels as a function of Au coverage for different Al interlayer thicknesses. Each curve corresponds to a different interlayer thickness.   Intensities are normalized to the cleaved surfaces. Insets show corresponding diffusion of anions and cations through the metal. Al interlayers increase anion outdiffusion for CdS.

10. Integrated SXPS peak areas for (a) Zn 3d and (b) Se 3d core levels as a function of Au coverage for different Al interlayer thicknesses. Intensities are normalized to the cleaved surfaces. Insets show corresponding diffusion of anions and cations through the metal. Each curve corresponds to a different interlayer thickness. Al interlayers decrease anion outdiffusion for ZnSe.

11. SXPS Se 3d core level spectra for (a) $\hbar\nu = 70$ eV and (b) $\hbar\nu = 130$ eV at successive stages of interlayer contact formation on CdSe $(10\bar{1}0)$. Alignment is with respect to the higher-energy fullwidth at half maximum points. One monolayer (ML) on CdSe equals 3.5×10^{14} atoms/cm^2. The bulk-sensitive spectra in (a) reveal an anomalous broadening due to rapid band bending below the CdSe surface. Surface-sensitive spectra in (b) display no such broadening. Surface sensitivity is defined according to the electron escape depth curve for inorganic compounds of Seah and Dench [65] in (c) (after Brucker *et al.* [71]).

12. Schematic energy band diagrams of the Al-(top) Au-(middle) and Au plus Al interlayer-UHV-cleaved CdS or CdSe $(10\bar{1}0)$ (bottom) interfaces. qV_B denotes the band bending, $\varnothing_{SB}$ the associated Schottky barrier height. W the barrier width over which the parabolic band bending takes place. and E_B the core level electron binding energy. The characteristic J-V curves for each interface indicate schematically the "ohmic" (top), rectifying (middle) and "softened" rectifying (bottom) behavior of the interfaces pictured at right (after Brucker *et al.* [66]).

References

1. C.A. Mead. Solid State Electron. 9 (1966) 1023 and references therein.

2. S. Kurtin, T.C. McGill. and C.A. Mead, Phys. Rev. Lett. 22 (1970) 1433.

3. J. Van Laar and A. Huijser, J. Vac. Sci. Technol. 13 (1976) 769.

4. See, for example, J. Vac. Sci. Technol. 15 (1978) 1217-1416 and references therein.

5. L.J. Brillson, C.F. Brucker, N.G. Stoffel. A.D. Katnari. and G. Margaritondo. Phys. Rev. Lett. 46 (1981) 838.

6. L.J. Brillson, C.F. Brucker, A.D. Katnani, N.G. Stoffel. and G. Margaritondo. J. Vac. Sci. Technol. 19 (1981) 661.

7. L.J. Brillson, Phys. Rev. Lett. 40 (1978) 260: L.J. Brillson, J. Vac. Sci. Technol. 15 (1978) 1378..

8. D.D. Wagman. W.H. Evans. V.B. Parker. I. Halow. S.M. Bailey, and R.H. Schumm. Natl. Bur. Stand. Technical Notes 270-3 – 270-7 (U.S.G.P.O., Washington, D.C., 1968-1971).

9. K.C. Mills. Thermodynamic Data for Inorganic Sulphides. Selenides. and Tellurides (Butterworths, London. 1974).

10. O. Kubachewski. E.L.L. Evans. and C.B. Alcock. Metallurgical Thermochemistry (Pergamon. New York, 1967).

11. L.J. Brillson, Surf. Sci. 51, (1975) 45: L.J. Brillson. Surf. Sci. 69 (1977) 62.

12. R.H. Williams, V. Montgomery, and R.R. Varma. J. Phys. C. II (1978) L735.

13. R.H. Williams, R.R. Varma. and V. Montgomery. J. Vac. Sci. Technol. 16 (1979) 1418.

14. N.C. Wyeth and A. Catalano, J. Appl. Phys. 51 (1980) 2286.

15. J. Baars, D. Bassett. and M. Schultz. Phys. Status Solidi (a) 49 (1978) 483.

16. J.O. McCaldin, T.C. McGill. and C.A. Mead, Phys. Rev. Lett. 36 (1976) 56.

17. J.O. McCaldin, T.C. McGill, and C.A. Mead, J. Vac. Sci. Technol. 13 (1976) 802.

18. L. Pauling, The Nature of the Chemical Bond (Cornell Univ. Press, Ithaca, N.Y., 1939).

19. J.C. Phillips and J.A. VanVechten, Phys. Rev. Lett. 23 (1969) 1115, Phys. Rev. B2 (1970) 2147.

20. J.O. McCaldin, T.C. McGill, and C.A. Mead, unpublished.

21. R.K. Swank, Phys. Rev. 153 (1967) 844.

22. G.G. Hall, Phil. Mag. 43 (1952) 338.

23. D.J. Chadi and M.L. Cohen, Phys. Stat. Solidi (b) 68 (1975) 405.

24. J.L. Birman, Phys. Rev. 115 (1959) 1493.

25. W.A. Harrison, Phys. Rev. B8 (1973) 4487.

26. W.A. Harrison and S. Ciraci, Phys. Rev. B10 (1974) 1516.

27. K. Kajiyama, Y. Mizushima, and S. Sakata, Appl. Phys. Lett. 23 (1973) L58.

28. J.W. Keller, A.P. Roth, and E. Fortin, Can. J. Phys. 58 (1980) 63.

29. K. Okamoto, C.E.C. Wood, and L.F. Eastman, Appl. Phys. Lett. 38 (1981) 636.

30. L.J. Brillson, J. Vac. Sci. Technol. 16 (1979) 1137.

31. I. Lindau, P.W. Chye, C.M. Garner, P. Pianetta, and W.E. Spicer, J. Vac. Sci. Technol. 15 (1978) 1332.

32. P.W. Chye, I. Lindau, P. Pianetta, C.M. Garner, and W.E. Spicer, Phys. Rev. B17 (1978) 2682.

33. H.H. Wieder, J. Vac. Sci. Technol. 15 (1978) 1498.

34. R.H. Williams, J. Vac. Sci. Technol. 16 (1979) 1418.

35. W.E. Spicer, I. Lindau, P.W. Chye, P. Skeath, and C.Y. Su, J. Vac. Sci. Technol. 16 (1979) 1422.

36. W.E. Spicer, I. Lindau, P.R. Skeath, C.Y. Su and P. Chye, Phys. Rev. Lett. 44 (1980) 420.

37. A. Hiraki, K. Shuts, F. Kim, W. Kammura, and W. Iwami, Appl. Phys. Lett. 31 (1977) 611, and references therein.

38. L.J. Brillson, C.F. Brucker, A.D. Katnani, N.G. Stoffel, and G. Margaritondo, Appl. Phys. Lett. 38 (1981) 784.

39. L.J. Brillson, G. Margaritondo, and N.G. Stoffel, Phys. Rev. Lett. 44 (1980) 667.

40. L.J. Brillson, G. Margaritondo, N.G. Stoffel, R.S. Bauer, R.Z. Bachrach, and G. Hansson, J. Vac. Sci. Technol. 17 (1980) 880.

41. G. Margaritondo, L.J. Brillson, N.G. Stoffel, and A.D. Katnani, Appl. Phys. Lett. 37 (1980) 917.

42. L.J. Brillson, C.F. Brucker, G. Margaritondo, J. Slowik, and N.G. Stoffel, Proc. XV International Conference on the Physics of Semiconductors (Kyoto, 1980). J. Phys. Soc. Japan 49 (1980) 1089.

43. V. Montgomery, R.H. Williams, and G.P. Srivastava, J. Phys. C 14 (1981) L191.

44. J. Massies, J. Chaplant, M. Laviron, and N.T. Linh, Appl. Phys. Lett. 38 (1981) 693.

45. J. Massies, F. Dezaly, and D.T. Linh, J. Vac. Sci. Technol. 17 (1980) 1134.

46. A.G. Milnes, Deep Impurities in Semiconductors (Wiley-Interscience, New York, 1973).

47. A.G. Milnes, Advances in Electronics and Electron Physics, in press.

48. A.K. Sinha and J.M. Poate, Appl. Phys. Lett. 23 (1973) 666.

49. R.H. Williams, A. McKinley, G.J. Hughes, V. Montgomery, and I.T. McGovern, J. Vac. Sci. Technol. 21 (1982) 594.

50. L.J. Brillson, R.S. Bauer, R.Z. Bachrach, and G. Hansson, Appl. Phys. Lett. 36 (1980) 326.

51. L.J. Brillson. R.S. Bauer. R.Z. Bachrach. and G. Hansson. Phys. Rev. B 23 (1981) 6204.

52. P. Skeath. C.Y. Su, I. Hino. I. Lindau. and W.E. Spicer. Appl. Phys. Lett. 29 (1981) 349.

53. W.G. Petro. I.A. Babalola. P. Skeath. C.Y. Su, I. Hino. I. Lindau. and W.E. Spicer. J. Vac. Sci. Technol. 21 (1982) 585.

54. L.J. Brillson. R.Z. Bachrach. and R.S. Bauer. Phys. Rev. Lett. 42 (1979) 397.

55. A.K. Sinha and J.M. Poate. in Thin Films — Interdiffusion and Reactions. Ed.. J.M. Poate, K.N. Tu. and J.W. Mayer (Wiley-Interscience. New York. 1978) p. 4078.

56. J.L. Freeouf and J.M. Woodall. Appl. Phys. Lett. 39 (1981) 727.

57. J.M. Woodall and J.L. Freeouf. J. Vac. Sci. Technol. 21 (1982) 574.

58. R.W. Grant. J.R. Waldrop. S.P. Kowalczyk. and E.A. Kraut. J. Vac. Sci. Technol. 19 (1981) 477.

59. L.J. Brillson. C.F. Brucker. A.D. Katnani. N.G. Stoffel. R.R. Daniels. and G. Margaritondo. J. Vac. Sci. Technol. 21 (1982) 564.

60. J.D. Dow. private communication.

61. L.J. Brillson. C.F. Brucker. N.G. Stoffel. A.D. Katnani. R. Daniels. and G. Margaritondo. Proc. XVI International Conference on the Physics of Semiconductors (Montpellier. 1982) in press.

62. C.F. Brucker and L.J. Brillson. unpublished.

63. L.J. Brillson, Phys. Rev. Lett. 38 (1977) 245.

64. L.J. Brillson. R.S. Bauer. R.Z. Bachrach. and J.C. McMenamin. J. Vac. Sci. Technol. 17 (1980) 476.

65. M.P. Seah and W.A. Dench. Surf. and Interface Analysis 1 (1979) 2.

66. C.F. Brucker and L.J. Brillson. J. Vac. Sci. Technol. 19 (1981) 617.

67. L.J. Brillson. Surface Science Reports 2 (1982) 123.

68. C.F. Brucker and L.J. Brillson, Appl. Phys. Lett. 39 (1981) 67.

69. E.C. Freeman and J. Slowik, Appl. Phys. Lett. 39 (1981) 96.

70. N.G. Stoffel, R.R. Daniels, G. Margaritondo, C.F. Brucker, and L.J. Brillson, J. Vac. Sci. Technol. 20 (1982) 701.

71. C.F. Brucker and L.J. Brillson, Thin Solid Films 93 (1982) 67.

72. C.F. Brucker, L.J. Brillson, A.D. Katnani, N.G. Stoffel, and G. Margaritondo, J. Vac. Sci. Technol. 21 (1982) 590.

SEMICONDUCTOR	PHILIPS IONICITY	PAULING IONICITY	$\dfrac{I_A(I+M)}{I_A(M)}$	$\dfrac{I_C(I+M)}{I_C(M)}$
CdS	0.685	0.59	⇑ 4.0	↓ 0.25
ZnS	0.623	0.59	⇑ 3.5	↓ <1
CdSe	0.699	0.58	⇑ 1.4	↓ 0.24
ZnSe	0.676	0.57	⇓ 0.47	↓ 0.15
CdTe	0.675	0.52	⇓ 0.35	↓ 0.29
ZnTe	0.546	0.53	⇓ 0.24	↓ 0.40

$I = 10\overset{\circ}{A} \text{ AAl}$
$M = 40\overset{\circ}{A} \text{ Au}$

A = ANION   C = CATION

VI II

40Å Au

II · VI

Table 1.

METAL

SEMICONDUCTOR

REACTED REGION

INTERDIFFUSED REGION

Fig. 1

Fig.2

Fig.3

Fig.4

Fig. 5

METAL-INDUCED
SURFACE STATES

S ⟶
⟵ Au
Cd ⟶

In ⟶
P ⟶
⟵ Au

⟵ Au
Ga ⟶
As ⟶
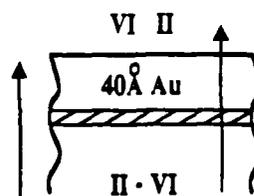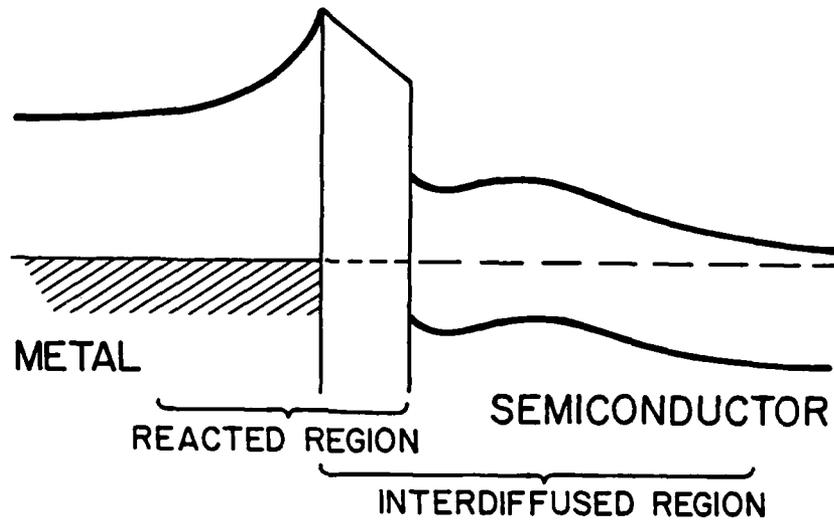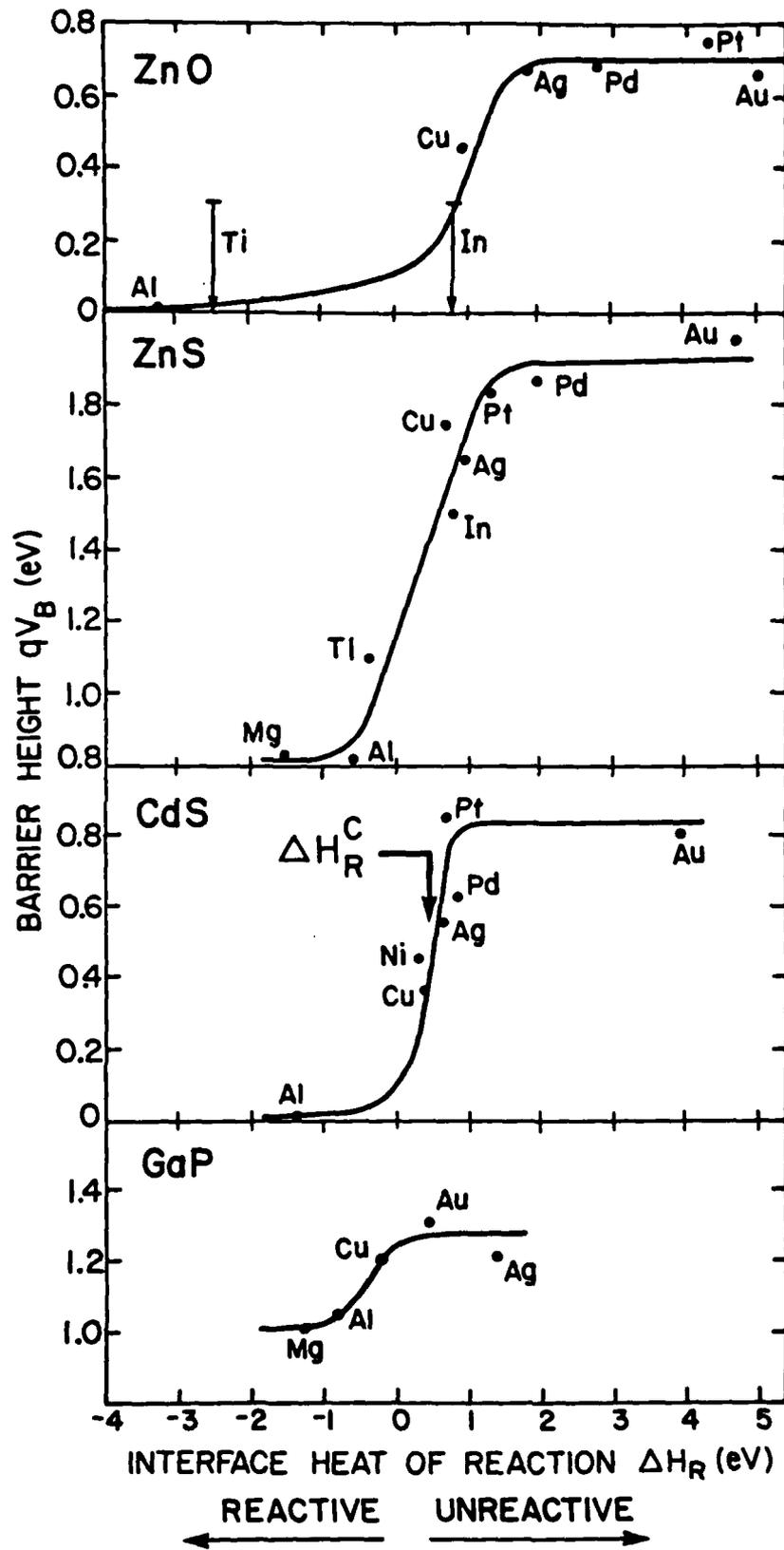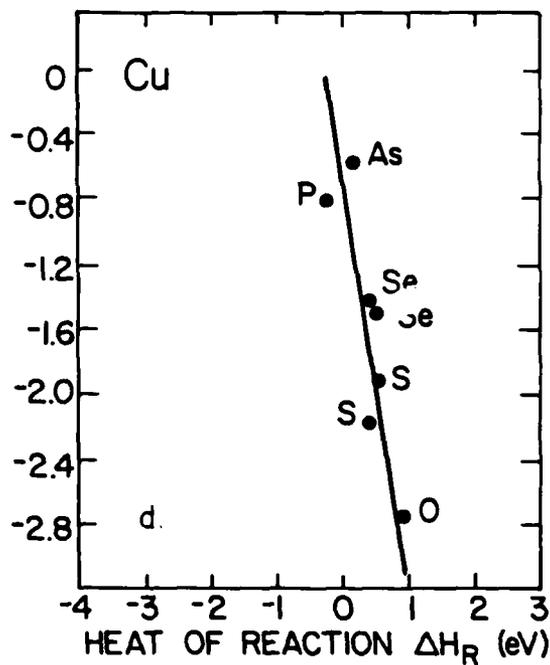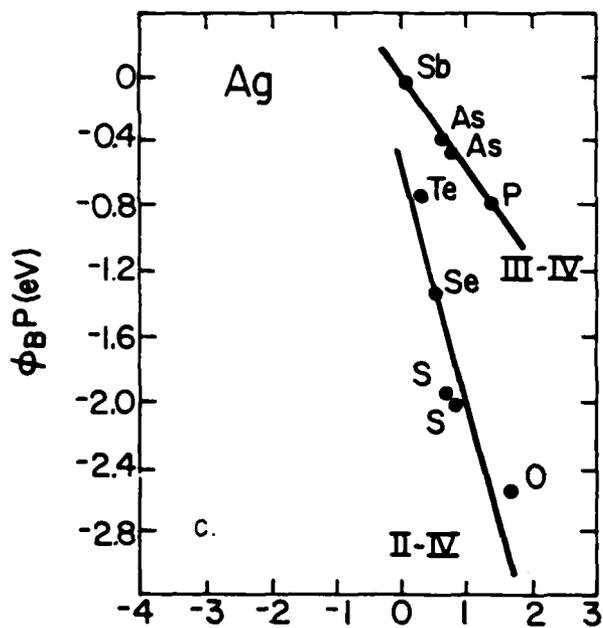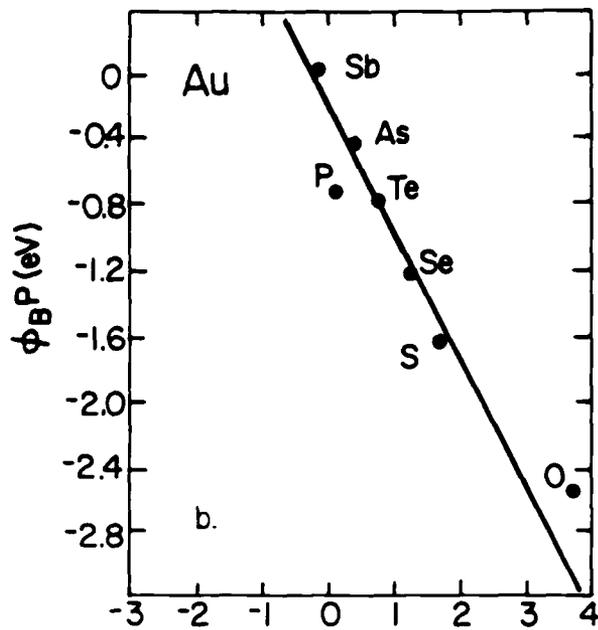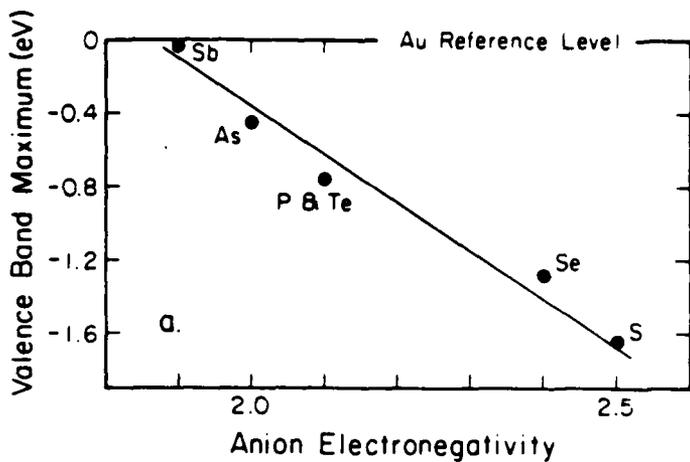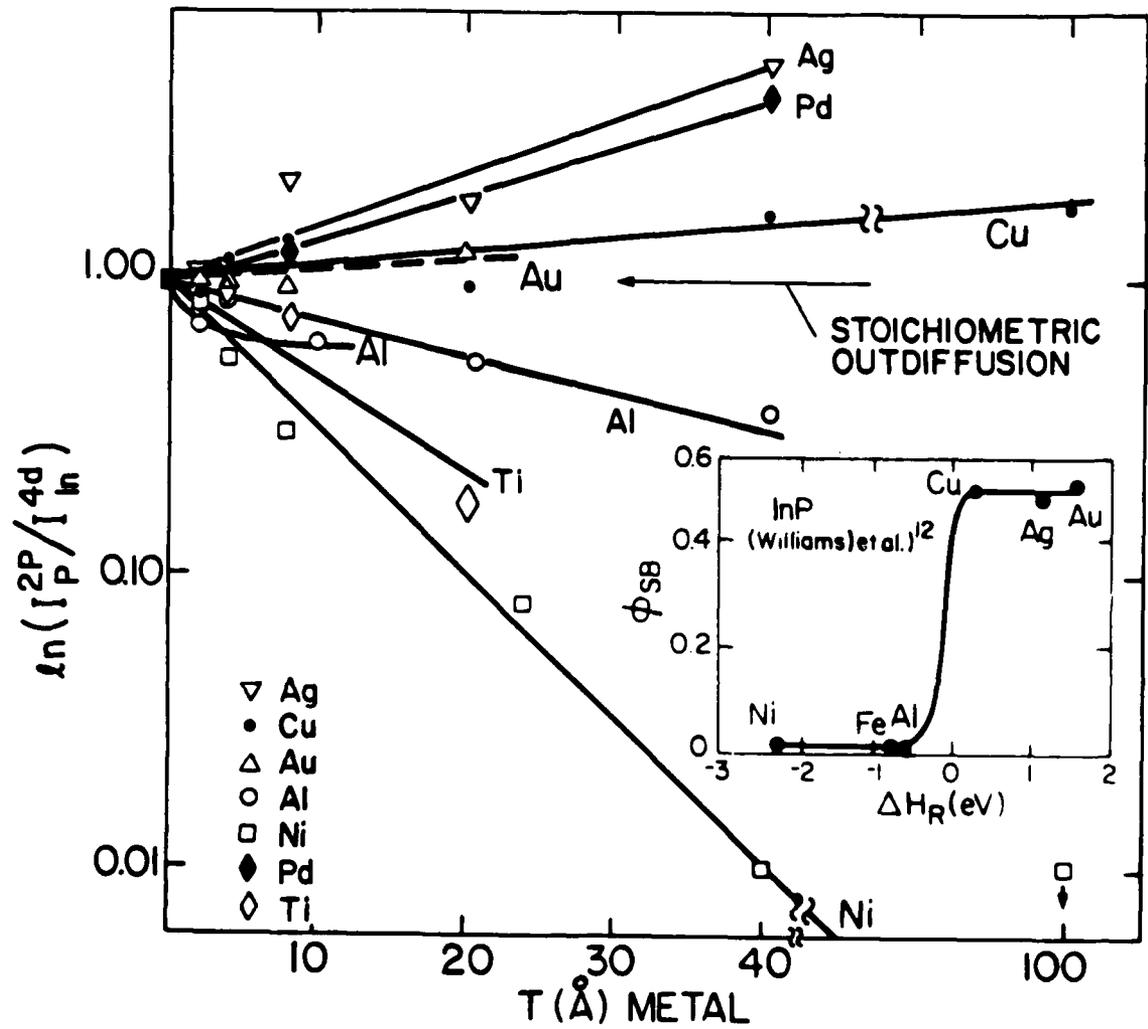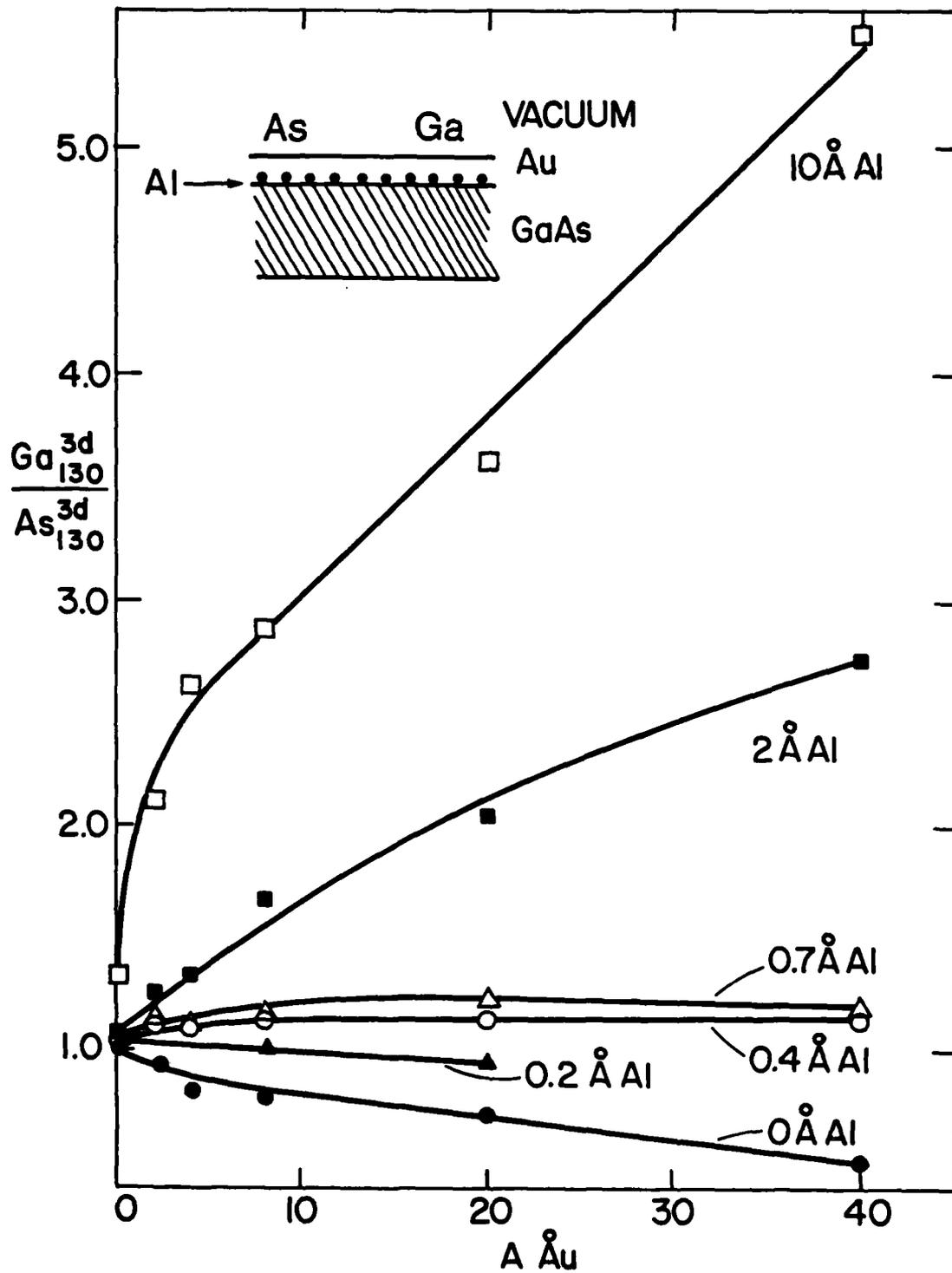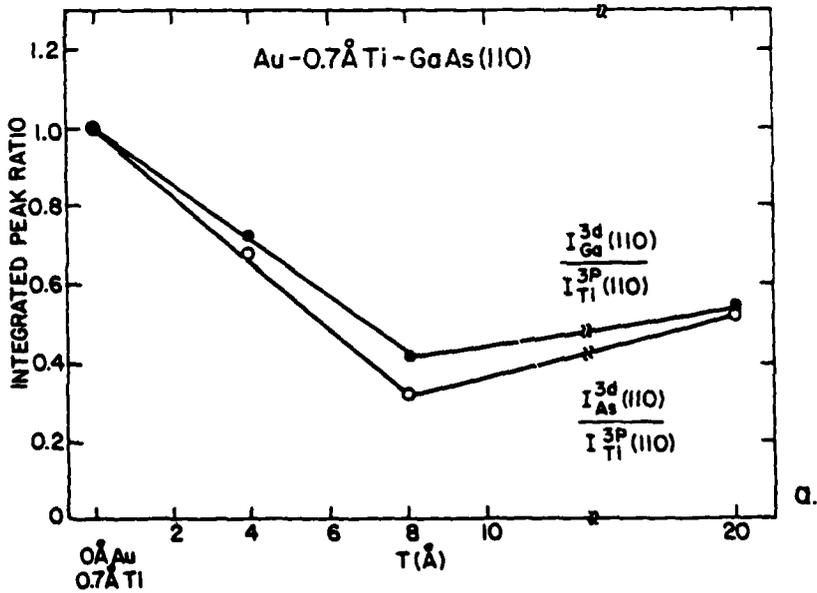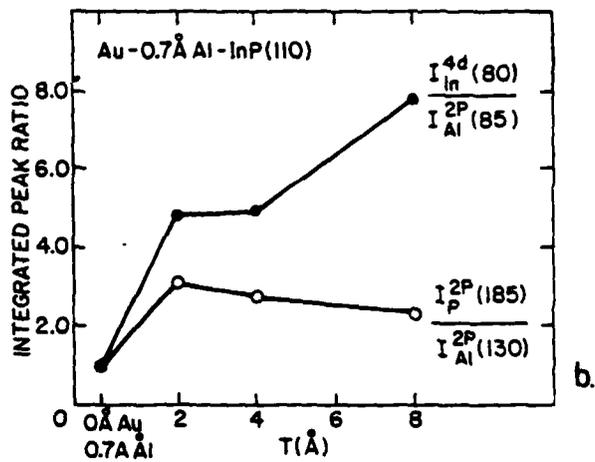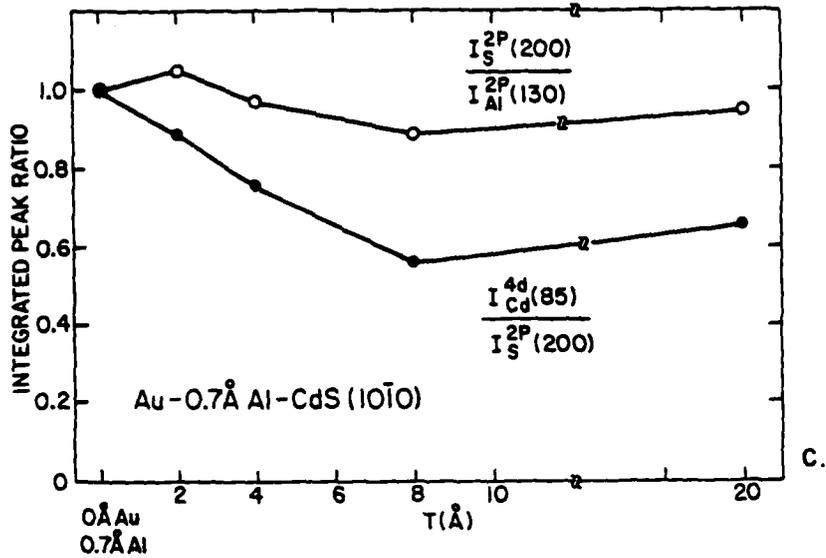
Fig.6

Fig.7

Fig.8

Fig.9

Fig.10

CdSe(10$\bar{1}$0) + Al + Au

(a) $\hbar\omega$ = 70 eV   (b) $\hbar\omega$ = 130 eV

Se3d

$\frac{1}{2}$ ML Al + 10Å Au

$\frac{1}{2}$ ML Al

CLEAVED

ELECTRON KINETIC ENERGY (eV)

(C)
(SEAH AND DENCH, 1979)

ESCAPE DEPTH (Å)

ENERGY (eV)
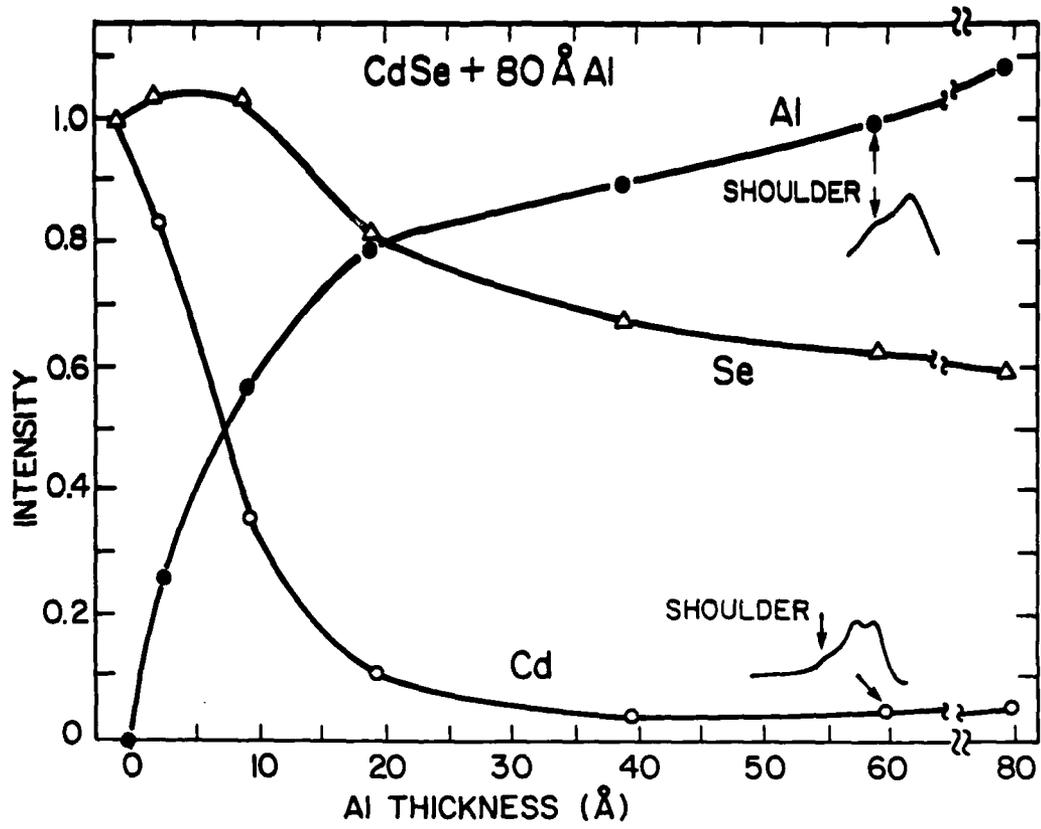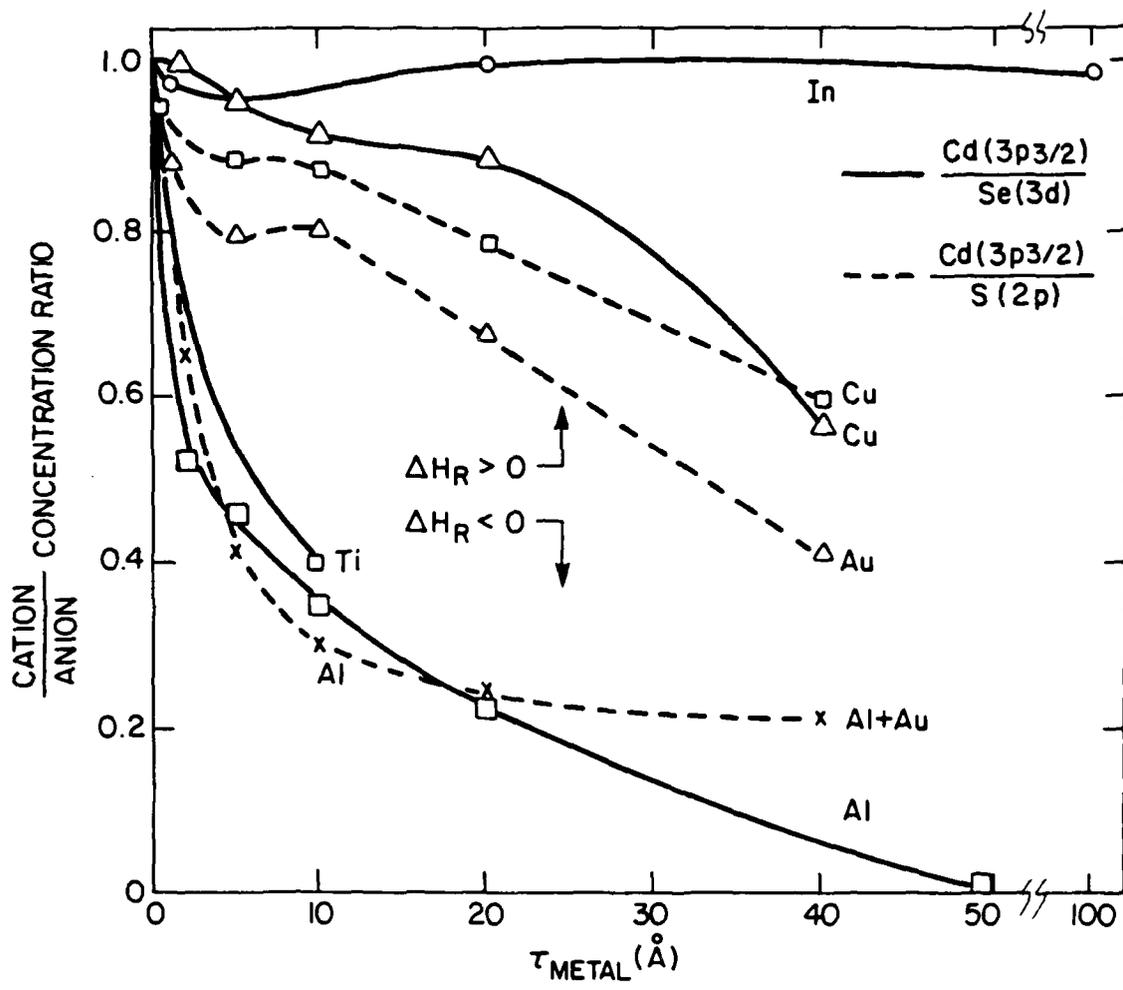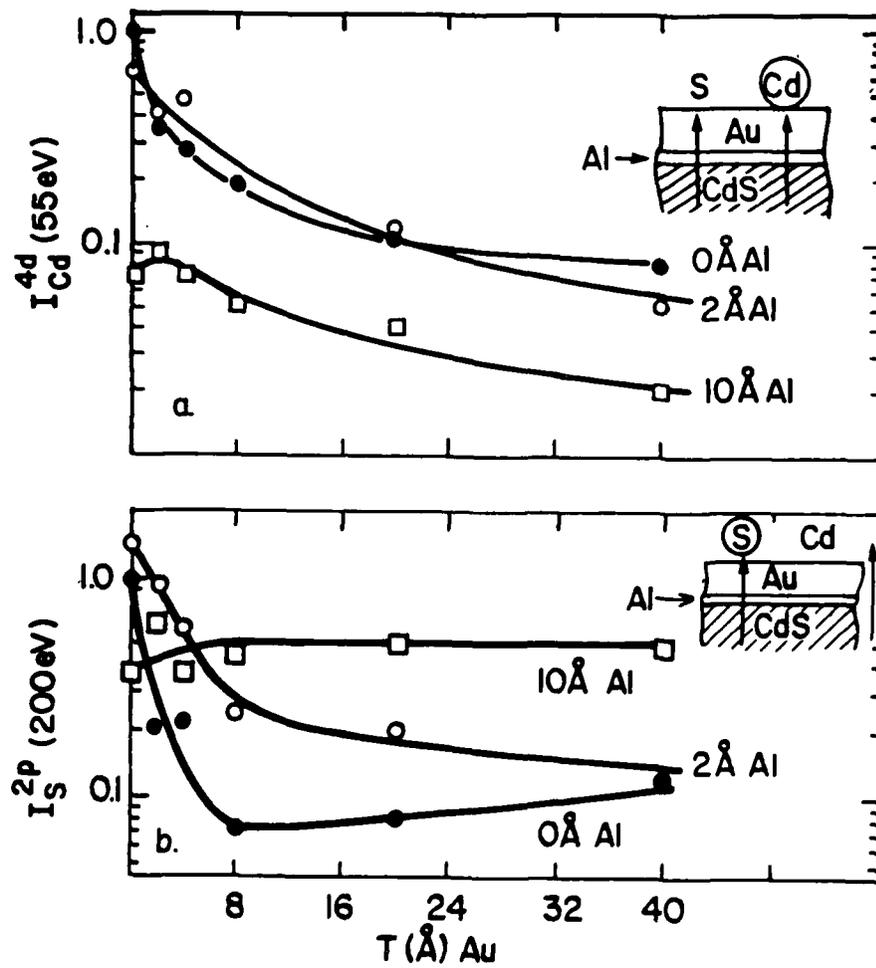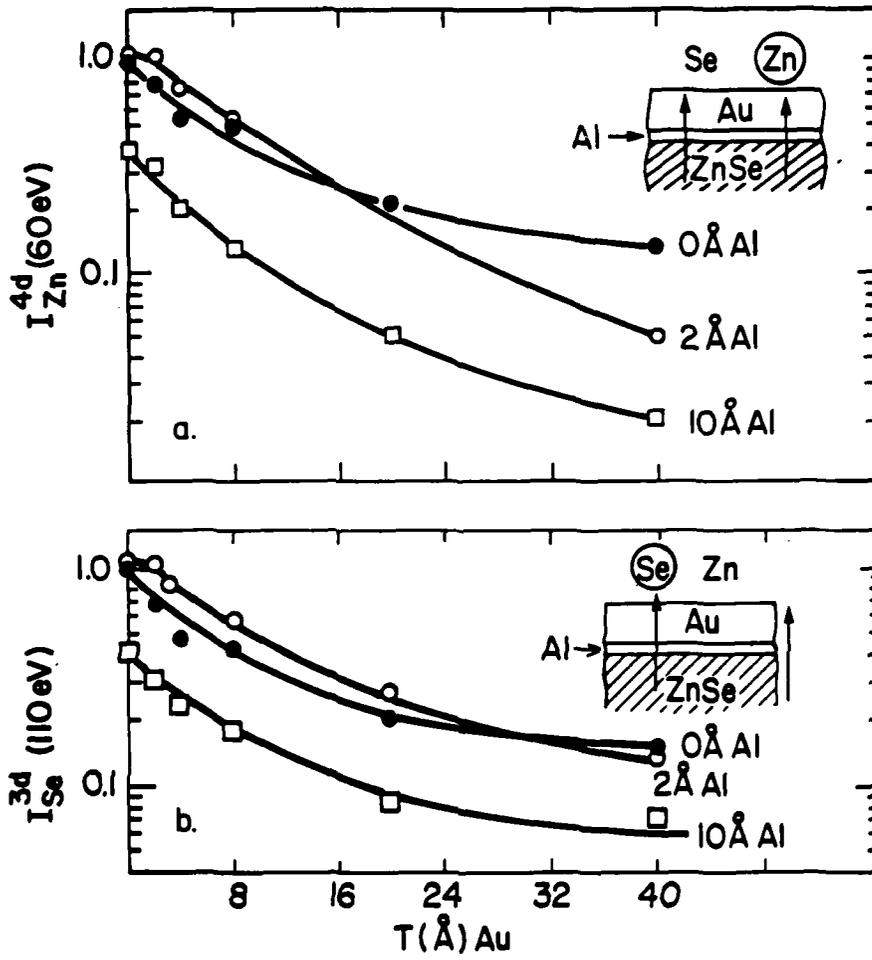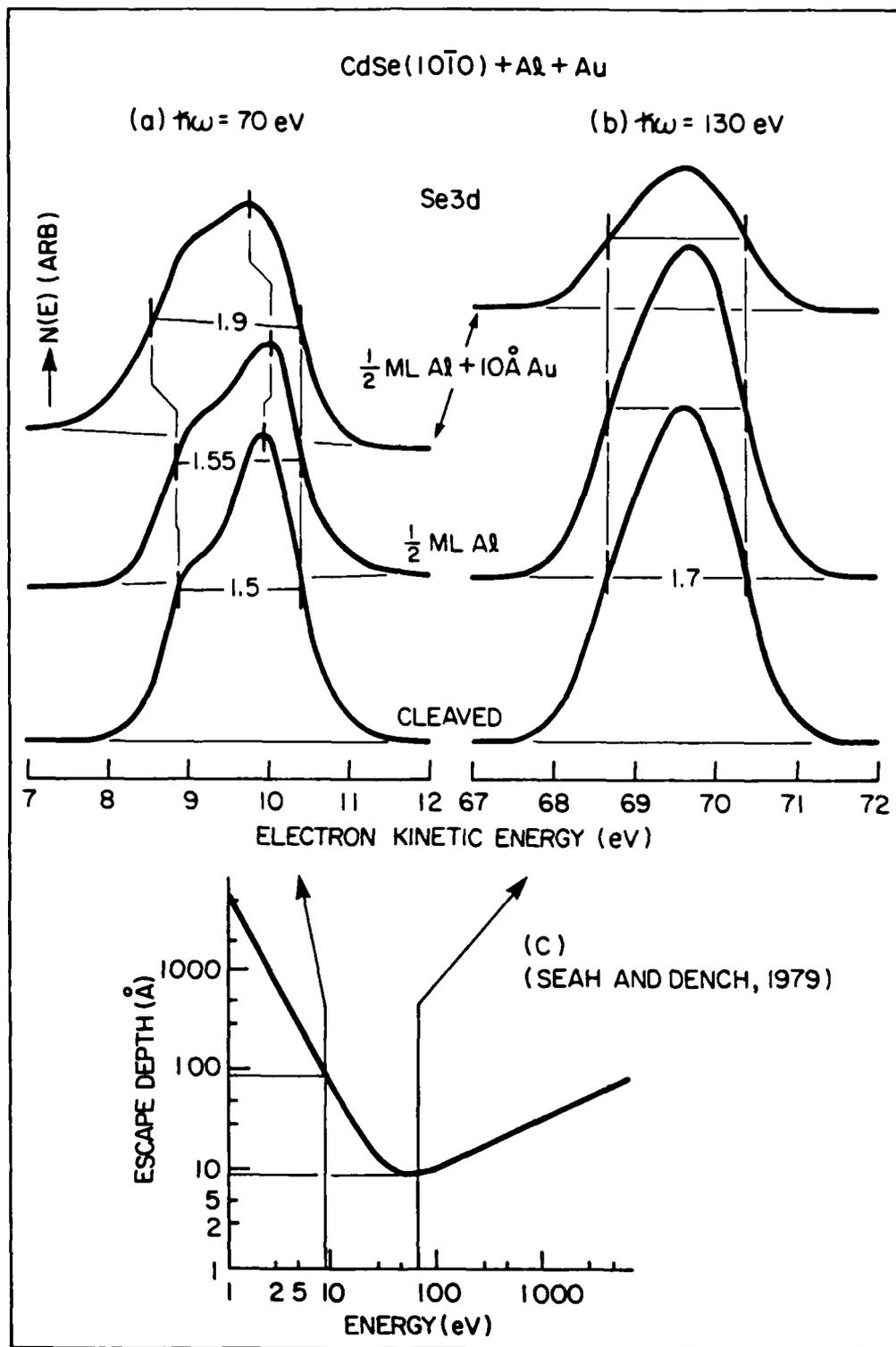
Fig.11
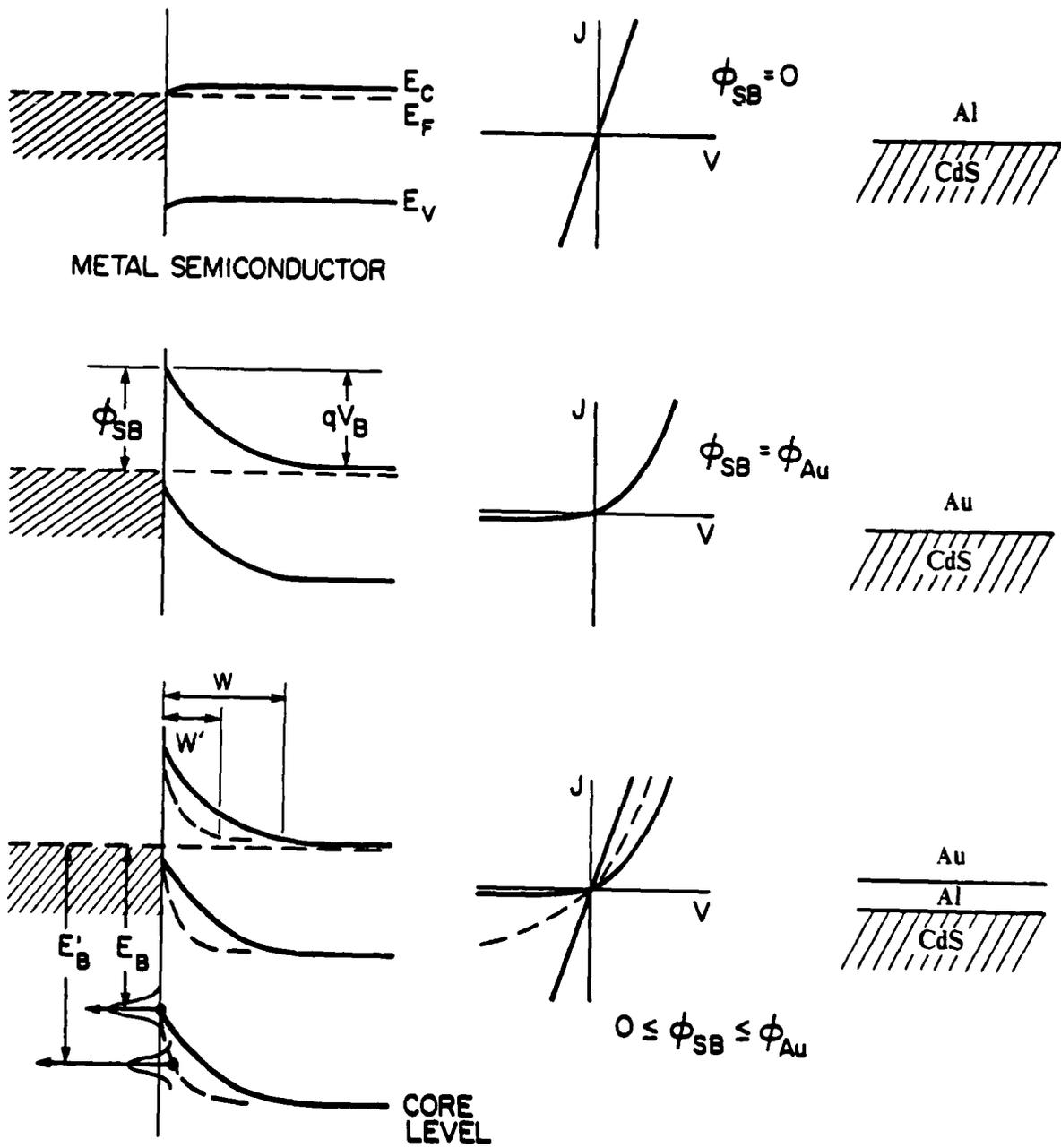
Fig.12

PHOTOEMISSION STUDIES OF REACTIVE DIFFUSION AND LOCALIZED DOPING AT II-VI COMPOUND SEMICONDUCTOR-METAL INTERFACES

L.J. Brillson, C.F. Brucker, N.G. Stoffel*, A. Katnani*, R. Daniels*, and G. Margaritondo

Xerox Webster Research Center, Rochester, NY, USA, 14644
*Dept. of Physics, University of Wisconsin, Madison, WI, USA, 53706

Soft x-ray photoemission spectroscopy measurements reveal strong differences in chemical bonding and diffusion between II-VI and III-V compound semiconductor-metal interfaces which provide a chemical basis for their systematic differences in Schottky barrier formation.

1. Introduction

In recent years, surface science techniques have shown that semiconductor-metal interfaces are far from the atomically abrupt junctions commonly envisaged. Instead, chemical reactions and diffusion can occur which broaden the interface over many atomic layers. These chemical effects can produce new electrically-active sites and/or dielectric layers which can contribute to the measured Schottky barrier height φ_{SB}. For III-V compounds, considerable discussion has centered on Fermi level pinning by defects related to cation and anion diffusion out of the semiconductor.[1,2] It was found that metals react in varying degree with (110) surfaces of III-V compounds, leading to anion vs. cation-rich outdiffusion.[3] In turn, these have been associated with high vs. low φ_{SB} for InP and GaAs.[4] In contrast, different metals on II-VI compound semiconductors generally produce a wider range of φ_{SB}.[5] Correspondingly, we have now found from soft x-ray photoemission spectroscopy (SXPS) data of a large set of II-VI compounds: a) qualitatively different chemical behavior between II-VI and III-V compound semiconductors and b) varying degree of chemical behavior which correlates with the compound ionicity.

2. Experiment and Discussion

Metal-semiconductor interfaces were prepared by cleaving II-VI crystals in ultrahigh vacuum (UHV) and depositing metal on the cleaved surface in stages. SXPS core level and valence band spectra were taken at each stage using photon energies selected for high surface sensitivity, i.e., which produced photoelectrons having kinetic energies with short inelastic mean free paths - typically 4-6A. The II-VI compounds studied were "Sonora" ZnS (n-type, intrinsic doping), ZnSe (doped n-type by a Zn extraction method), ZnTe (p-type, intrinsic doping), CdS (n-type), CdSe (n-type), and CdTe (p-type). The crystal structures and their cleavage surface were wurzite and (10$\bar{1}$0) for

CdS and CdSe and zincblende (110) for the remainder. Charging distorted SXPS features severely for ZnS and ZnSe but was reduced substantially with high intensity illumination from a focussed projector lamp.

Figure 1 provides an illustration of the strong chemical effects present at II-VI/metal interfaces. Significant diffusion of Zn and Se out of the semiconductor into the metal overlayer(s) occurs since the SXPS core level intensities attenuate slowly with metal coverage, despite the 4-6A electron escape depth. With an initial 10A Al deposition, the Zn 3d peak in Fig. 1 develops a second smaller feature, shifted 1.1 eV to lower binding energy which corresponds to dissociated Zn. Such dissociation is expected since the Al bonds strongly with Se.[6,7] With Au added to this surface the Zn peak splitting decreases, indicative of charge transfer between Zn and Au. For Al deposition alone (not shown), the dissociated cation
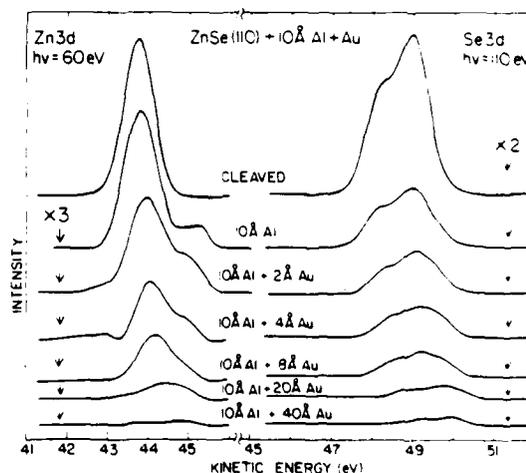

Fig. 1: SXPS spectra for Zn 3d and Se 3d core levels as a function of metal coverage on UHV-cleaved ZnSe (110) surfaces.

intensity decreases much more rapidly than the anion intensity, suggesting that free cations are localized preferentially near the interface.[6,7] Such cation localization is not observed for reactive metals on III-V compounds.[3,8] For Au deposition exclusively (not shown), no dissociated cation peaks are evident, but both substrate anion and cation peaks shift due to both band bending and bond charge transfer. With Au or Au + Al on all six II-VI compounds, the cation intensities decrease with metal coverage. Cation attenuation is more pronounced than for metals on III-V compounds.[3,8]

Al interlayers at semiconductor-Au interfaces highlight a particularly significant difference between II-VI and III-V compounds. Whereas multilayer Al interlayers retard anion outdiffusion for all III-V compounds, such interlayers retard or enhance anion outdiffusion for each II-VI compound depending upon the semiconductor ionicity. Figure 2 illustrates the contrast between anion outdiffusion from CdS vs. ZnSe. Increasing thicknesses of Al reduce the Se 3d SXPS core level intensity I_{Se}^{3d} but actually enhance I_{S}^{2p} for the same metal deposits on CdS. The anion enhancement suggests a reactive diffusion in which the S is pulled out of the CdS and through the Al as it forms new Al-S bonds. For CdS and CdSe, Cu interlayers produce a similar anion enhancement.[7] The effect of a 10A Al interlayer in fact varies monotonically with the
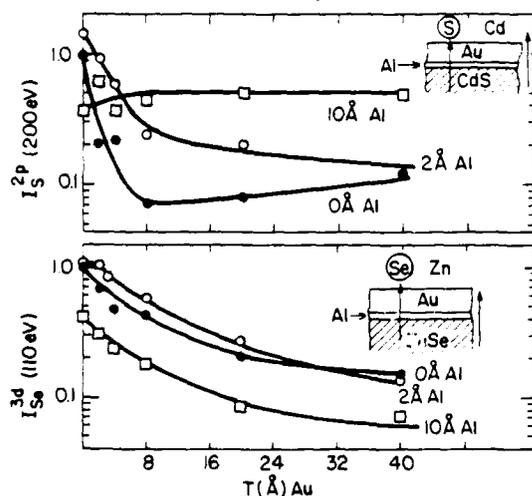

Fig. 2: Integrated SXPS peak areas for (a) S 2p and (b) Se 3d core levels as a function of metal coverage for different Al interlayer thicknesses. Areas are normalized to the cleaved surface. Insets show corresponding diffusion of anions and cations through the metals. Al interlayers increase (decrease) anion outdiffusion for CdS (ZnSe).

ionicity[9,10] of the II-VI semiconductor. For a 40A Au overlayer with vs. without the 10A Al interlayer, the relative changes in SXPS anion intensity are 4.0, 3.5, 1.4, 0.47, 0.35, and 0.24 for CdS, ZnS, CdSe, ZnSe CdTe, and ZnTe respectively. Thus, the more ionic the semiconductor, the more pronounced are its differences in interface chemistry with III-V compounds.

For all of these interfaces, the 10A Al interlayer always decreased the SXPS cation intensities without any obvious trend in semiconductor properties. Furthermore, the semiconductor outdiffusion was either anion-rich or stoichiometric. This behavior differs from III-V diffusion through metals, for which reactive (unreactive) metals lead to cation- (anion-) rich outdiffusion. If Fermi level (E_F) pinning is due to defects associated with semiconductor outdiffusion, then only one type of defect should dominate for both reactive and unreactive metals on II-VI compounds and E_F movement should not be restricted by levels within the band gap associated with anion and cation deficiencies, as proposed for the III-V compounds.[2] This is consistent with the wider range of φ_{SB} for II-VI vs III-V compound semiconductor-metal interfaces.[5]

The enhanced anion outdiffusion with reactive metals produces a net accumulation of partially dissociated cations which are localized near the metal-semiconductor interface. For Au-CdS and CdSe interfaces with Al interlayers, the cation localization results in an effective doping of the semiconductor surface. Se 3d core level spectra exhibit an anomalous broadening which is attributed to sharp band bending at the CdSe surface for $h\nu = 70$ eV and minimum surface sensitivity (escape depth 90-100A) and which is absent for $h\nu = 130$ eV spectra and maximum surface sensitivity (escape depth 6-10A).[11] No such broadening occurs for the junctions without the interlayer. Capacitance-voltage (C-V) measurements of the interfaces with Al interlayers reveal a narrowing of the surface space charge region and an increase in doping density.[7] Current-voltage (J-V) measurements display a strong reduction in φ_{SB} with monolayer thicknesses of Al interlayer.[12] The barrier lowering can be attributed to a substantial tunneling through the surface space charge region, which is heavily doped by electrically-active cations released by the interface chemical reaction.[12,13] SXPS core level and electrical measurements rule out analogous phenomena at III-V interfaces.

For both II-VI and III-V (GaAs, GaSb, InAs, and InP) semiconductors studied, anion and cation outdiffusion

decreases linearly with increasing heat of formation[14] H_F^{SC}, thereby establishing that interface dissociation and diffusion scale predominantly with semiconductor stability. As shown in Fig. 3a, Cd- and Zn- chalcogenides exhibit the same dependence of anion and cation outdiffusion on H_F^{SC}, despite differences in cation, crystal structure, and n- vs. p-type doping. The attenuation values in Fig. 3 were obtained from anion and cation peak intensities at a Au coverage of 20A relative to those for the cleaved surface, as indicated schematically by the insets. A regular but quantitatively different dependence of III-V outdiffusion on H_F^{SC} appears in Fig. 3b. The stronger III-V vs. II-VI attenuation for a given H_F^{SC} value indicates slower diffusion of III and V atoms at room temperature, consistent with their lower self-diffusion coefficients.[15] As a result, any barriers to diffusion across the metal-semiconductor interface are correspondingly more effective for III-V vs. II-VI compounds. These facts may account for the order-of-magnitude more rapid stabilization (in minutes vs. hours, respectively) of III-V vs. II-VI/metal interface chemistry, as measured by the changes in SXPS intensities and spectral lineshapes with time. The evolution of the interface chemical structure in times much larger than those needed to dissipate heats of condensation suggest that atom movement out of the semiconductor rather than just the energy released by the initial metal-surface bonding can be a limiting factor in the semiconductor outdiffusion.
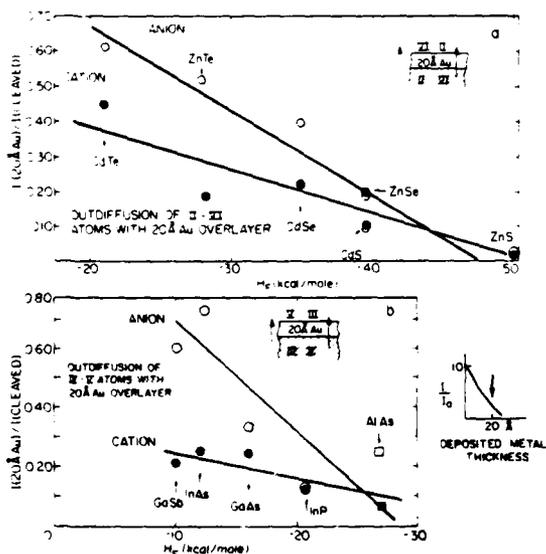
In conclusion, a qualitative difference in interface chemistry exists between II-VI and III-V compound semiconductors with metals. II-VI interfaces exhibit a wide range of diffusion behavior which resembles that of III-V interfaces with decreasing semiconductor ionicity. Several differences between the two semiconductor classes can account for wider range of II-VI/metal φ_{SB}: a) a reversal in stoichiometry of semiconductor outdiffusion for III-V's which is absent for II-VI's, b) a φ_{SB} lowering due to effective doping of II-VI/metal interfaces by dissociated cations, and c) II-VI/metal interfaces with new dielectric properties which are more spatially extended than their III-V counterparts.

References

[1]   Lindau, I., Chye, P.W., Garner, C.M., Pianetta, P. and Spicer, W.E., J. Vac. Sci. Technol 15 (1978) 1332; Wieder, H.H., J. Vac. Sci. Technol. 15 (1978) 1498; Williams, R.H., J. Vac. Sci. Technol. 16 (1979) 1418.

[2]   Spicer, W.E., Lindau, I., Skeath, P.R., Su, C.Y. and Chye, P., Phys. Rev. Lett. 44 (1980) 420.

[3]   Brillson, L.J., Brucker, C.F., Stoffel, N.G., Katnani, A. and Margaritondo, G., Phys. Rev. Lett. 46 (1981) 838.

[4]   Brillson, L.J., Brucker, C.F., Katnani, A.D., Stoffel, N.G. and Margaritondo, G., Appl. Phys. Lett. 38 (1981) 784.

[5]   Mead, C.A., Solid State Electron. 9 (1966) 1023.

[6]   Brillson, L.J., Bauer, R.S., Bachrach, R.Z. and McMenamin, J.C., J. Vac. Sci. Technol. 17 (1980) 476.

[7]   Brucker, C.F. and Brillson, L.J., J. Vac. Sci. Technol. 19 (1981) 617.

[8]   Brillson, L.J., Margaritondo, G. and Stoffel, N.G., Phys. Rev. Lett. 44 (1980) 667.

[9]   Phillips, J.C. and Van Vechten, J.A., Phys. Rev. Lett. 23 (1969) 1115

[10] Pauling, L., The Nature of the Chemical Bond (Cornell Univ. Press. Ithaca, NY, 1939).

[11] Brucker, C.F., Brillson, L.J., Katnani, A.D., Stoffel, N.G. and Margaritondo, G., J. Vac. Sci. Technol., in press.

[12] Brucker, C.F. and Brillson, L.J., Appl. Phys. Lett. 39 (1981) 67.

[13] Freeman, E.C. and Slowik, J.H., Appl. Phys. Lett. 39 (1981) 96.

[14] Mills, K.C., Themodynamic Data for Inorganic Sulphides, Selenides, and Tellurides (Butterworths, London, 1974).

[15] Shaw, D., Atomic Diffusion in Semiconductors (Plenum, NY, 1973).

[16] Bauer, R.S., Bachrach, R.Z. Bachrach, Hansson, G.V. and Chiaradia, P., J. Vac. Sci. Technol. 19 (1981) 674.

Fig. 3: Outdiffusion of a) II-VI and b) III-V atoms with 20A Au overlayers, as indicated schematically by the insets, vs. semiconductor heat of formation. AlAs data from ref. 16.

Soft X-Ray Photoemission Techniques for Characterizing Metal-Semiconductor Interfaces

L.J. Brillson

Xerox Webster Research Center, 800 Phillips Road, W-114, Webster, NY 14580

Abstract

The wide energy range and tunability of synchrotron radiation provide soft x-ray photoemission spectroscopy (SXPS) with several effective methods for characterizing metal-semiconductor interfaces on an atomic scale. These SXPS techniques reveal that metal-semiconductor interfaces are in general not abrupt and that the detailed atomic structure is a controlling factor in determining interface electronic structure.

1. Introduction

Over the past several years, considerable progress has been made in understanding the properties of metal-semiconductor interfaces.[1-5] Perhaps the most effective solid state technique used in characterizing the metal-semiconductor interface to date has been soft x-ray photoemission spectroscopy (SXPS). SXPS results have led to a number of advances in understanding the metal-semiconductor contact - chief among them that the interface is far from the abrupt junction commonly envisioned and that the detailed chemical structure on an atomic scale influences, and in some cases, dominates the interface electronic properties. In this paper, I will review those SXPS techniques which have provided the most

information on the variations in chemical composition and bonding, band bending and the relative movement of atoms near the metal-semiconductor interface.

Several other synchrotron radiation techniques provide information on semiconductor surfaces as well. These include constant final state spectroscopy for monitoring unoccupied states induced by chemisorption,[6] angle-resolved SXPS for determining the symmetry of metal chemisorption on semiconductors,[7] and surface extended x-ray absorption fine structure of atoms SEXAFS, for determining positions of metal atoms in the semiconductor surface.[8] Space precludes discussion of these methods, some of which are discussed elsewhere in this volume.

2. SXPS Used for Interface Characterization

The basis for using the SXPS technique in studying interfaces is the extremely short and variable photoelectron escape depth,[9] which can be controlled by selecting an appropriate incident photon energy via a monochromator between the synchrotron radiation source and the experimental chamber. For example, with a "grasshopper"[10] monochromator at the Tantalus ring of the University of Wisconsin, photoelectrons with energies ranging from 40 eV to

200 eV can be monochromatized and directed to the surface or interface under study in ultrahigh vacuum (UHV).

The photoelectron kinetic energy is given by

$$E_k = h\nu - E_B - (E_{VAC} - E_F) \tag{1}$$

where $h\nu$ is the incident photon energy and E_B is the binding energy relative to E_F, the Fermi level. E_{VAC} is the vacuum level which the electron must exceed in energy to escape from the solid. If the kinetic energies of the excited electronics lie in the range of ~ 50 - 100 eV, then SXPS can have extremely high surface sensitivity, e.g., 4-5 Å, since only electrons within this depth below a surface can escape into vacuum without energy loss. The inelastic collision mean free path increases significantly at much higher or lower energies, so that by tuning in incident wavelength, one can tune the escape depth away from the minimum in order to probe several atomic layers or more into the surface.

The SXPS technique can be coupled to UHV surface science techniques so that electronic and chemical properties at or below a surface can be analyzed as an interface is built up monolayer by monolayer in a clean and controllable fashion.
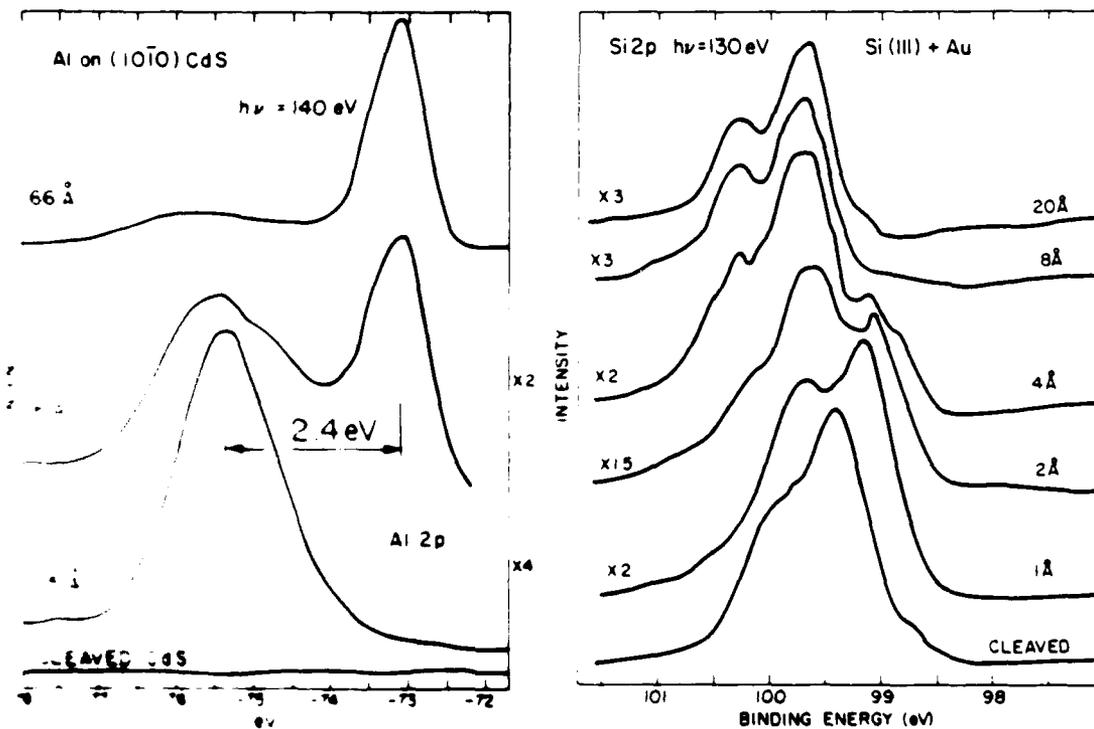
1. SXPS Al 2p core level spectra at $h\nu$ = 140 eV as a function of Al overlayer coverage on cleaved CdS (10$\bar{1}$0).
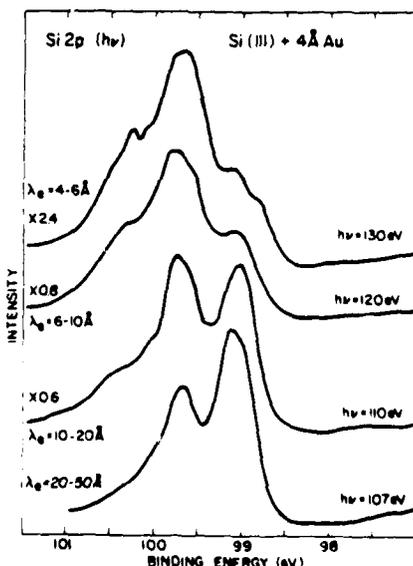
2. SXPS Si 2p core level spectra at $h\nu$ = 130 eV as a function of increasing Au coverage on cleaved Si (111).

3. Interface Chemical Bonding

Figure 1 illustrates the use of SXPS for determining chemical bonding at a metal-semiconductor interface on a monolayer scale. A photon energy of 140 eV was used to excite Al 2p core electrons from a $(10\bar{1}0)$ surface of CdS cleaved in UHV and overlaid with atomic layers of Al.[12] The choice of hν and core level binding energy results in extreme surface sensitivity. With this initial deposition of ~ 1 monolayer, the Al 2p spectrum exhibits only a single peak, characteristic of Al bonded to the substrate. With additional Al coverage, a second peak appears shifted to lower binding energy, charateristic of metallic Al. The appearance of only a single peak at monolayer Al coverage indicates that no island formation takes place. At thick Al coverages, the metallic Al feature completely dominates the spectrum. Chemical shifts of the Cd 4d and S 2p core level features are also observed as a function of metal coverage.

The inelastic strengths of the "reacted" vs. metallic Al peaks vary as a function of incident photon energy. With higher or lower hν, the photoelectron escape depth increases from its minimum value and electrons from further below the surface are photoemitted from the solid. Thus for 6 Å Al on CdS, the reacted Al 2p peak intensity increases relative to the metallic peak intensity, indicating the reacted layer lying below the surface and the metallic phase above it.

The evolution of interface chemical bonding with metal deposition can be seen clearly in Fig. 2. With increasing Au deposition on the cleaved Si (111) surface, the Si 2p core level changes from its characteristic spin-orbit split shape to a mixture of two peaks, characteristic of the substrate and of a strong Au-Si charge transfer, shifted to higher binding energy. The absence of significant attenuation of the latter peak with Au coverage suggests that the Au-Si phase forms near the free surface of and within the bulk of the deposited Au film.

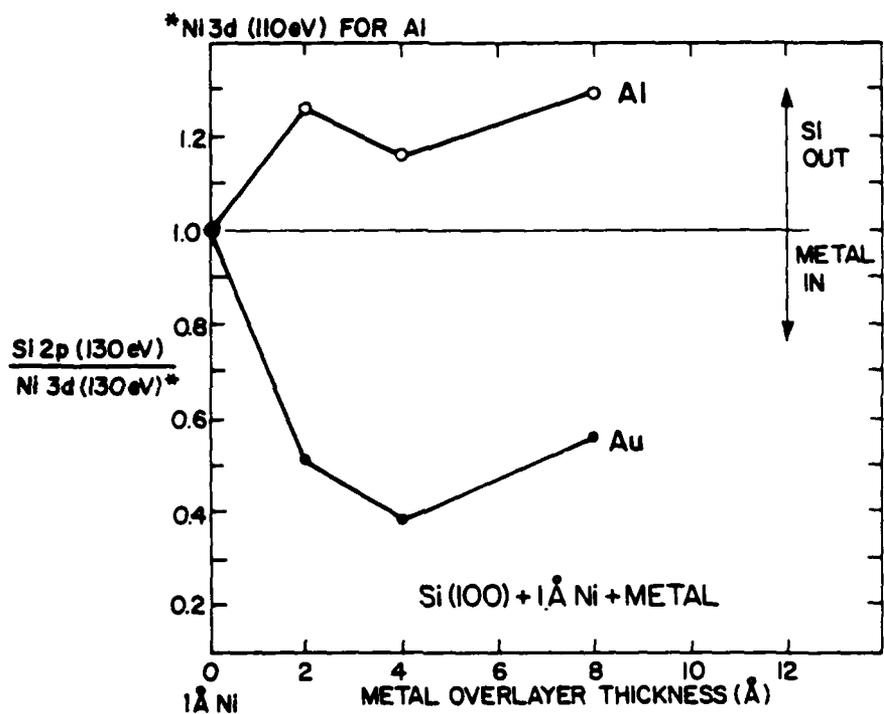3. SXPS Si 2p core level spectra at 4 Å Au on cleaved Si (111) as a function of hν.

This point is confirmed by studies of the Si 2p core level lineshape as a function of photon energy. Figure 3 shows that with the most surface-sensitive $h\nu = 130$ eV, the escape depth λ_e is 4-6 Å and the Si 2p feature is dominated by the Au-Si phase.[13] For a more bulk sensitive $h\nu = 107$ eV ($\lambda_e = 20$-50 Å), only a well-resolved Si 2p feature from the substrate is apparent. For 20 Å Au on Si (111), these different energies produce no obvious variation in lineshape from that of the Au-Si phase, indicating that the Au-Si phase extends throughout the Au overlayer thickness.

Similar experiments using Al instead of Au provide qualitatively different results. In this case, increasing Al thickness produces only small changes in Si 2p core level lineshape, in particular, the appearance of a weak contribution from dissociated Si at the Al surface at multilayer Al coverages. Depth-dependent changes with $h\nu$ confirm that dissociated Si is indeed segregated to the free Al surface.[13] These results highlight the use of four SXPS methods to characterize the interface: i) peak intensity *vs.* overlayer thickness to gauge diffusion, ii) peak intensity *vs.* $h\nu$ to measure chemical distribution at *vs.* below a surface, iii) peak energy *vs.* overlayer thickness to monitor the evolution of chemical bonding as the interface is slowly formed, and iv) peak energy *vs.* $h\nu$ to determine the spatial variation in bonding below a layer already formed.

4. Interdiffusion

Since the atomic structure at a surface or interface is known to affect the associated electronic structure (e.g., densities-of-states, Fermi level position, Schottky barrier formation),[14,15] the movement of metal and semiconductor atoms at their interface is of considerable interest. In particular, the movement of metal atoms into the semiconductor or the diffusion of semiconductor atoms out of their lattice can lead to impurity and defect states in the semiconductor band which influence the Fermi level position. In order to distinguish these processes, one requires not only fine depth resolution but also a marker at the original interface. SXPS provides orders-of-magnitude better depth resolution than conventional Rutherford backscattering[16] and is free of the roughening artifacts produced by Auger sputter depth profiling.[17] By "marking" the semiconductor surface with low (e.g., monolayer or submonolayer) coverage of a strongly chemisorbed species, one can distinguish metal and semiconductor atomic movements across the interface. The first demonstration of this technique was the SXPS-marker analysis of Au on GaAs (110).[18,19] Here Ga and As core level intensities decreased relative to an Al marker layer on the Al-GaAs surface. Thus Au diffused past the interface into the GaAs, effectively diluting or screening the GaAs subsurface. Further Au deposition caused an increase in both Ga and As intensities relative to Al, indicating an outdiffusion of GaAs into the Au overlayer. Brillson and coworkers observed analogous diffusion of Au into CdS and InP in similar fashion.[20]

Figure 4 illustrates results obtained for the Au-Si and Al-Si interfaces already mentioned above, using one monolayer of Ni as a marker layer.[13] As shown, initial Au deposition of up to 4 Å leads to a net decrease of the Si vs. Ni intensity ratio (Au indiffusion) followed by an increase at higher coverage (Si outdiffusion). By contrast, the Si vs. Ni intensity increases for Al coverages on Si, indicating Si outdiffusion. These conclusions are supported by the spectral features described in Section 3. The SXPS-marker experiments are difficult to perform because the marker layer must be kept thin enough in order to minimize effects on the diffusion process itself. This point is discussed further in Section 6. As a result, SXPS marker or interlayer intensities are weak and are attenuated even further by the metal overlayers.

*Ni 3d (110 eV) FOR Al

$$\frac{Si\ 2p\ (130\ eV)}{Ni\ 3d\ (130\ eV)^*}$$

Si (100) + 1 Å Ni + METAL

1 Å Ni   METAL OVERLAYER THICKNESS (Å)

4. SXPS intensity ratios of I_{Si}^{2p} (130 eV)/I_{Ni}^{3d} (130 eV) for Au and
I_{Si}^{2p} (130 eV)/I_{Ni}^{3d} (110 eV) for Al   overlayers on Si (100). Intensity ratios
arbitrarily normalized to unity at zero overlayer coverage.

5. Microscopic Interfacial Phases

The extreme surface sensitivity of SXPS permits interfacial phases only a few monolayers thick to be detected. Thus, for example, metals which react strongly with III-V compound semiconductors to form stable metal-V complexes are observed to produce exchange reactions near room temperature.[21-24] As a result, dissociated cation spectral features appear. No significant anion spectral changes occur, since the anions remain strongly bonded. Figure 5 illustrates this effect for Ti on UHV-cleaved InP (110).[23] With increasing Ti coverage, the In 4d core level in Fig. 5a evolves into two peaks, each with its own spin-orbit splitting (which in fact overlap). No significant energy shift appears in the P 2p spectra of Fig. 5b, as expected. Figure 5a shows that for Ti coverages below 2 Å, a hybrid peak feature appears unlike that of the dissociated or substrate peaks.

This hybrid feature appears for Au, Pd, Cu, Ni and Ag deposition on InP as well but not for Al. Significantly, Al is the only one of these metals in which In has no significant solubility.[25] This correlation suggests that bulk phase diagrams may be useful in predicting metal-cation alloying at the microscopic metal-semiconductor interface.
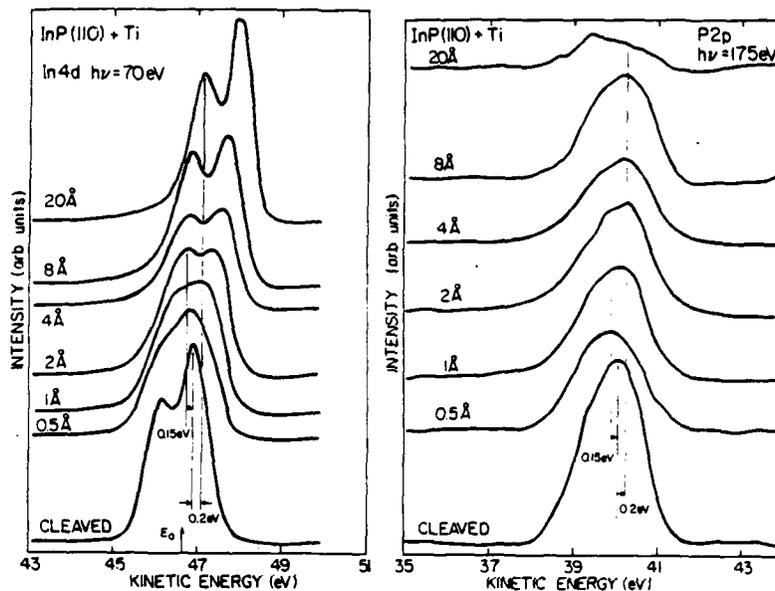

5. SXPS In 4d (a) and P 2p (b) core level spectra as a function of increasing Ti coverage on cleaved InP (110) using 70 eV and 175 eV respectively.
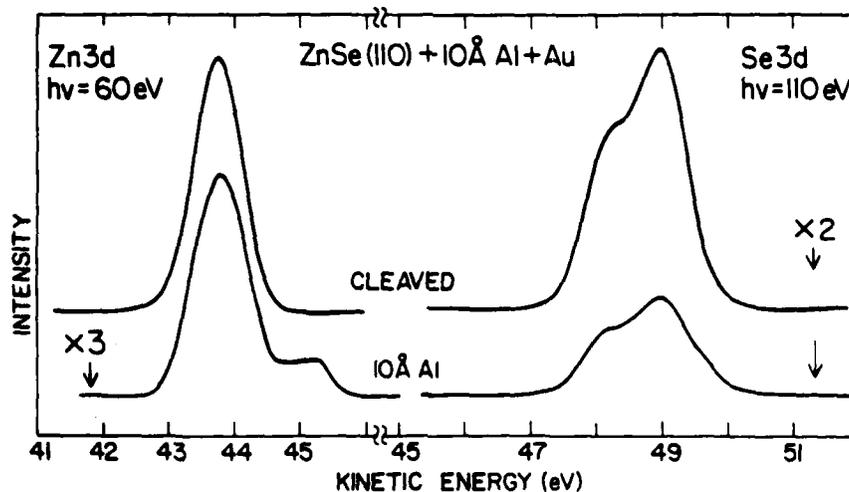
6. SXPS Zn 3d and Se 3d core level spectra for Al on cleaved Zn Se (110).

Interfacial phases for II-VI compound semiconductors appear to be qualitatively different. Figure 6 illustrates Zn 3d and Se 3d core level spectra for 10 Å Al on Zn Se. Significant outdiffusion of Zn and Se into the Al occurs since the core level intensities attenuate slowly with metal coverage, despite the 4-6 Å escape depth. With an initial 10 Å Al deposition, the Zn 3d peak in Fig. 6 develops a second smaller feature, shifted 1.1 eV to lower binding energy which corresponds to dissociated Zn. The Se 3d spectrum exhibits a somewhat slower attenuation and no additional peak features. Further Al deposition (not shown) produces more rapid attenuation of the cation vs. anion intensity,[26] suggesting that free cations are localized preferentially near the interface.[12,26-28] Such cation localization is not observed for reactive metals on III-V compounds.[29,30] It is significant that the diffusion behavior of II-VI compounds resembles that of III-V compounds with decreasing semiconductor ionicity.[20,31]
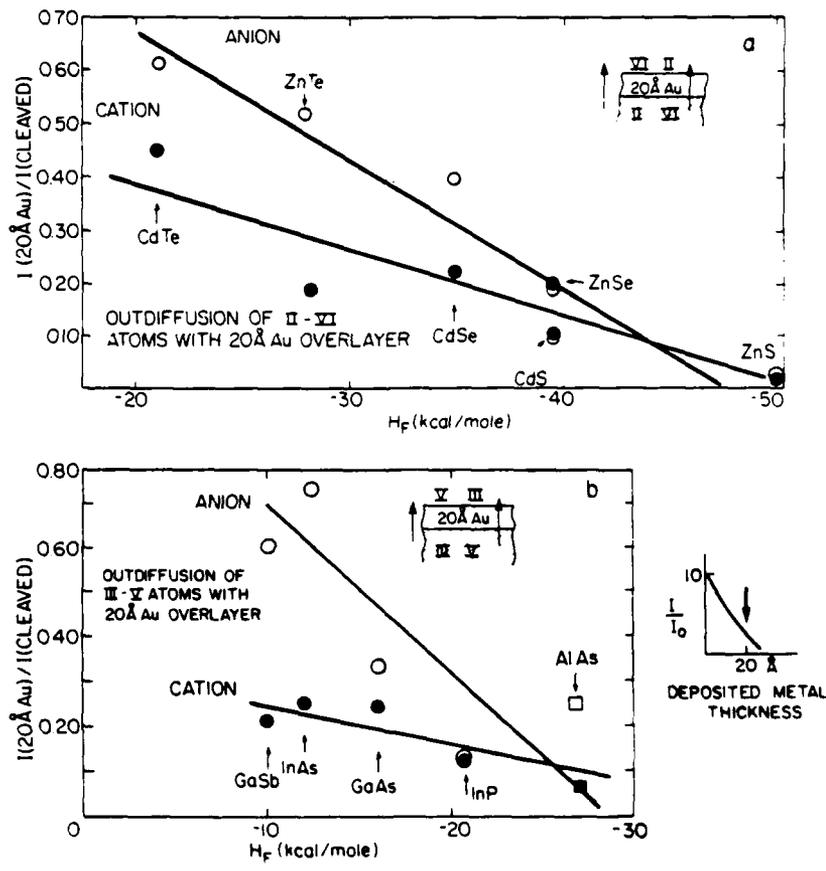
7. Outdiffusion of a) II-VI and b) III-V atoms with 20 Å Au overlayers, as indicated schematically by the insets, vs. semiconductor heat of formation.

6. Dynamics of Semiconductor Outdiffusion

The attenuation of semiconductor core level intensities as a function of metal overlayer thickness provides a measure of semiconductor diffusion into the overlayer, particularly if the overlayer is deposited uniformly rather than in island form. Au deposition on semiconductor surfaces appears to form uniform, 2-dimensional overlayer, since the valence band features of the adsorbate are characteristic of dispersed vs. metallic Au.[32,33] When measured at a Au coverage of 20 Å, the extent of outdiffusion for both II-VI (Fig. 7a) and III-V (Fig. 7b) compound atoms scales monotonically with decreasing heat of formation[34,35] (e.g., semiconductor stability). This correlation across different semiconductor systems is all the more remarkable since it includes both p- and n-type specimens as well as different crystal structures (zincblende and wurzite). Figure 7 demonstrates that a rate-limiting step to semiconductor outdiffusion is the breaking of anion-cation bonds, and that the less stable the bulk compound, the greater the outdiffusion.[20] These conclusions are not affected by the uniformity of the Au overlayer.
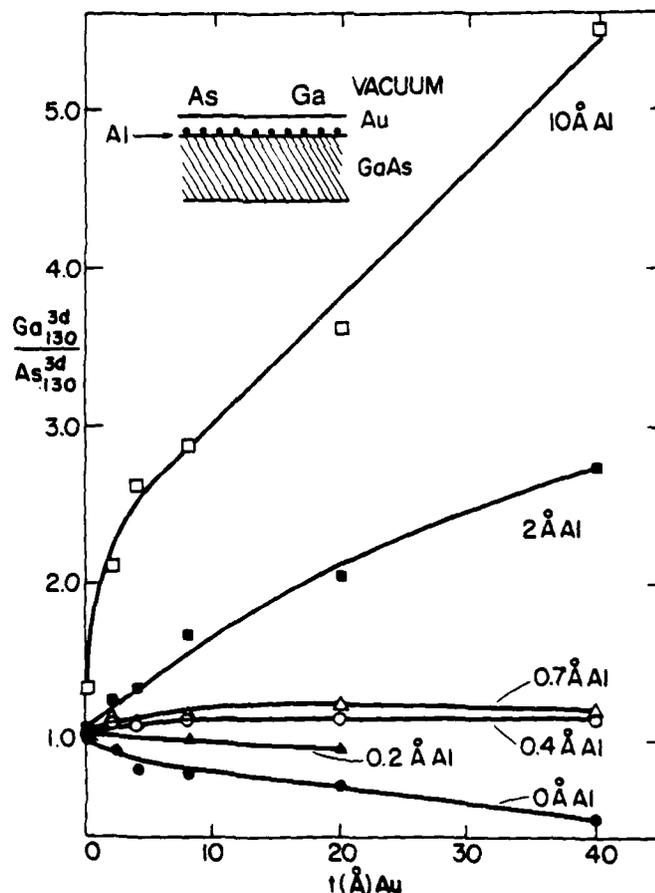
8. SXPS intensities of I_{Ga}^{3d} (130 eV)/I_{As3d} (130 eV) as a function of Au overlayer thickness T. Each curve corresponds to a different initial Au coverage.

A second rate-limiting step is the diffusion of semiconductor atoms into the metal. Brillson et al.[36] showed that "reactive" metals (i.e., metals which can form a stable metal-anion compound)[37] cause a preferential attenuation of anion atoms due to metal-anion bonding at the metal-semiconductor interface. As shown by the inset in Fig. 8, reactive Al interlayers between Au and GaAs serve to preferentially attenuate As relative to Ga outdiffusion. Indeed, Al coverages of only one monolayer or less can affect the difusion process and an interlayer of only 10 Å can cause a relative change of an order of magnitude. Similarly, by varying the reactivity of the interlayer between Au and GaAs (by varying the metal), one can obtain even larger variations with a 10 Å interlayer.[38] Such experiments can be performed successfully because of the extreme surface sensitivity of the SXPS technique.

The anion attenuation by reactive metal overlayers suggest that the metal-semiconductor interface has a "width" characterized by the extent of metal-anion bonding which decreases with metal-semiconductor reactivity.[29,37] Furthermore, the chemical trapping of the outdiffusing anions acts to reverse the stoichiometry of the normally-anion-rich outdiffusion in III-V compound semiconductors. For InP and possibly other III-V compounds this reversal of stoichiometry in fact correlates with two pinning positions of the Fermi level at the Schottky contact - depending on the reactivity of the metal-semiconductor junction. This result suggests that interfacial chemistry controls the type of defects formed near the Schottky junction and in turn the size of electronic barriers formed.[39]

## 7. Fermi Level Pinning and Semiconductor Band Bending

In addition to correlations between interface chemistry and reported barrier heights, SXPS provides a means to measure Fermi level position with respect to the semiconductor band edges. This technique has been used widely to study Schottky barrier formation[40,41] and involves energy measurement of core levels and/or the valence band edge. Thus, for example, a rigid shift of all semiconductor core levels to higher kinetic energy with the chemisorption of metal indicates an increase in n-type band bending. The flat band condition must be determined separately. Using this approach, Rowe and Margaritondo demonstrated that band bending at metal-Si interfaces evolves completely over only a few monolayers of metal.[40,42] Spicer et al.[41] showed that such Fermi level movements were even more rapid for certain metal-III-V compound semiconductor systems.

Figure 9 illustrates Fermi level movements for various metals on InP (110).[23] Solid lines signify E_F shifts extracted from rigid shifts of both In 4d and P 2p core levels. Dashed lines derive from only In 4d peak shifts and are therefore less certain. Nevertheless, one may conclude from Fig. 8 that a wide variety of E_F behavior occurs for different metals - both in terms of the energy shifts at thick coverages and their rate of change at monolayer coverages. The wide energy range (~ 0.6 eV) is in contrast to the narrow (~ 0.2 eV) range observed for selected adsorbates on GaAs (110) surfaces.[41,42]
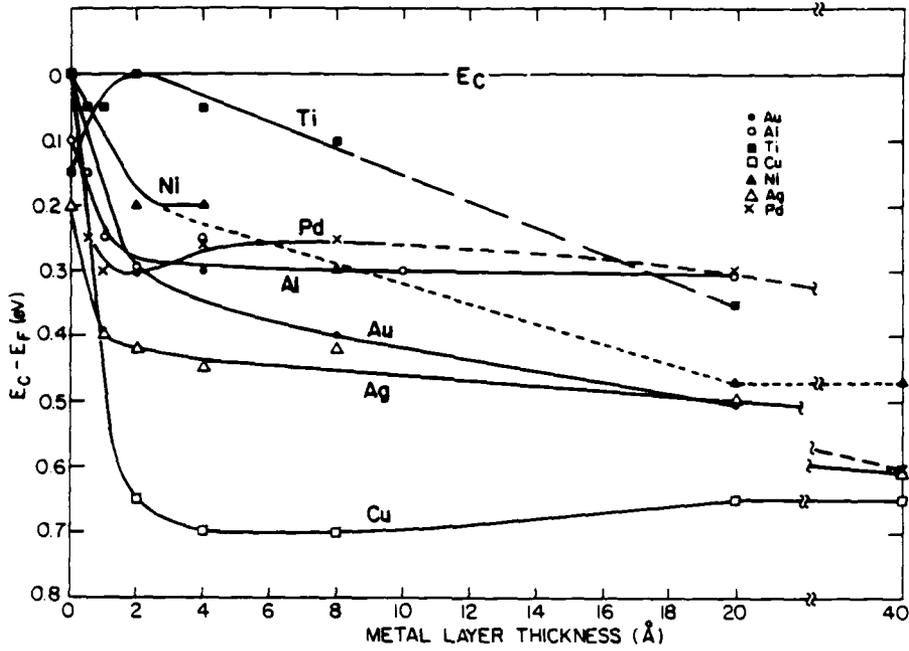
9. Position of the Fermi level E_F below the conduction band edge E_C as a function of
    metal coverage for Ti, Al, Ni, Au, Pd, Ag, and Cu. $E_C - E_F$ for the cleaved surfaces
    is derived from absolute In 4d and P 2p binding energies.

SXPS results also reveal that the band bending associated with E_F movements need not be parabolic, as
conventionally assumed. Instead, new phases near the interface may lead to rapid band bending over distances
which are narrow compared to the width of the surface space charge region of the bulk semiconductor. A case
in point is the Al-CdS junction at which, as in Fig. 6, dissociated cations accumulate at the interface. Such a
cation excess can produce degenerate n-type doping of the CdS just below its free surface and an effective
barrier height reduced by tunneling.[27,28] Indeed, whereas the Au-CdS ($10\bar{1}0$) interface exhibits $E_F - E_C =$
0.8 eV, where E_C is the condition band edge, and a C-V barrier of 0.76 eV, the Au - 2 Å Al - CdS ($10\bar{1}0$)
interface exhibits a similar $E_F - E_C$, but an "ohmic contact".[27,28] These results can be reconciled by a rapid
band bending at the latter interface. By varying the escape depth of core level photoelectrons at similar Au-Al-
CdSe ($10\bar{1}0$) interface, Brucker et al.[27,28] demonstrated an anomalous broadening of the Se 3d core level, as
shown in Fig. 10, when bulk vs. surface regions were probed. For $h\nu = 130$ eV, only the surface ($\lambda_e = 5$-10
Å) region was probed, whereas for $h\nu = 70$ eV both the surface and bulk ($\lambda_e = 50 - 100$ Å) was examined.
Surface core level shifts would be expected to broaden the surface-sensitive spectra.[43] Instead, the surface-
sensitive spectra exhibit a constant width, while the bulk-sensitive spectra broaden by ~ 30%. Al on CdSe or
CdS produces no significant band bending. The broadening in Fig. 10 becomes apparent only after the E_F
movement induced by Au deposition.
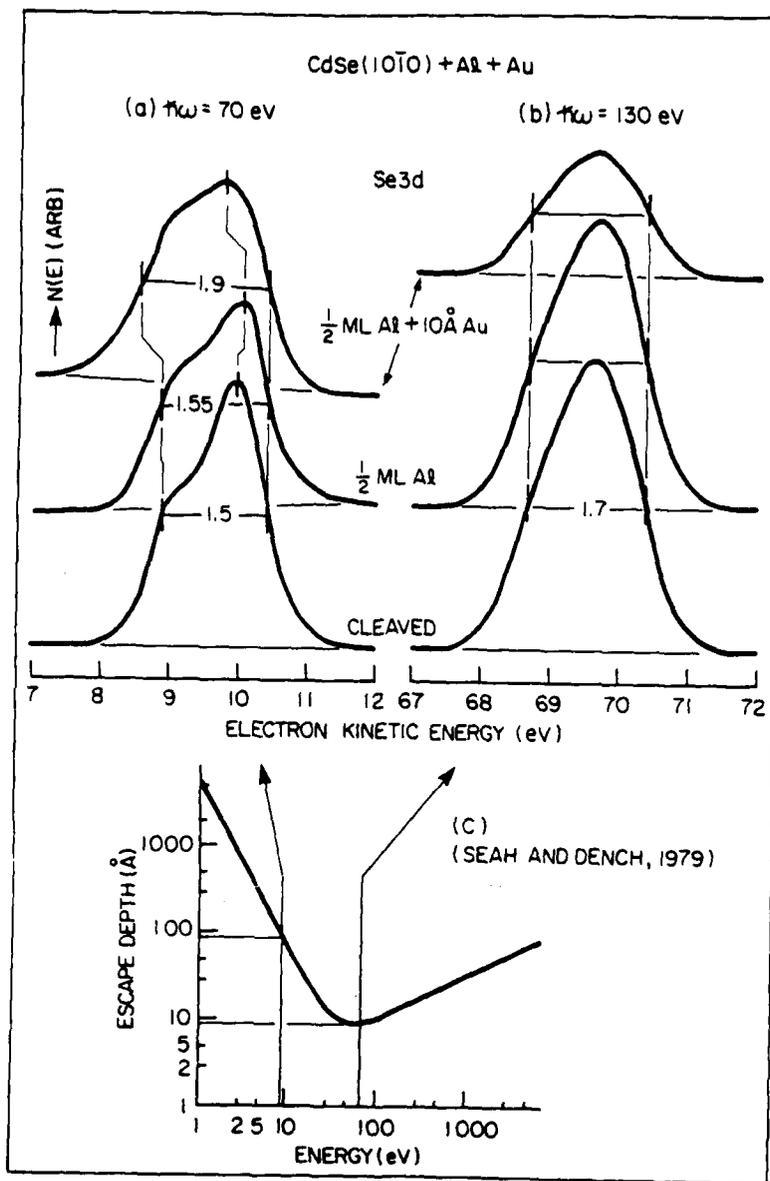
10. Surface-sensitive ($h\nu$ = 130 eV) vs. bulk-sensitive ($h\nu$ = 70 eV) Se 3d core level spectra for Au and Al on cleaved CdSe (10$\bar{1}$0) FWHM values for each peak are given in eV.

8. Conclusions

SXPS techniques provide considerable information about the metal-semiconductor interface, including chemical bonding and composition, band bending, and atomic movements near the metal-semiconductor interface. These measurements provide a characterization on an atomic scale which was hitherto unavailable. The results demonstrate that metal-semiconductor interfaces are in general not abrupt, that new interfacial

phases-reacted and/or diffused may be present, and that these detailed microscopic features can dominate the electrical properties of the macroscopic contact.

References

1. L.J. Brillson, Surf. Sci. Rep. 2, 123 (1982).
2. L.J. Brillson, J. Phys. Chem. Solids 44, 703 (1983).
3. G. Margaritondo, Solid State Electron. 26, 449 (1982).
4. R.H. Williams, Contemp. Phys. 23, 329 (1982).
5. R.Z. Bachrach, in Metal-Semiconductor Schottky Barrier Junctions, Ch. 2, edited by B.L. Sharma (Plenum Press, New York) in press.
6. See, for example, D.E. Eastman and J.L. Freeouf, Phys. Rev. Lett. 33, 1601 (1974).
7. G.W. Hansson, R.Z. Bachrach, R.S. Bauer, and P. Chiaradia, Phys. Rev. Lett. 46, 1033 (1981).
8. J. Stöhr and R. Jaeger, J. Vac. Sci. Technol. 21, 619 (1982).
9. M.P. Seah and W.A. Dench, Surface Science Interface Anal. 1, 2 (1979).
10. F.C. Brown, R.Z. Bachrach, R.B.M. Hagstrom, N. Lien, and C.H. Pruett, in Vacuum Ultraviolet Radiation Physics, edited by E. Koch, R. Haensel and C. Kurz (Pergamon, Elmsford, NY 1975) p. 785
11. J.H. Weaver and G. Margaritondo, Science 206, 151 (1979).
12. L.J. Brillson, R.S. Bauer, R.Z. Bachrach, and J.C. McMenamin, J. Vac. Sci. Technol. 17, 476 (1980).
13. L.J. Brillson, A.D. Katnani, M. Kelly and G. Margaritondo, J. Vac. Sci. Technol., in press.
14. M.L. Cohen, Advan. Electron. Electron. Phys. 51, 1 (1980).
15. C.B. Duke, J. Vac. Sci. Technol. 6, 152 (1967).
16. W.K. Chu, J.W. Mayer, and M.A. Nicolet, Backscattering Spectroscopy (Academic, New York, 1977).
17. E. Zinner, J. Electrochem. Soc., in press.
18. L.J. Brillson, R.S. Bauer, R.Z. Bachrach, and G. Hansson, Appl. Phys. Lett. 36, 326 (1980).
19. L.J. Brillson, R.S. Bauer, R.Z. Bachrach, and G. Hansson, Phys. Rev. B23, 6204 (1981).
20. L.J. Brillson, C.F. Brucker, N.G. Stoffel, A.D. Katnani, R. Daniels, and G. Margaritondo, Surf. Sci. Proc. Second IUPAP Semicond. Symposium on Surfaces and Interfaces, Surf. Sci., in press.
21. R.Z. Bachrach, J. Vac. Sci. Technol. 15, 525 (1978); R.Z. Bachrach and R.S. Bauer, J. Vac. Sci. Technol. 16, 1149 (1979).
22. L.J. Brillson, C.F. Brucker, A.D. Katnani, N.G. Stoffel, and G. Margaritondo, J. Vac. Sci. Technol. 19, 661 (1981).
23. L.J. Brillson, C.F. Brucker, A.D. Katnani, N.G. Stoffel, R. Daniels, and G. Margaritondo, J. Vac. Sci. Technol. 21, 564 (1982).
24. T. Kendelewicz, W.G. Petro, I.A. Babalola, J.A. Silberman, I. Lindau, and W.E. Spicer, J. Vac. Sci. Technol. B1, 623 (1983).
25. M. Hansen and K. Anderko, Constitution of Binary Alloys (McGraw-Hill, New York, 1958)
26. C.F. Brucker and L.J. Brillson, J. Vac. Sci. Technol. 19, 617 (1981).
27. C.F. Brucker and L.J. Brillson, Thin Solid Films 89, 67 (1982).
28. C.F. Brucker and L.J. Brillson, Appl. Phys. Lett. 39, 67 (1981).
29. L.J. Brillson, G. Margaritondo, and N.G. Stoffel, Phys. Rev. Lett. 44, 667 (1980)

30. L.J. Brillson, C.F. Brucker, A.D. Katnani, N.G. Stoffel, and G. Margaritondo, Phys. Rev. Lett. 46, 838 (1981).

31. L.J. Brillson, C.F. Brucker, N.G. Stoffel, A.D. Katnani, R. Daniels and G. Margaritondo, Physica B&C 117, 848 (1983).

32. K.S. Liang, W.R. Salaneck, and I.A. Aksay, Solid State Commun. 19, 329 (1976).

33. P.W. Chye, I. Lindau, P. Pianetta, C.M. Garner, C.Y. Su, and W.E. Spicer, Phys. Rev. B18, 5545 (1978).

34. D.D. Wagman, W.H. Evans, V.B. Parker, I. Halow, S.M. Bailey, and R.H. Schumm, Natl. Bur. Stand. Technical Notes 270-3 (1968) and 270-4(1969).

35. O. Kubachewski, E.L.L. Evans, and C.B. Alcock, Metallurgical Thermochemistry (Pergamon, New York, 1967).

36. L.J. Brillson, G. Margaritondo, N.G. Stoffel, R.S. Bauer, R.Z. Bachrach, and G. Hansson, J. Vac. Sci. Technol. 17, 880 (1980).

37. L.J. Brillson, Phys. Rev. Lett. 40, 260 (1978).

38. L.J. Brillson, C.F. Brucker, G. Margaritondo, J. Slowik, and N.G. Stoffel, J. Phys. Soc. Jpn. 49, 1089 (1980).

39. L.J. Brillson, C.F. Brucker, A.D. Katnani, N.G. Stoffel, and G. Margaritondo, Appl. Phys. Lett. 38, 784 (1981).

40. See, for example, G. Margaritondo, J.E. Rowe, and R.B. Christman, Phys. Rev. B14, 5396 (1976).

41. W.E. Spicer, I. Lindau, P. Skeath, and C.Y. Su, J. Vac. Sci. Technol. 17, 1019 (1980).

42. I. Lindau, P.W. Chye, C.M. Garner, P. Pianetta, C.Y. Su, and W.E. Spicer, J. Vac. Sci. Technol. 15, 1337 (1978).

43. For example, F.J. Himpsel, P. Heiman, T.C. Chiang, and D.E. Eastman, Phys. Rev. Lett. 45, 1112 (1980).

Contact Technology in 3-5 Device Analysis and Modification of Metal-Semiconductor Contact Interfaces in 3-5 Devices

L.J. Brillson

Xerox Webster Research Center, Webster, New York 14580

Surface science techniques reveal that microscopic chemical phenomena dominate the electronic properties at metal-semiconductor interfaces. Thus, it is now possible to modify Schottky barrier properties substantially via atomic layers at the intimate contact.

Considerable progress has been made over the past few years in the characterization and understanding of contact metallurgy and their key role in the evolution of electronic structure at compound semiconductor interfaces.[1] Ultrahigh vacuum (UHV) surface science techniques have revealed new chemical and electronic phenomena at metal-semiconductor interfaces which can account for Schottky barrier formation on an atomic scale. These techniques show that metal-semiconductor interfaces are not abrupt, as commonly portrayed, but are extended over tens or hundreds of Å. With the aid of soft x-ray photoemission spectroscopy (SXPS), one finds that an entire class of (reactive)[2] metals on 3-5 compounds exhibit metal-anion bonding over a finite width. Because of the extreme surface sensitivity (4-6 Å) of the SXPS technique,

photoelectrons excited from core levels in the substrate can be monitored to gauge the growth of the reacted layer and the attenuation of the substrate emission. Figure 1 illustrates that this characteristic width scales with chemical reactivity of the metal with the semiconductor - the stronger the metal-anion bonding, the more abrupt the interface.[3] The outdiffusing anions are
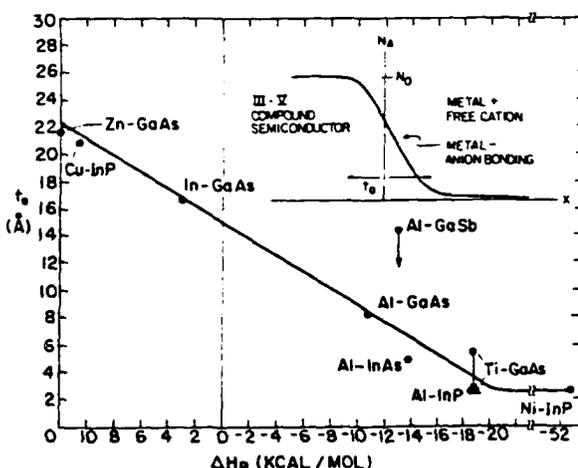
1. Characteristic interface width verses interface heat of reaction for III-V compound semiconductor junctions. Inset shows schematic anion profile.

"chemically trapped" at the interface.[4,5] With metals which form only weak bonds to 3-5 compounds (such as Au) both anion and cation

dissocaite from the semiconductor lattice and diffuse into the metal. Again using SXPS to gauge the intensity of dissociated anion and cation signals as a function of metal overlayer thickness, one finds that this contact degradation scales with the heat of formation - that is, the more stable the semiconductor, the lower the dissociation and outdiffusion to the metal.[6] Figure 2 shows that 2-6 as well as 3-5 compound semiconductor follow this trend.
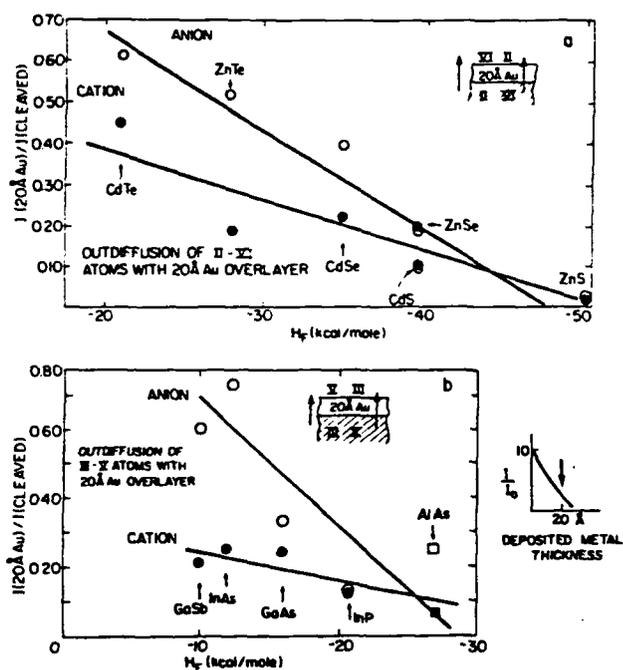

2. -Outdiffusion of a) 2-6 and b) 3-5 atoms with 20 Å Au overlayers, as indicated schematically by the insets, versus heat of semiconductor formation.

For metal such as Al which bond strongly to 3-5 compound surfaces, the chemical trapping of outdiffusing anions leads to cation-rich diffusion into the metal. Indeed, reactive metal "interlayers" only a few monolayers thick at 3-5 interfaces with unreactive metals can reverse the

stoichiometry of outdiffusion. Figure 3 illustrates the effect of atomic thicknesses of Al at Au-GaAs (110) interfaces.[4] Less than a monolayer of Al substantially affects the Ga/As stoichiometry of outdiffusion. A 10 Å Al interlayer increases the Ga/As intensity ratio by an order of magnitude.

This reversal in stoichiometry manifests itself electrically as a change in the nature of
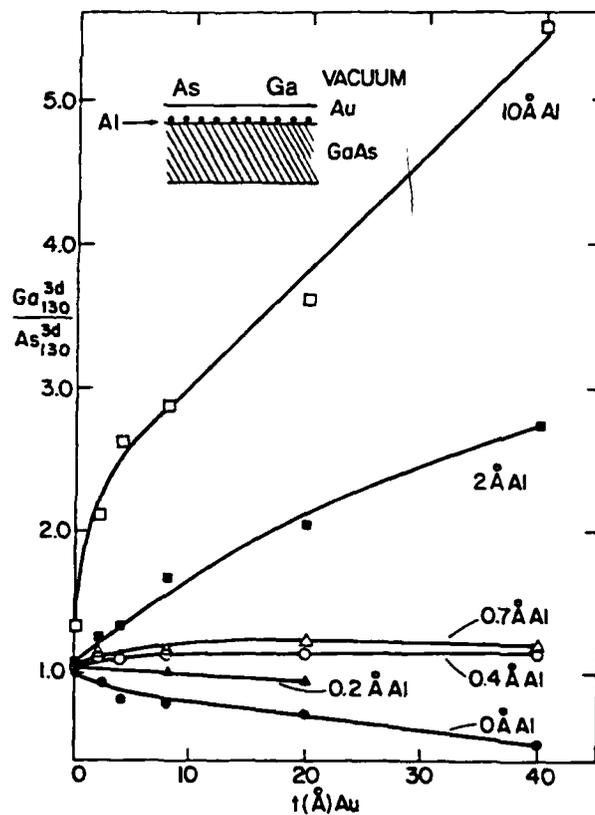
3. SXPS ratio of surface cation/anion core level intensities at hν = 130 eV, $Ga_{130}^{3d}/As_{130}^{3d}$, relative to the UHV-cleaved GaAs surface and versus Au overlayer thickness t. Each curve corresponds to a different Al coverage. Inset shows interlayer configuration schematically.

electrically-active defects.[7,8,9] and local band bending. Figure 4 illustrates the anion-rich outdifusion for unreactive metals such as Ag, Pd,

Cu, and Au on InP and the cation-rich outdiffusion for the reactive metals Al, Ti, and Ni. This figure provides a natural explanation for the well-defined transition[2] between high and low Schottky barriers for unreactive vs. reactive bonding at the metal-InP interface.[10]
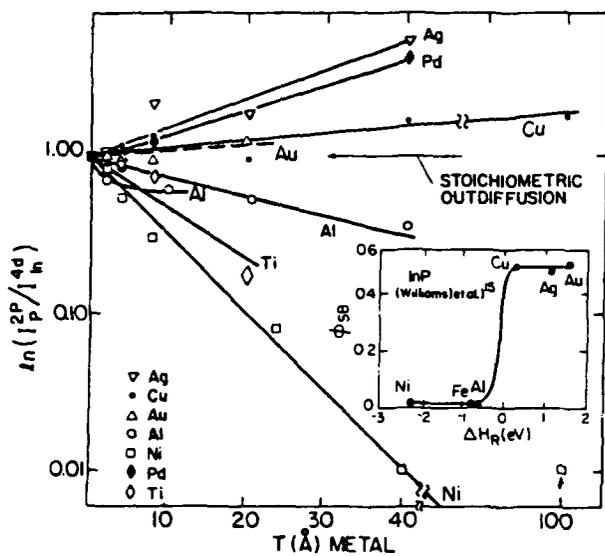
4. SXPS ratio of surface anion/cation core level intensities $I_p{}^{2p}/I_{In}{}^{4d}$ versus Cu, Au, Pd, Ag, Ni, Ti or Al coverages on InP (110) relative to the UHV-cleaved ratio. Schottky barrier height φ_{SB} vs. heat of reaction ΔH_R is plotted in the inset for metals on InP.[10]

The regular behavior illustrated for 3-5 interfaces in Figs. 1, 3 and 4 differs markedly from that of 2-6 interfaces, where reactive metals cause a cation accumulation at the Schottky contact, an increase in majority carrier concentration, and consequent ...ing of the effective barrier height due to tunneling.[11] The more ionic the 2-6 semiconductor, the more pronounced are its differences in interface chemistry with 3-5 compounds.[12] These trends provide a basis for

the well-known, qualitative differnece in 3-5 vs. 2-6 diode formation.[13]

The chemical correlations described in Fig. 4 suggest that interface the atomic structure can directly influence the electronic properties of the macroscopic contact. One method of altering the chemical structure and thereby φ_{SB} is by introducing interlayers of different reactivities and thickness at the metal-semiconductor interface. For example, introducing a 10 Å Al interlayer between Au dots on UHV-cleaved InP (110) produced a 0.1 eV φ_{SB} decrease relative to Au-InP diodes without interlayers on the same surface.[14] Montgomery et al. have described substantial decreases of InP-Au and Ag barriers with exposure of InP to H_2O or Cl,[15] and Massies et al. have reported a 0.4 eV modulation of the Al-GaAs (100) barrier by H_2O exposure.[16] Grant, Waldrop and coworkers have produced substantial Fermi level pinning behavior with different surface treatments on GaAs[17] and InP[18].

All of these results suggest that the metal-semiconductor contact in 3-5 devices is spatially extended, with regions of chemical reaction and/or diffusion, anion-rich or cation-rich outdiffusion as well as metal indiffusion - all of which contribute to the 3-5 device performance. With this understanding gained from surface science techniques, we are now provided with a number of new avenues for controlling Schottky barrier formation on an atomic scale.

1. L.J. Brillson, Surf. Sci. Repts. 2, 123 (1982).

2. L.J. Brillson, Phys. Rev. Lett. 40, 260 (1978).

3. L.J. Brillson, C.F. Brucker, A.D. Katnani, N.G. Stoffel, and G. Margaritondo, Phys. Rev. Lett. 46, 838 (1981).

4. L.J. Brillson, G. Margaritondo, and N.G. Stoffel, Phys. Rev. Lett. 44, 667 (1980).

5. Y. Shapira and L.J. Brillson, J. Vac. Sci. Technol. B1, 618 (1983).

6. L.J. Brillson, J. Vac. Sci. Technol. 20, 652 (1982).

7. H.H. Wieder, J. Vac. Sci. Technol. 15, 1498 (1978).

8. I. Lindau, P.W. Chye, C.M. Garner, P. Pianetta, and W.E. Spicer, J. Vac. Sci. Technol. 15, 1332 (1978).

9. R.H. Williams, J. Vac. Sci. Technol. 16, 1418 (1979).

10. V. Montgomery, A. McKinley, and R.H. Williams, Surf. Sci. 89, 635 (1979).

11. C.F. Brucker and L.J. Brillson, Appl. Phys. Lett. 39, 617 (1981).

12. L.J. Brillson, C.F. Brucker, N.G. Stoffel, A.D. Katnani, R. Daniels, and G. Margaritondo, Physica B&C 117, 848 (1983).

13. C.A. Mead, Solid State Electron. 9, 1023 (1966).

14. L.J. Brillson, C.F. Brucker, A.D. Katnani, N.G. Stoffel, and G. Margaritondo, Appl. Phys. Lett. 38, 784 (1981).

15. V. Montgomery, R.H. Williams, and G.P. Srivastava, J. Phys. C. (Solid State Phys) 14 L191 (1981).

16. J. Massies, J. Chaplant, M. Laviron and N.T. Linh, Appl. Phys. Lett. 38, 693 (1981).

17. R.W. Grant, J.R. Waldrop, S.P. Kowalczylk, and E.A. Kraut, J. Vac. Sci. Technol. 19, 477 (1981).

18. J.R. Waldrop, S.P. Kowalczyk, and R.W. Grant, Appl. Phys. Lett. 42, 454 (1983).

InP Surface States and Reduced Surface Recombination Velocity

L.J.Brillson and Y.Shapira[a]
Xerox Webster Research Center, Webster, NY 14580

and

A. Heller
Bell Laboratories, Murray Hill, NJ, 07974

Abstract

Surface photovoltage and Auger electron spectroscopy studies of ultrahigh -vacuum cleaved (110) and chemically-treated (100) InP reveal direct optical transitions to and from surface states in the band gap for a wide variety of surface conditions. These states correlate with reported Fermi level pinning behavior but can not account for the unique reduction in surface recombination velocity at $KAg(CN)_2^-$-treated surfaces. This reduction is identified instead with formation of a surface layer which excludes ambient-induced recombination states.

The chemical interaction between InP and metal overlayers is found to have a strong influence on the Schottky barrier formation.[1-5] Here we report on investigations of InP surfaces and interfaces carried out using surface photovoltage spectroscopy , a surface-sensitive technique particularly useful for observing surface states within the band gap[6], and Auger electron spectroscopy, aimed at understanding the relation between surface electronic and chemical states and the large increase in efficiency[7-9] of p-InP photoelectrochemical cells after semiconductor treatment with $KAg(CN)_2^-$. The surface electronic features are found to be dominated by extrinsic surface states produced by adsorbates, lattice damage, and possible nonstoichiometry. The results provide a spectroscopic basis for the Fermi level pinning and band bending associated with these surface treatments and indicate that a layer forms at p-InP surfaces treated with $KAg(CN)_2^-$ which suppresses ambient-induced recombination states.

The InP crystals studied were either polished intrinsic n- and low Zn-concentration p-InP (100) slices or 5x5x15mm bars cleaved in UHV to expose (110) faces. The bars had $p = 4.3 \times 10^{15}$ cm^{-3}(Zn) or $n = 3.2 \times 10^{15}$cm^{-3} doping and were supplied by MCP Electronic Materials Ltd. (Alperton, Middlesex, UK). The surface photovoltage apparatus has been described elsewhere.[10] The contact potential difference (cpd) between Au reference probe and semiconductor surface was monitored continuously as a function of photon energy hν with a resolution $\leq$ 75 meV. Differences in energy position could be distinguished in some cases to within 50mev. Changes in slope Δcpd/Δhν correspond to onsets of transitions which either populate or depopulate states within the band gap. For downward band bending(electron accumulation, common for p-type materials), a negative Δcpd/Δhν change at energy E_0 corresponds to an optical transition which removes

electrons from a surface level E_0 below the conduction band edge (E_c). A transition which fills a surface level E_1 above the valence band edge (E_v) produces a positive $\Delta cpd/\Delta h\nu$. For upward(hole accumulation,"n-type") band bending, the signs are reversed for band-to-band transitions but remain the same for subband transitions. For all surfaces, the sign of band bending was identified according to the characteristic band-to-band transitions at 1.34ev and 1.5ev. These bulk transitions were identified by their constant presence in spectra from different surfaces. Auger measurements involved a 2kV grazing incidence electron beam and double-pass cylindrical mirror analyzer, as well as a rastered grazing incidence ion gun operated at 0.5 keV and 10 μA Ar^+ beam current for depth profiling.

Figure 1 illustrates surface photovoltage curves obtained from p-InP (100) surfaces which reveal a wide variety of surface states dependent on surface conditions. $KAg(CN)_2^-$ treatment (etching in 0.2% Br_2-methanol followed by immersion in 0.1M $KAg(CN)_2^-$ plus KCN solution) yielded optical transitions corresponding to surface states at E_v + 0.9 eV and E_c − 1.25 eV (Fig. 1a). Br_2-methanol etching produces only states at E_v + 1.05 eV (Fig. 1b). Etching in aqua-regia (1:2:2 = $H_2O:HCl:HNO_3$) produces a similar result. Thus the 1.25 eV state can be associated with the $KAg(CN)_2^-$ treatment alone. When the $KAg(CN)_2^-$ treated surface is allowed to stand in UHV, the 1.25 eV features fades and the P content of the surface (determined by Auger) decreases. Since a) no volatile Ag compounds are known, b) P-oxides are volatile, and c) Auger electron spectroscopy confirms a loss of surface P, we conclude that silver treatment produces a volatile P compound which is responsible for the 1.25 eV state. The 0.9 eV state is due to Ag adsorption. Surface states at this energy have been inferred from electrical barrier height data[2] as well as Fermi level pinning position deduced from core level

shifts.[11] Its surface photovoltage signal does not change upon standing in vacuo. Ar$^+$ bombardment (Fig. 1c) removes the states reported in Figs. 1a and b. Therefore, these states must be surface-related. Significantly, the surface work function φ_S of the KAg(CN)$^-$ treated and Br$_2$-methanol-etched surfaces decrease by 0.6 and 0.9 eV respectively, relative to the Ar$^+$ bombardment-cleaned surface. This is consistent with the large p-type band bending expected.[6,7]

Vapor deposition of atomic Ag on aqua-regia-etched p-InP (100) (Fig. 1d) produces states at E_v + 0.9 eV, similar to aqueous KAg(CN)$_2{}^-$-treatment. However, Ag does not produce the 1.25 eV "peak" feature. Thus, KAg(CN)$_2{}^-$ treatment must involve more than Ag deposition. Vapor-deposited Au on the aqua-regia etched surface (Fig. 1e) produces states at $\sim E_v$ + 0.8 eV, which corresponds to the ultimate Fermi level (E_F) position of the Au-InP Schottky barrier contact.[2] Relative to the aqua-regia-etched surface alone, φ_S increases by 0.3 eV with Au as E_F moves lower in the gap, while φ_S decreases by 0.2 eV with Ag deposition-consistent with their different work functions. A 10^{12} Langmuir (L) 0_2 exposure of this surface (Fig. 1f) removes the Au-induced features and introduces new states at E_v + 1.15 eV. This is consistent with the E_F movement observed by Spicer et al. for oxidized p-InP.[11] For n-type InP (100) surfaces etched with aqua-regia, only states at $E_c - 0.5$ eV are apparent and Ag deposition produces only a state at $E_c - 1.25$ eV which is difficult to distinguish from the surface photovoltage response to the absorption edge. Apparently, etched n- and p-InP (100) behave differently, unless there exists a broad distribution of gap states. Nevertheless, Ag deposition again decreases φ_S by 0.2 eV for the aqua-regia-etched n-type (100)surface.

Figure 2 illustrates surface photovoltage curves obtained from ultrahigh-vacuum-cleaved InP crystals, whose surfaces are free of any ambient contamination.

Ultrahigh-vacuum-cleaved p-InP (110) exhibited different surface photovoltage features from cleave to cleave which fall into three categories. Curves for Type I cleaves (Fig. 2a) indicate states at E_v + 1.5 eV and E_c − 1.25 eV. Thus, the latter states are not unique to Ag deposition. Au deposition on this surface does not significantly alter that of Fig. 2a but increases φ_S by 0.7 eV. Ag deposition on this surface (Fig. 2b) shifts the E_v + 1.15 eV feature to 1.1 eV without affecting the 1.25 eV feature. For the ultrahigh-vacuum-cleaved (110) as well as the etched (100) p-InP surfaces, Ag deposition decreases φ_S (by < 0.2 eV) while Au increases φ_S.

Surface photovoltage curves for type II cleaves exhibits (Fig. 2c) features suggesting states at E_v + 1.25 eV and possibly E_c − 1.30 eV near the valence band edge. The latter could be masked by the absorption edge response. Ar^+ bombardment of Type II cleaves (Fig. 2d) shifts the states at E_v + 1.25 eV to E_v + 1.2 or less and decreases φ_S by 1 eV. The shift of E_v + 1.25 eV features by this surface treatment, which we observe to reduce surface P, suggests that these states may be associated with a surface excess of P.

Spectra for Type III cleaves (Fig. 2e) exhibit the most n-type band bending (based on the $E \geq E_g$ features) and only states near E_v. That Types I, II, and III are successively more n-type is supported by φ_S increases of 0.2 eV and 0.4 eV from Type I to II and Type II to III respectively. The dramatic decrease in φ_S with Ar^+ bombardment of Type II (and III) surfaces supports this interpretation. For comparison, Fig. 2f illustrates SPS features of ultrahigh-vacuum-cleaved n-InP (110), which also display a subband gap transition from states at E_c − 1.15 V. The variation of surface photovoltage features between ultrahigh-vacuum-cleaved p-InP (110) surfaces suggests cleavage-dependent surface states near the valence band edge, even though no apparent differences could be discerned between the visually

smooth, mirror-like surfaces. One can not rule out a (highly unusual) density of surface states which accounts for combinations of some of the cleaved spectral features, but these features are explained naturally in terms of a regular increase in density of states near E_v and are consistent with band bending and work function differences. Consistent with Williams et $al.$,[12] we observe no intrinsic surface states on the ultrahigh-vacuum-cleaved InP surface. An absolute correlation between the intensity of the E_c-1.25ev feature and a P excess is difficult since the surface stoichiometry of InP and other III-V compounds does fluctuate by as much as several percent, as determined by photoemission core level intensities. Monch and Gant[13] have also recently reported As excesses on cleaved GaAs(110) surfaces using Auger techniques. However, orders -of-magnitude lower densities of states are required to produced the spectral features in Fig.2. These results have serious implications for Fermi level pinning studies[3,4,11] based on cleaved compound semiconductor surfaces.

1ML Ag on Type III-cleaved p-InP (110) (Fig. 2g) reduces (increases) the effect of states at E_c − 1.15 eV (E_v + 1.2 eV) and decreases φ_S by 0.1 eV − consistent with a movement of E_F toward E_c. Oxidation (10^{12}L) of Type III-cleaved InP (110) after Ar^+ bombardment (Fig. 2h) reintroduces p-type band bending and states at E_v + 1.2, similar to those of Fig. 1f. Thus, the n-type band bending produces by UHV-cleavage can be overriden by surface treatments to reestablish p-type band bending and states identified with chemical treatments. In the process, the surface photovoltage response to states near E_v (E_c) are reduced (enhanced).

Auger spectra of ultrahigh-vacuum-cleaved and chemically-treated InP surfaces (Fig. 3) reveal a P excess on cleaved (3a) relative to chemically treated (3b-d) surfaces. Gentle (500 eV) Ar^+ sputter-profiling of UHV cleaved InP decreases the

P d^2N/dE^2 KLL signal rapidly at first and then slowly due to preferential P sputtering. In contrast, all three chemically-treated surfaces exhibit P-deficiency initially. Figures 3b-d exhibit the presence of C and O. LMM features of Ag on $KAg(CN)_2^-$ -treated InP are weak but observable in d^2N/dE_2 spectra. While all three chemically-treated surfaces are P-deficient, they each show a unique set of multiply-bonded P features. Furthermore, $KAg(CN)_2^-$ -treated InP exhibits a pronounced shift of In and O peaks to higher binding energy. This is strong evidence for oxygen functional groups associated with hydrogen bonding (e.g., $In(OH)_3$, $InO.OH$, $InPO_4$ $(xH_2O))$.[14] From the changes in Auger signals with sputtering, we estimate this surface layer to be < 10 - 20 Å thick. We believe this unique surface layer induced by $KAg(CN)_2^-$ to be responsible for the reduced surface recombination velocity.

The work of Casey and Buehler[15] and of Suzuki and Ogawa[16] shows that oxidation of the surface of n-InP drastically reduces the surface recombination velocity. We note that the formation of an oxide, upon etching in methanol -0.2% bromine or in aqua regia, involves the transformation of an initially phorphorus-rich face to an indium-rich face. This is consistent with the formation of a stable hydrated indium oxide surface layer, of 6-10 Å thickness, when p-InP is used as a photocathode in an acid electrolyte.[17] Since there are no intrinsic surface states within the band gap of InP,[12] the high surface recombination velocity prior to oxidation must be due to gap states induced by adsorbed impurities. The surface oxide layer and its variant promoted by chemisorbed silver act to prevent the adsorption of impurities on the semiconductor that introduce states causing rapid recombination.

In conclusion, we find many different types of band bending and states within the InP band gap. $KAg(CN)^{-}_{2}$ treatment produces gap states near the expected Fermi level pinning position for chemically-treated p-InP(100) and high p-type band bending, but does not reduce any density of recombination states. Instead, $KAg(CN)^{-}_{2}$ treatment produces a unique surface layer which retards *impurity* adsorption and increased surface recombination velocity. Thus formation of a chemically-modified interface dominates solar cell performance of InP in an electrochemical bath..

[a]On sabbatical leave from Tel Aviv University, Tel Aviv, Israel.

References

1. See, for example, H.H. Wieder, J. Vac. Sci. Technol. 17, 1009 (1980).

2. R.H. Williams, V. Montgomery, and R.R. Varma, J. Phys. C 11, L735 (1978); L.J. Brillson, Phys. Rev. Lett. 40, 260 (1978).

3. L.J. Brillson, C.F. Brucker, A.D. Katnani, N.G. Stoffel, and G. Margaritondo, J. Vac. Sci. Technol. 19, 661 (1981); 21, 256 (1982); Appl. Phys. Lett. 38, 784 (1981).

4. R.H. Williams, A. McKinley, G.J. Hughes, V. Montgomery, and I.T. McGovern, J. Vac. Sci. Technol. 21, 594 (1982).

5. E. Hökelek and G.Y. Robinson, Appl. Phys. Lett. 40, 426 (1982).

6. A. Heller, R.G. Vadinsky, W.D. Johnston, Jr., K.E. Strege, H.J. Leamy, and B. Miller, in Proceedings of the 15th IEEE Photovoltaic Specialists Conference (IEEE, New York, 1981), p. 1422.

7. A. Heller, B. Miller, and F.A. Thiel, Appl. Phys. Lett. 38, 282 (1981); A. Heller and R.G. Vadimsky, Phys. Rev. Lett. 46, 1153 (1981).

8. A. Heller, J. Vac. Sci. Technol. 21, 559 (1982).

9. H.C. Gatos and J. Lagowski, J. Vac. Sci. Technol. 10, 130 (1973).

10. L.J. Brillson, Surf. Sci. 51, 45 (1975).

11. W.E. Spicer, P.W. Chye, C.M. Garner, I. Lindau, and P. Pianetta, Surf. Sci. 86, 763 (1979).

12. R.H. Williams, R.R. Varma, and A. McKinley, J. Phys. C: Solid State Phys. 10, 4545 (1977).

13. W.Monch and H.Gant,Surf.Sci.,in press.

14. D.T. Clark, T. Fok, G.G. Roberts, and R.W. Sykes, Thin Solid Films 70, 261 (1980).

15. H.C. Casey, Jr., and E. Buehler, J. Electron. Mater. 3, 279 (1974).

16. T. Suzuki and M. Ogawa, Appl. Phys. Lett. 34, 447 (1979).

17. H.J. Lewerenz, D.E. Aspnes, B. Miller, D.L. Malm and A. Heller, J. Amer. Chem. Soc. 104, 3325 (1982).

Figure Captions

1. SPS features of p-InP (100) surfaces under various conditions. Monolayers(ML) of metal are vapor-deposited. E_c-$E(E_v + E)$ features correspond to transitions to the conduction band(form the valence band) which depopulate (populate) the surface state.

2. SPS features of UHV-cleaved InP(100) surfaces under various conditions.Monolayers (ML) of metal are vapor-deposited.

3. Integrated AES spectra of UHV-cleaved InP(110) and chemically-treated InP (100) surfaces. Using 2KeV electron beam energy, 2eV modulation voltage, and $< 2\mu A$ beam current over .1mm diameter spot size.
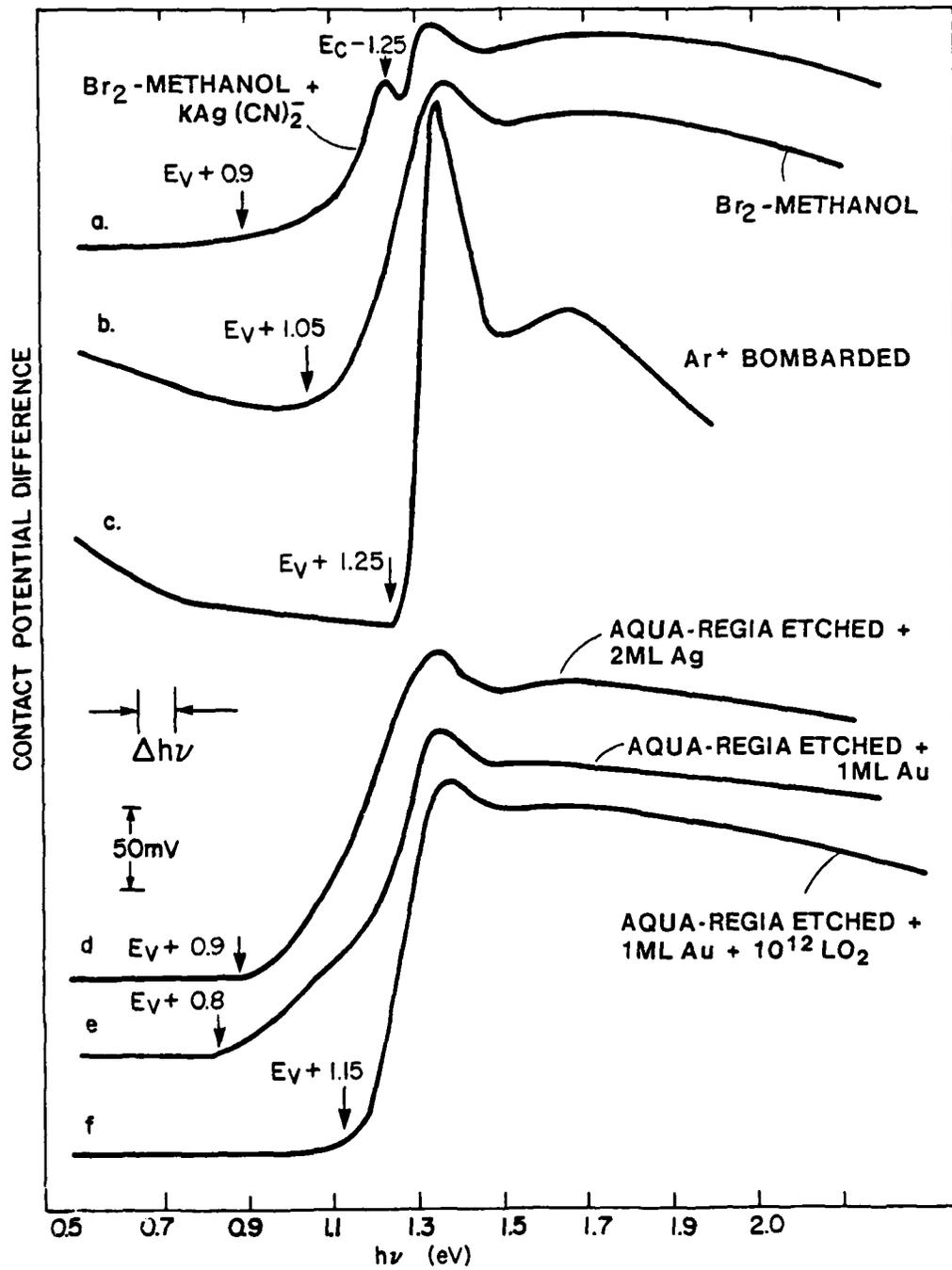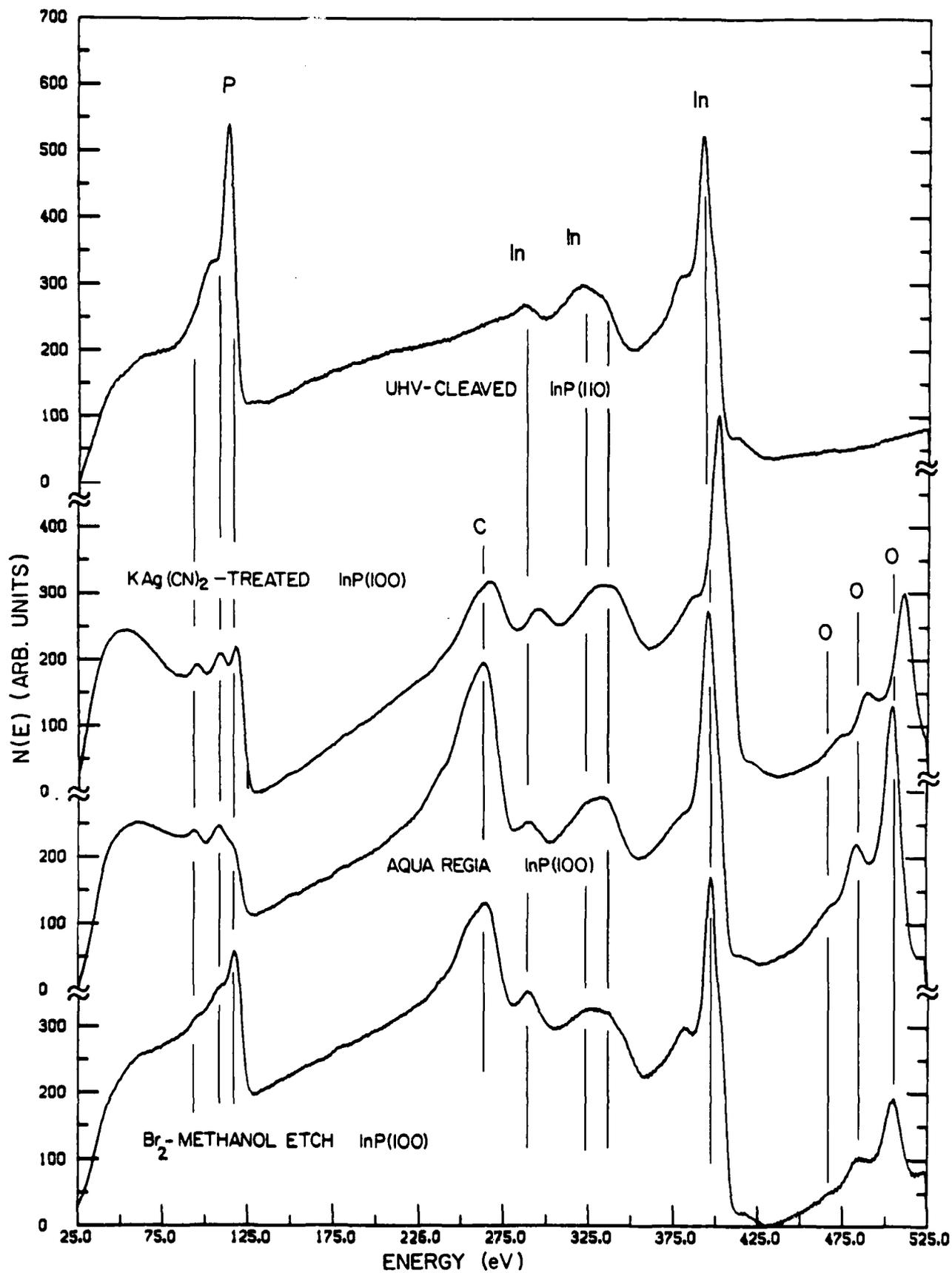
Fig. 1
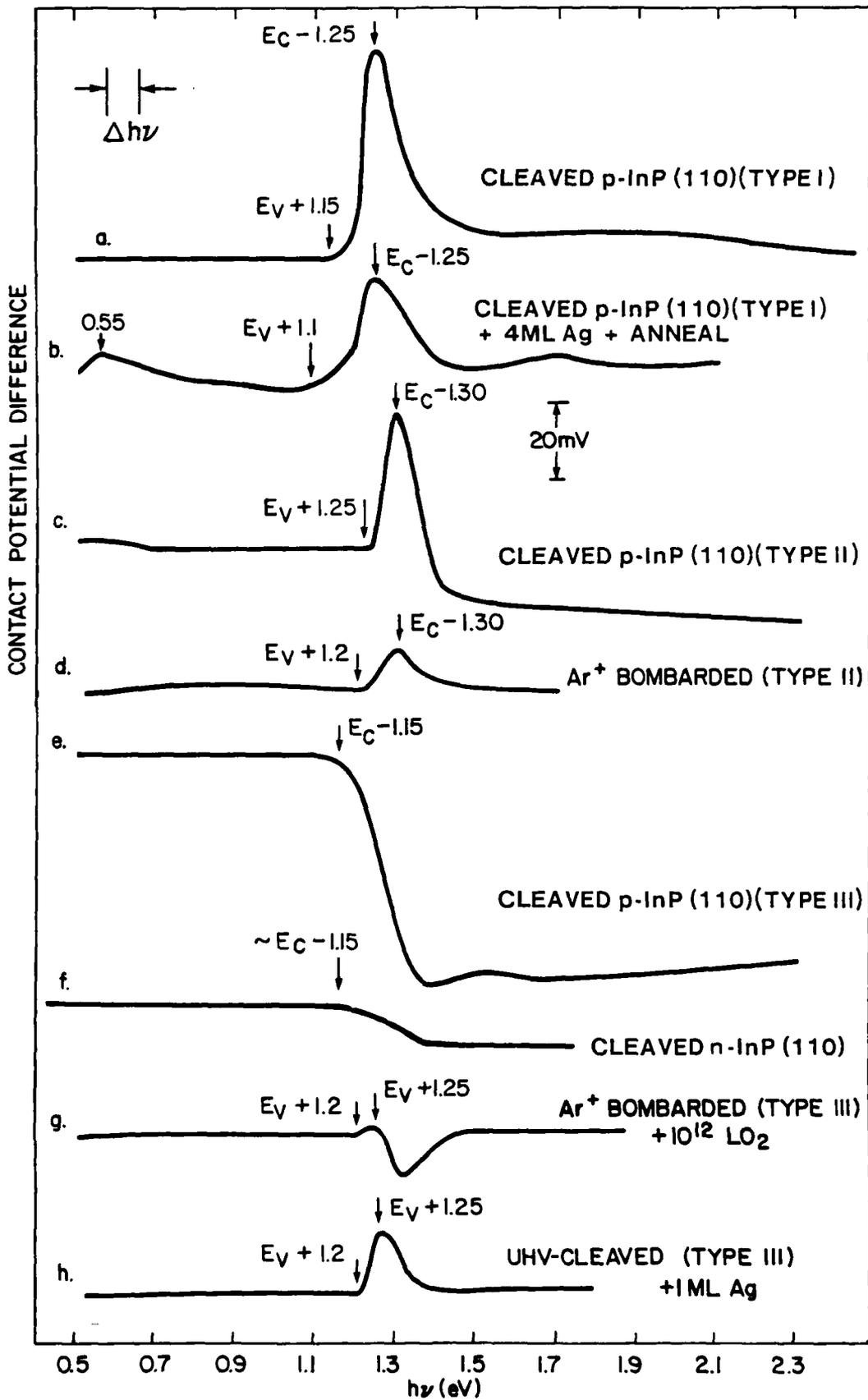
Fig. 2

Fig. 3

Investigation of InP Surfaces and Metal Interfaces by Surface Photovoltage and Auger Electron Spectroscopies

Y. Shapira* and L.J. Brillson

Xerox Webster Research Center, 800 Phillips Road, W114, Webster, NY 14580

and

A. Heller

Bell Telephone Laboratories, 600 Mountain Avenue, Murray Hill, NJ 07974

Abstract

We have used surface photovoltage spectroscopy (SPS) and Auger electron spectroscopy (AES) to investigate the extrinsic surface states produced within the InP band gap by a variety of wet chemical treatments as well as by UHV metal chemisorption, oxidation, and Ar^+ bombardment. UHV-cleaved surfaces display no intrinsic surface states, only extrinsic states associated with an excess of surface P. We have attempted to correlate the various SPS features with the chemical composition of these surfaces, particularly with $KAg(CN)_2^-$ -treated surfaces, for which the surface recombination velocity on P-InP is known to decrease significantly.

On Sabbatical leave from the School of Engineering, Tel Aviv Univ., Israel

I. Introduction

The surface properties of InP have attracted considerable attention in recent years for several reasons, chief among them their role in the formation of metal-InP Schottky barriers[1-5] and in the photoelectrochemical performance of InP solar cells.[6-9] UHV studies have employed a variety of surface spectroscopic and electrical techniques to demonstrate the dominant influence of surface and interface chemistry on the corresponding electronic properties.[10,11] Here we report an investigation of InP surfaces and interfaces using surface photovoltage spectroscopy (SPS), a surface-sensitive technique which is particularly useful for identifying surface states within the semiconductor band gap.[12] Particular attention was directed to the p-InP surface treated with $KAg(CN)_2{}^-$ in solution. Such treatment of p-InP photoelectrochemical cells yields a large increase in solar collection efficiency due to a decrease in surface recombination velocity (SRV).[9] In order to account for this SRV effect, we have investigated such surfaces by SPS and Auger electron spectroscopy (AES) and compared the results with those of various etched and cleaved surfaces of n- and p-type InP single crystals. Surface electronic features were correlated with extrinsic surface states produced by adsorbates, lattice damage and nonstoichiometry. In particular, we report SPS results for InP surfaces treated with different etchants, after Ar^+ bombardment, oxidation or Au and Ag deposition. The use of SPS yields a variety of extrinsic surface states distributed within the InP band gap. Furthermore, SPS reveals the presence of extrinsic surface states on some UHV-cleaved InP (110) surfaces, a result which can be attributed to the presence of a P excess at the cleaved surface determined by AES. Correlation of SPS and AES results suggests a basis for the effect of $KAg(CN)_2{}^-$ on the SRV of InP.

In the next section, we describe the UHV techniques employed to characterize the InP surfaces as well as the surface preparation methods. The SPS and AES results are presented in Sec. 3 for a representative variety of surfaces. In Sec. 4 we correlate the electronic and chemical results and provide a chemical basis for the special behavior of $KAg(CN)_2^-$ surfaces.

2. Experimental

The SPS experiments were performed in a UHV chamber which contained facilities for crystal cleavage, Ar^+ bombardment, metal deposition, and gas handling. Base pressure of this system was $p = 5 \times 10^{-11}$ torr. SPS measurements were carried out using monochromatic light from a wide-band Leiss double-prism monochromator (0.5eV $<$ hν $<$ 6 eV) which was directed through a sapphire viewport and focussed onto surfaces positioned near a vibrating Kelvin probe. The contact potential difference (cpd) between specimen and vibrating Kelvin tip could be monitored continuously as a function of incident photon energy hν by a detection circuit employing negative feedback from a lock-in amplifier. Experimental details of the SPS arrangement have been published previously.[13,14] Spectra were acquired with 0.5 $<$ hν $<$ 2.3 eV and with a monochromator resolution of $\triangle$hν ~ 0.075 eV. Gradual changes in cpd slope could be determined to within 0.1 eV. Changes in cpd slope with energy $\triangle$cpd/$\triangle$hν correspond to onsets of transitions which either populate or depopulate energy levels within the band gap. For a p-type semiconductor, a positive $\triangle$cpd/$\triangle$hν slope change at an energy $E_0 =$ hν corresponds to an optical transition which removes electrons from a level E_0 below the conduction band edge. Conversely, a negative $\triangle$cpd/$\triangle$hν slope change at an energy E_1 corresponds to a transition filling a level E_1 above the valence band. For n-type semiconductors, the signs are reversed.

A more complete description of the SPS technique is given elsewhere.[12]

AES measurements were performed using a double-pass cylindrical mirror analyzer (CMA) and grazing incidence electron gun. All spectra were acquired with a 2 keV electron beam energy and 2 eV CMA modulation voltage. Electron gun current was restricted to $\leq$ 2μA at a 0.1 mm diameter spot in order to minimize electron beam effects. Ar$^+$ bombardments were performed with a 500 eV beam energy and a 10μA beam current.

Several types of InP crystals were studied. Polished p- and n-InP 15x10x2 mm^3 slices oriented with (100) large faces were etched by a 0.2% Br$_2$-methanol solution and mounted on stainless steel holders by cementing their ohmic back contacts with "Ohmex". The ohmic contacts were prepared by Sn evaporation followed by annealing. Some of the p-InP samples underwent Ag treatment, which consisted of etching in a 0.2%-methanol solution followed by immersion in a 0.1M KAg(CN)$_2$$^-$ plus KCN solution. The same surfaces were also investigated after etching with dilute aqua regia (1:2:2 = H$_2$O:HCl:HNO$_3$). Other samples included n- and p-InP 5x5x15 mm^3 bars supplied by MCP Electronic Materials Ltd. (Alperton, Middlessex, UK) with p = 4.3x10^{15} cm^{-3} (Zn) or n = 3.2x10^{15} cm^{-3} (nominally undoped). Cleavage in UHV exposed clean (110) faces for the SPS and AES experiments.

3. Experiments

Figure 1 displays surface photovoltage spectra obtained from a wide variety of chemically-treated InP (100) surfaces. For a surface etched in Br-methanol and treated with KAg(CN)$_2$$^-$, Fig. 1a displays characteristic slope changes at hν = 0.9, 1.25, 1.31, 1.35, 1.5, and $\simeq$ 1.7 eV. Figure 1b was obtained from a Br$_2$-methanol-etched surface without kAg(CN)$_2$$^-$ treatment and is

distinguished by a shift of the 0.9 eV feature to 1.05 eV and the absence of the 1.25 and 1.3 eV features. Similar features are evident for surfaces etched with aqua regia, as displayed in Fig. 1d. Ar^+ bombardment of the Br_2-methanol-etched surface results in the spectral feature shown in Fig. 1c. The lowest energy change in cpd slope occurs at 1.25 eV with a very prominent feature at 1.35 eV, as well as the 1.5 and 1.7 eV features common to the other spectra. Thus, ion bombardment removes all SPS features from the band gap region. The only remaining features corresponds to the absorption edge at 1.25 eV - i.e., transitions from the valence band maximum (E_V) to the conduction band (E_C) at $Eg = 1.34$ eV and transitions from the spin-orbit-split valence band to the conduction band at $Eg + \Delta_0 = 1.5$ eV, where $\Delta_0 = 0.2$ eV is the spin-orbit splitting.[15] Both types of transitions act to reduce the band bending within the surface space charge region.

Deposition of two monolayers (ML) of Ag on the aqua-regia-etched InP (100) surface lowers the energy onset for sub-band gap transitions from 1.1 eV for the aqua-regia-etched surface to 0.9 eV, as shown in Fig. 1e. This behavior is analogous to the effect of $KAg(CN)_2^-$ in Fig. 1a. Similarly, the effect of IML Au deposition on the aqua-regia-etched surface is to shift the same energy onset to 0.8-0.85 eV. This corresponds to transitions to a state 0.5 eV below E_C. The negative $\Delta cpd/\Delta h\nu$ slope at $h\nu \sim 0.5$ eV may signal the complementary transition from this state to the conduction band. The 1.35 eV band gap feature is unchanged. Finally, the apparent effect of exposing the Au-covered surface in Fig. 1f to one atmosphere of O_2 [10^{12} Langmuir (L)] is to remove the Au-induced states in the band gap and to reintroduce the onset in surface state transitions at $h\nu = 1.15$ eV - even higher in energy than that of the original aqua-regia-etched surface.

The spectra in Fig. 1 illustrate the sensitivity of band gap features to specific chemical treatments. Furthermore, although these surfaces are not as well-defined as for instance UHV-cleaved surfaces, they display a set of pronounced SPS features in common which can be identified with bulk transitions. In turn, these can be used to identify the n- or p-type character of the surface band bending - a consideration we will come to shortly.

Figure 2 displays surface photovoltage spectra obtained for several UHV-cleaved InP (110) surfaces. The cleaved p-type InP spectrum in Fig. 2a is characterized by a $\triangle$cpd/$\triangle$hν onset at 1.15 eV and a peak at 1.25 eV. The 1.25 eV peak is similar to the 1.25 eV peak in Fig. 1a and its origin will be discussed in the next section. This peak appears to be superimposed on a relatively weak set of bulk features (similar to those of Fig. 1) for energies hν > E_g. This is a surprising result in view of the absence of intrinsic surface states reported previously for UHV-cleaved InP (110) faces.[16] Instead, Fig. 2a indicates pronounced transitions both into and out of the band gap. Deposition of Ag produces only minor changes in the surface photovoltage spectrum. As shown in Fig. 2b, the $\triangle$cpd/$\triangle$hν onset shifts only slightly to lower energies, even after mild (100-200°C) annealing. A different class of UHV-cleaved p-type InP surface can be distinguished by the SPS technique. This Type II (vs. Type I in Figs. 2a and b) cleaved surface exhibits a similar $\triangle$cpd/$\triangle$hν onset and peak feature but a decrease of the cpd for energies hν > E_g relative to sub-band gap values. A third class of p-type InP (110) cleaves (Type III) shown in Fig. 2d exhibit a large decrease in cpd at hν $\simeq$ E_g, suggestive of n-type band bending. This interpretation is supported by the shape of the E > E_g features. That Types I, II, and III are successively more n-type is supported by Kelvin measurements of surface work function φ_s, which increases by 0.2 eV and 0.4 eV from Type I to II and Type II to III respectively.

Figure 2e illustrates the features of a UHV-cleaved n-type InP (110) surface and also reveals the presence of a sub-band gap transition.

All of the p-type UHV-cleaved InP (110) surfaces we have studied exhibit features similar to or intermediate between those of Types I, II, and III shown in Fig. 2. This variability is suggestive of cleavage-dependent surface states, even though no apparent differences could be discerned between the visually-smooth, mirror-like surfaces.

In order to determine a chemical origin for these UHV-cleaved InP (110) features as well as those of the chemically-treated InP (100) surfaces, we performed AES measurements on many of these surfaces. Figure 3a displays the AES spectrum of a freshly cleaved InP (110) surface. Only In and P features are present. The UHV-cleaved surface after a 40 min. Ar^+ bombardment exhibits the spectrum shown in Fig. 3b. Note the pronounced decrease in the In/P peak ratio. Figure 3b represents a state of prolonged Ar^+ bombardment which does not change with further sputtering. From the evolution of AES spectra with time (i.e., sputter profiling) we observed that Ar^+ bombardment depleted the surface P preferentially. However, sputter-profiling measurements[17] revealed that an additional decrease in P occurred initially for the UHV-cleaved surface which was over and above the characteristic P depletion for all surfaces. Similar P excesses were found for both n- and p-type cleavages. For the chemically-treated surfaces in Figs. 3c, d, and e, the AES techniques reveals the presence of considerable C and O contamination. This is particularly evident for the aqua-regia-etched surface in Fig. 3c, which shows evidence for surface Cl as well. Only slight evidence for surface Ag can be detected in Fig. 3e. More importantly, each of these treatments results in significant differences in P Auger lineshape - indicative of

multiple bonding sites for surface P which vary in proportion from surface to surface. Furthermore, Fig. 3e displays an anomalous shift of the In and O peak features to higher energies relative to In and O peaks for other surfaces. Such shifts can be referenced to the P and C peak features, which remain unshifted.

4. Discussion

From a correlation of the SPS and AES results presented, we may draw a number of conclusions concerning the extrinsic surface states within the InP band gap. The optical transitions corresponding to SPS features in Figs. 1 and 2 are represented schematically in Fig. 4. Also shown are the bent band regions, the signs of which are extracted from the $h\nu > E_g$ band gap response and the magnitudes of which are approximated from the relative changes in surface work function.[17] For the $KAg(CN)_2^-$-treated surface, the optical transitions in Fig. 4a corresponds to states at $E_V + 0.9$ eV. In contrast, the p-InP (100) surface after a Br_2-methanol etch (Fig. 4b) exhibits only states at $E_V + 1.0$ eV. The aqua regia etch produces a similar result. Thus the 1.25 eV transition in Fig. 4a must be associated with the $KAg(CN)_2^-$ treatment. Ar^+ bombardment (Fig. 4c) removes the states in Figs. 4a and b, so that these states must be surface-related. Moreover, the Ar^+ bombardment-induced lattice damage introduces no new deep levels within the band gap, in contrast with similar experiments on CdS,[13,18] CdSe,[14] and trigonal Se.[19] Ag on aqua-regia-etched p-InP (100) produces states at $E_V + 0.9$ eV (Fig. 4d), similar to those of Fig. 4a, but does not produce the 1.25 eV transition. Thus the $KAg(CN)_2^-$ treatment must involve more than just the deposition of Ag in forming extrinsic surface states. Au on the aqua-regia-etched surface produces states at approximately $E_V + 0.8$ eV (Fig. 4e). This energy level within the InP band gap corresponds to the ultimate Fermi level position of the

Au-InP Schottky barrier contact.[2] A 10^{12}L oxygen exposure of this Au/aqua-regia-etched surface removes the Au-induced gap states and introduces a new level at E_V + 1.1 eV (Fig. 4f). This shift in surface state position is consistent with the Fermi level movement observed by Spicer et al.[20] for oxidized p-InP.

Optical transitions for several cleaved InP (110) surfaces appear in Figs. 4g-j. Surface photovoltage transitions at UHV-cleaved p-InP (110) (Type I cleave) surfaces provide evidence for states at E_V + 1.15 eV and E_c - 1.25 eV (Fig. 4g). Ag on this surface shifts the upper state (Fig. 4h). These results provide further evidence that the 1.25 eV state is not directly related to Ag chemisorption. SPS results for a Type II UHV-cleaved p-InP (110) surface suggest transitions to states at E_V + 1.25 eV and from states at E_c - 1.30 eV (Fig. 4i). Because of the anomalous cpd decrease for $h\nu > E_g$ (Fig. 2c), this surface may have upward (n-type) band bending. This reversal is almost certainly present for Type III cleave p-InP (110) surfaces, where the $h\nu > E_g$ features can be identified with bulk transitions (Fig. 2d). The extent of this reversal and the strength of the optical transition from states near E_V appear to be cleavage-dependent. Finally, the UHV-cleaved n-type InP (110) exhibits SPS transitions from a state at E_c - 1.15 eV. The states at E_c - 1.15eV and E_c - 1.25 eV on n- and p-type InP (110) surfaces respectively may have the same origin.

The AES features in Fig. 3 suggest that the cleavage-dependent effects discussed with Figs. 2 and 4 may be related to a P excess on the cleaved InP (110) surface. It is not clear whether such effects are confined to crystals from this one supplier or if they are a general phenomenon. What is more certain is that such a surface nonstoichiometry has pronounced electronic effects. The states produced near E_V by UHV-cleavage and $KAg(CN)_2^-$ treatment may not
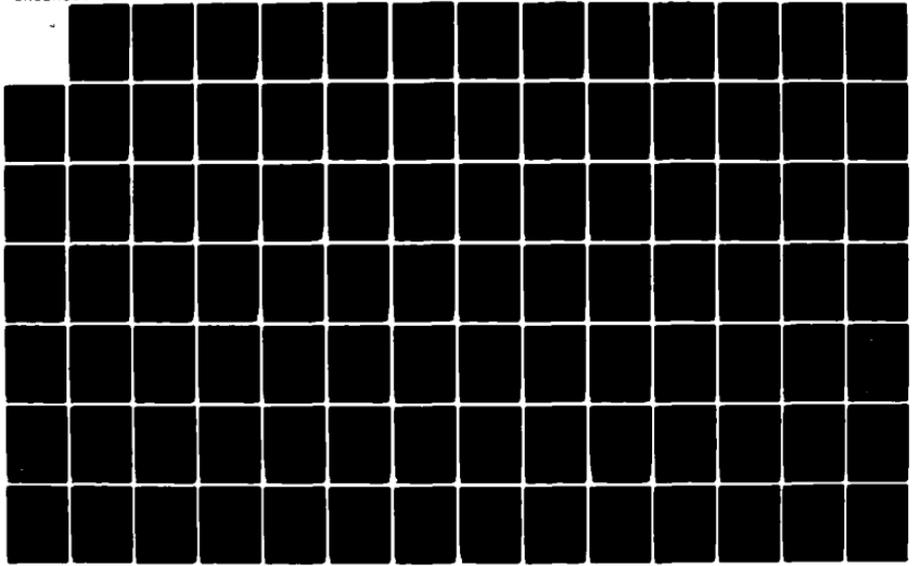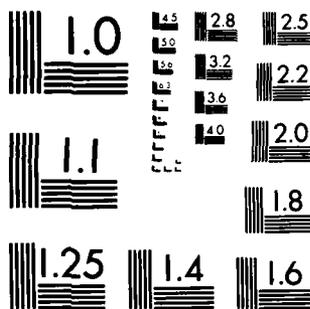
MICROCOPY RESOLUTION TEST CHART
NATIONAL BUREAU OF STANDARDS-1963-A

necessarily be the same. Whereas UHV-cleavage produces a P-rich surface, $KAg(CN)_2^-$ treatment yields a P-deficient surface. However, the $KAg(CN)_2^-$ treatment does produce a unique set of surface P species, according to the Auger lineshape in Fig. 3e, and yields In and O species which have a different chemical bonding environment from those of the other surfaces investigated. These features may indicate the presence of a particular type of In-oxide which stabilizes the surface against formation of additional extrinsic states. Such stabilization may account for the reduction in SRV observed for such treated surfaces when employed in photoelectrochemial cells.[9]

5. Conclusions

Comparison of SPS and AES results for a wide variety of InP surfaces shows that extrinsic surface states within the InP band gap are highly-sensitive to surface chemical treatment. All states observed within the band gap could be attributed to extrinsic factors, including those of UHV-cleaved surfaces, which are due to creation of P-rich faces for the particular InP material we studied. The unique surface state features of the $KAg(CN)_2^-$ -treated InP (100) surface appear to be related to formation of a particular type of In-oxide.

Acknowledgements

Figure Captions

1. Surface photovoltage spectra of (100) InP under various surface conditions: (a) Br-methanol-etched and treated with a $KAg(CN)_2^-$ solution, (b) Br-methanol-etched only, (c) Ar^+ bombarded, (d) aqua-regia-etched, (e) aqua-regia-etched plus 2ML Ag, (f) aqua-regia-etched plus 1ML Au, and (g) aqua-regia-etched plus 1ML Au plus $10^{12}L$ O_2 exposure.

2. Surface photovoltage spectra of UHV-cleaved (110) InP under various surface conditions: (a) p-type (Type I), (b) p-type (Type I) plus 4ML Ag plus mild annealing, (c) p-type (Type II), (d) p-type (Type III), and (e) n-type.

3. Auger electron spectra of various InP surfaces: (a) UHV-cleaved InP (110), (b) UHV-cleaved InP (110) plus Ar^+ bombardment, (c) aqua-regia-etched InP (100), (d) Br-methanol-etched InP (100), and (e) $KAg(CN)_2^-$-treated, Br-methanol-etched InP (100).

4. Schematic diagram of optical transitions involving states within the InP band gap and the conduction band (E_C) and valence band (E_V) edges for various conditions on etched p-InP (100) surfaces - (a) Br-methanol-etched and treated with $KAg(CN)_2^-$ solution, (b) Br-methanol-etched only, (c) Br-methanol-etched plus Ar^+ bombardment, (d) aqua-regia-etched plus 1ML Ag, (e) aqua-regia-etched plus 1ML Au, and (f) aqua-regia-etched plus 1ML Au plus $10^{12}L$ O_2 exposure - as well as for UHV-cleaved InP (110) surfaces - (g) p-type (Type I), (h) p-type (Type I) plus 4ML Ag + mild annealing, (i) p-type (Type II), and (j) n-type. Energy level positions are derived from surface photovoltage spectra in Figs. 1 and 2.

References

1. R.H. Williams, V. Montgomery, and R.R. Varma, J. Phys. C: Solid State Phys. 11, L735 (1978).

2. R.H. Williams, R.R. Varma, and V. Montgomery, J. Vac. Sci. Technol. 16, 1418 (1979).

3. P.W. Chye, I. Lindau, P. Pianetta, C.M. Garner, C.Y. Su, and W.E. Spicer, Phys. Rev. B 18, 5545 (1978).

4. L.J. Brillson, C.F. Brucker, A.D. Katnani, N.G. Stoffel, and G. Margaritondo, J. Vac. Sci. Technol. 19, 661 (1981).

5. L.J. Brillson, C.F. Brucker, A.D. Katnani, N.G. Stoffel, R. Daniels, and G. Margaritondo, J. Vac. Sci. Technol. 21, 546 (1982).

6. A. Heller, B. Miller, H.J. Lewerenz, and K.J. Bachmann, J. Am. Chem. Soc. 102, 6556 (1980).

7. A. Heller, B. Miller, and F.A. Thiel, Appl. Phys. Lett. 38, 282 (1981).

8. A. Heller and R.G. Vadimsky, Phys. Rev. Lett. 46, 1153 (1981).

9. A. Heller, R.G. Vadimsky, W.D. Johnson, Jr., K.E. Strege, H.J. Leamy, and B. Miller, Proc. 15th IEEE Photovoltaic Spec. Conf. (June 1981) p. 1422.

10. L.J. Brillson, C.F. Brucker, A.D. Katnani, N.G. Stoffel, and G. Margaritondo, Appl. Phys. Lett. 38, 784 (1981).

11. R.H. Williams, J. Vac. Sci. Technol. 18, 929 (1981).

12. H.C. Gatos and J. Lagowski, J. Vac. Sci. Technol. 10, 130 (1973).

13. L.J. Brillson, Surf. Sci. <u>51</u>, 45 (1975).

14. L.J. Brillson, Surf. Sci. <u>69</u>, 62 (1977).

15. W. Richter, in <u>Springer Tracts in Modern Physics</u> <u>78</u>, 174 (1976).

16. R.H. Williams, R.R. Varma, and A. McKinley, J. Phys. C: Solid State Phys. <u>10</u>, 4545 (1977).

17. Y. Shapira, L.J. Brillson, and A. Heller, unpublished.

18. L.J. Brillson, J. Vac. Sci. Technol. <u>12</u>, 76 (1975).

19. L.J. Brillson and C.H. Griffiths, J. Vac. Sci. Technol. <u>15</u>, 529 (1978).

20. P.W. Chye, C.Y. Su, I. Lindau, C.M. Garner, P. Pianetta, and W.E. Spicer, Surf. Sci. <u>88</u>, 439 (1979).
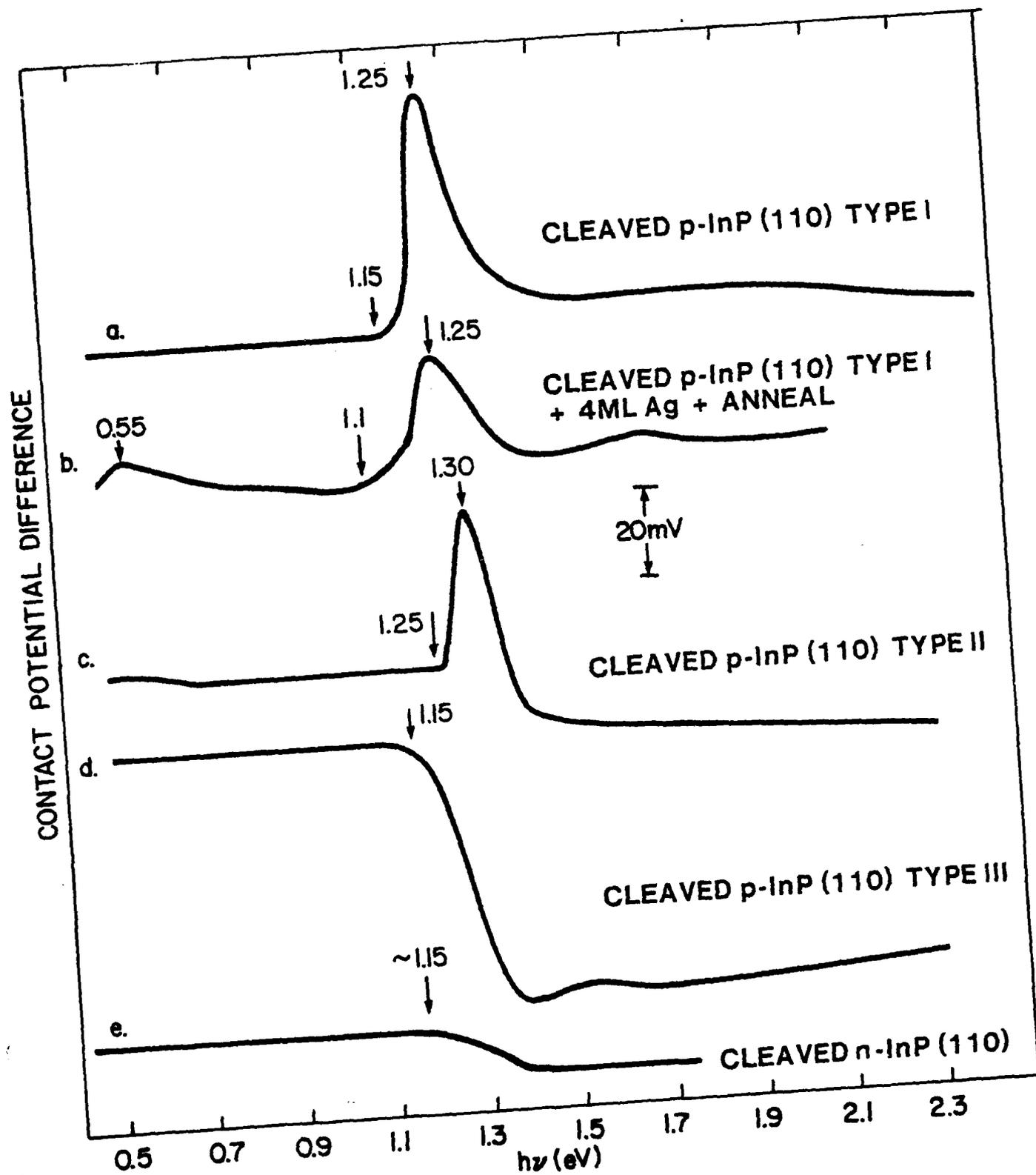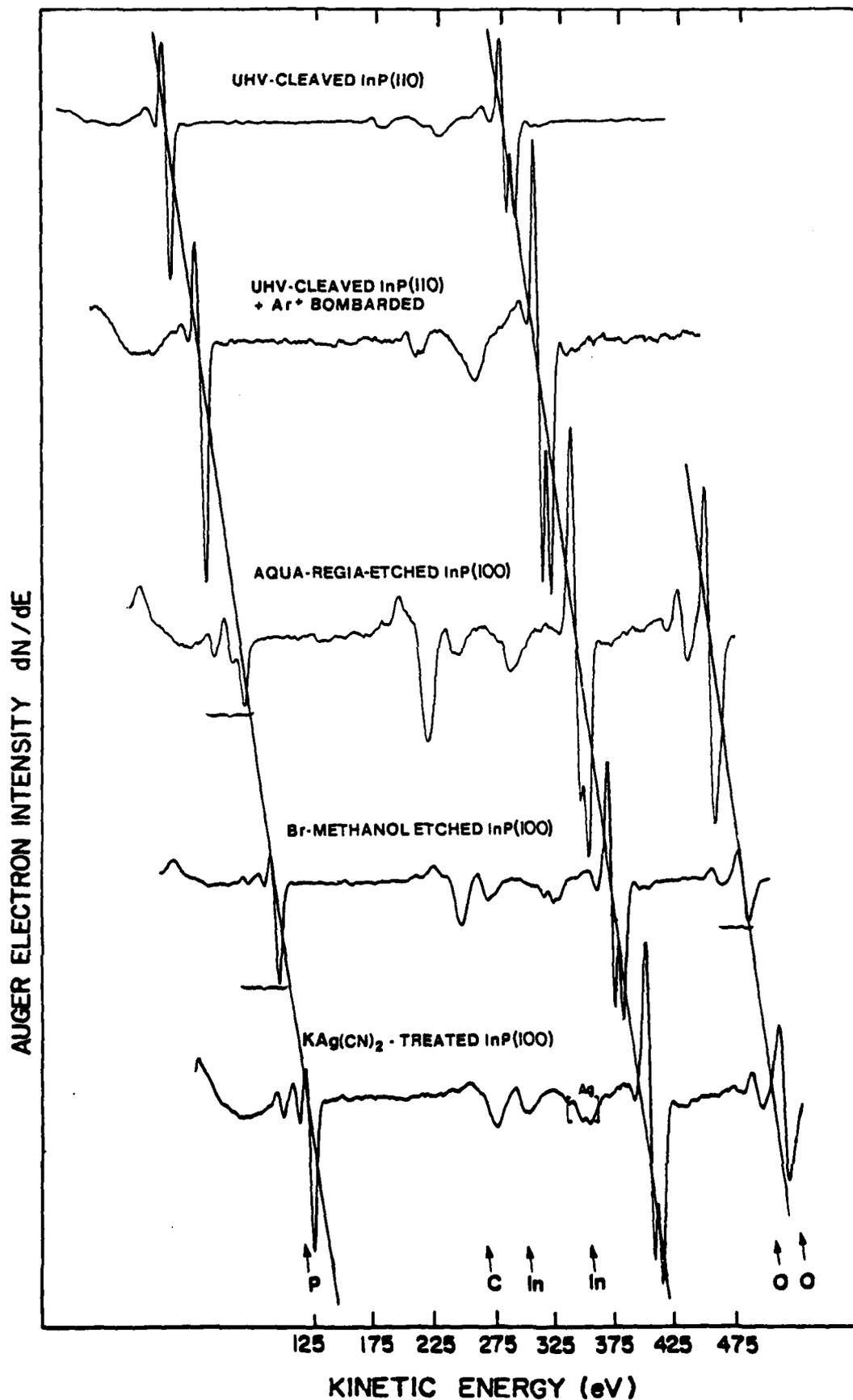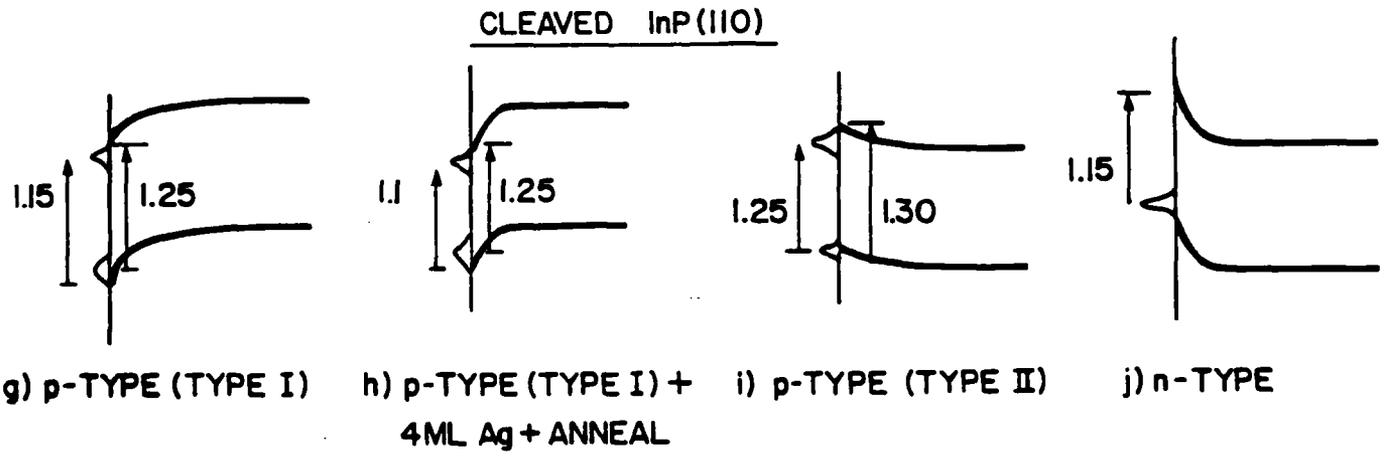
Fig. 1

CONTACT POTENTIAL DIFFERENCE

1.25 ↓

CLEAVED p-InP (110) TYPE I

1.15 ↓

a.

↓ 1.25

CLEAVED p-InP (110) TYPE I
+ 4ML Ag + ANNEAL

0.55

1.1 ↓

b.

1.30 ↓

20mV

1.25 ↓

c.

CLEAVED p-InP (110) TYPE II

↓ 1.15

d.

CLEAVED p-InP (110) TYPE III

~1.15 ↓

e.

CLEAVED n-InP (110)

0.5   0.7   0.9   1.1   1.3   1.5   1.7   1.9   2.1   2.3

hν (eV)

Fig.2

UHV-CLEAVED InP(110)

UHV-CLEAVED InP(110)
+ Ar⁺ BOMBARDED

AQUA-REGIA-ETCHED InP(100)

Br-METHANOL ETCHED InP(100)

KAg(CN)₂ - TREATED InP(100)

AUGER ELECTRON INTENSITY dN/dE

KINETIC ENERGY (eV)

P   C In   In   O O

125   175   225   275   325   375   425   475

Fig.3

Fig.4

STUDIES OF SURFACE RECOMBINATION VELOCITY REDUCTION
ON InP PHOTOELECTROCHEMICAL SOLAR CELLS

Y. Shapira

Faculty of Engineering, Tel-Aviv University, Ramat Aviv, Israel

L.J. Brillson

Xerox Research Centre, Webster NY 14580 USA

A. Heller

Bell Laboratories, Murray Hill NJ 07974 USA

Summary

We report on results of Auger electron spectroscopy and surface photo- voltage spectroscopy performed on a wide range of InP surfaces and metal- interfaces, as well as Ar^+ bombarded, oxidized and chemically-treated surfaces. The spectroscopic tools enabled us to determine the origin of the significantly reduced surface recombination velocity reported on $KAg(CN)_2^-$ - treated InP surfaces. This reduction which can increase the collection efficiency of InP-based PEC solar cells by about 500, is attributed to formation of a surface oxide layer which excludes ambient-induced recombination states.

1.INTRODUCTION

Photoelectrochemical (PEC) solar cells based on p-InP are know to convert sunlight into either electrical power or fuels such as hydrogen. While single crystalline InP-based cells with 12% efficiency have been known for some time (1), Heller et al. have recently reported on polycrystalline InP photocathode - based PEC cells with similar efficiency combined with good stability (2-4). The high current collection efficiency of these cells is a consequence of a passivating treatment by $KCN+KAg(CN)_2$ solution, which causes a thousandfold reduction in the surface recombination velocity (5). This significant reduction was attributed to strengthening of chemical bonds at InP surfaces and grain boundaries. However, the role of Ag in this passivating treatment was not sufficiently clear. Our approach was to determine the nature of the passivation layer from the viewpoint of chemical composition and electronic structure. On this basis, other methods might systemically be devised in order to improve the performance of solar cells based on InP and other semiconductors. We have conducted measurements of Auger electron spectroscopy (AES) and surface photovoltage spectroscopy (SPS) on $KAg(CN)_2^-$ - treated p-InP (100) surfaces as well as on etched, vacuum-cleaved, metal-covered and ion-bombarded p- and n-InP surfaces, the latter of which served as references. The results point to a unique oxide layer on the InP surface which prevents chemisorption of ambient impurities. These im-

purities create surface states which can act as recombination centers. The results demonstrate the capabilities of the spectroscopic techniques used and provide a methodical basis for improvements in solar cells performance.

2. EXPERIMENTAL METHODS

The InP crystals studied were either polished, intrinsic n- and low Zn concentration p-InP (100) slices, which were etched by Br_2-methanol or dilute aqua-regia followed in some cases by 0.1M KCN + 0.1M $KAg(CN)_2^-$ dip or 5x5x15 mm^3 bars cleaved in ultra high vacuum (UHV) to expose (110) surfaces. The spectroscopies used were performed in the same UHV system, where cleavage, metal deposition or Ar^+ bombardment had been carried out. AES measurements involve energy analysis of (Auger) electrons which are emitted from atoms at a surface layer (5 - 20Å thick) hit by an electron beam. Since the energetic (2keV, in our case) electron beam causes electron emission by well-defined electronic transitions, specific to each element, chemical composition of surfaces can be determined by this spectroscopy. AES can provide a depth profile of the material constituents (6) when coupled with Ar^+ bombardment, which erodes the surface layer by layer. The complementary technique used was surface photovoltage spectroscopy (SPS), a surface-sensitive method for observing energy states within the semiconductor band gap. SPS was performed by capacitively measuring the contact potential difference (CPD) between the surface and a reference Au electrode difference (CPD) between the surface and a reference Au electrode while illuminating the surface with a tunable monochromatic light of energy $h\nu$. Changes in the slope of the CPD vs. $h\nu$ curve indicate the energy and type of surface states in the band gap. Details of sample preparation and of both techniques used in this study were published elsewhere (7).

3. EXPERIMENTAL RESULTS

Fig. 1 shows AES integrated results for a UHV-cleaved InP (110) surface as well as those of some chemically-treated (100) surfaces. The peaks are marked according to the element represented. The topmost curve corresponds to a UHV-cleaved surface
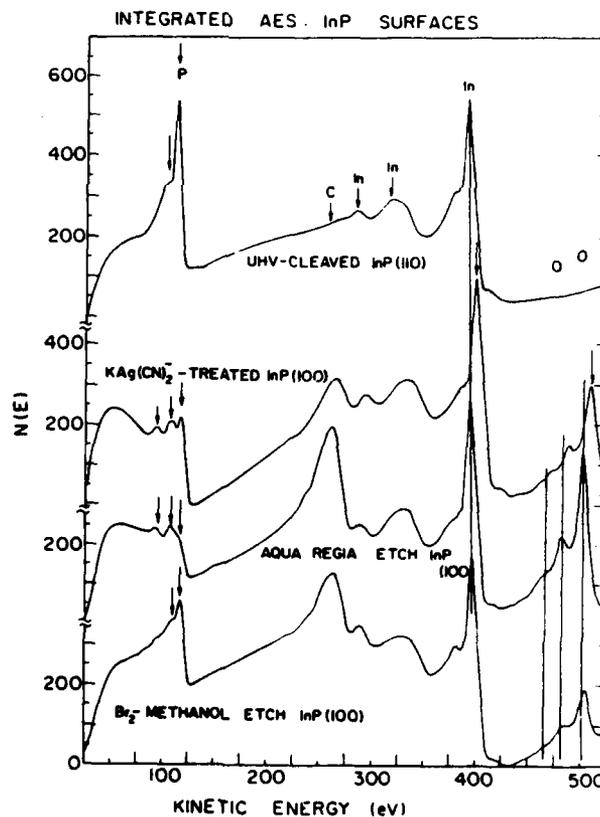

Fig. 1. Integrated Auger electron spectra of UHV-cleaved InP (110) and chemically treated InP (100) surfaces.
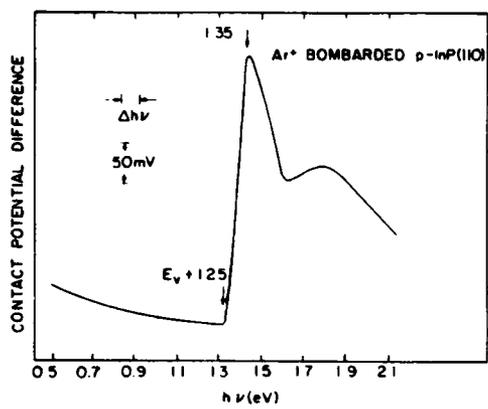
Fig. 2. SPS features of an Ar^+ bombarded p-InP (110) surface.
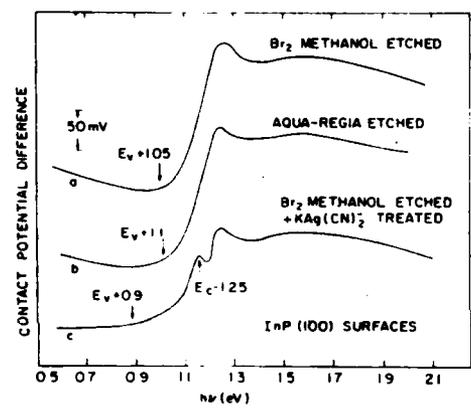

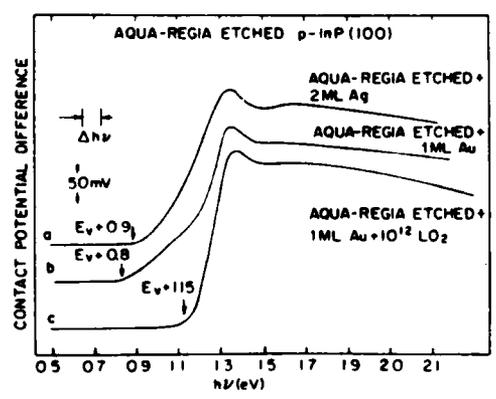Fig. 3. SPS features of InP (100) surfaces chemically treated as marked.

Fig. 4. SPS features of aqua-regia-etched p-InP (100) surfaces after (a) Ag deposition or (b) Au deposition and (c) oxygen exposure.

and displays In and P only, as expected. InP surfaces etched with dilute aqua-regia or 0.2% Br_2 —methanol solutions show signs of surface carbon and oxygen but also a significant increase of the In:P concentration ratio. Further treatment with $KAg(CN)_2$ produces an Auger spectrum which in addition to increased In concentration, reveals an anomalous shift of the In and O peaks and a significant difference in the P lineshape, the peak energy of which remains unshifted.

In order to determine the effects of the chemical treatment on the electronic structure of the InP surfaces, we performed SPS measurements, which yielded following results. Fig. 2 displays the surface photovolt spectrum obtained from an Ar^+ bombarded surface. For photon energies below 1.25 eV, the spectrum is featureless, pointing to the absence of any energy states in the gap. Only between 1.2 eV and 1.35 eV, there is a large increase in $\Delta cpd/\Delta h\nu$, which is attributed to transitions from the valence band edge, E_v to the conduction band edge, E_c ($E_c-E_v=E_g$ (InP)= 1.35 eV). This adsorption edge response is followed by other transitions from the spin-orbit split valence band to E_c. Relative to this reference spectrum, we see that chemical surface treatments produce considerable changes in the SPS features as shown by Fig.3. It shows that etching produces a positive $\Delta cpd/\Delta h\nu$ change at lower energies ($h\nu= 1.05$ or 1.1 eV) corresponding to creation of surface states at $E_v + 1.1$ eV (curves a and b). Surface treatment with $KAg(CN)_2^-$ (curve c) further shifts the surface states position to $E_v + 0.9$ eV and produces another feature corresponding to a surface state at $E_c - 1.25$ eV (negative slope!). The surface nature of these changes is obvious from the fact that they can be removed by mild Ar^+ bombardment.

The same conclusion can be reached by observing fig.4, which contains SPS features of aqua-regia etched p-InP, and noting the shift of the onset from 1.1 eV (fig. 3b) to 0.9 eV (fig. 4a) caused by vapor deposition of only 2 monolayers (ML) of silver (roughly 3A) on the etched surface. This change in slope, attributed to surface states at $E_v + 0.9$ ev, is also consistent with the reported Schottky barrier height of ~0.5 V reported for Ag-InP junctions (8). Deposition of 1 ML of gold on an aqua-regia etched InP surface (curve b) is enough to shift the slope change onset to 0.8 eV, which is also consistent with the reported Schottky barrier height of Au-InP junctions. Curve c of fig. 4 shows that exposure of the same Au-covered surface, which yielded spectrum 4b, to atmospheric pressure of oxygen, removes the Au-induced states at $E_v + 0.8$ eV and reintroduces the transition at 1.15 eV, even higher in energy than the original aqua-regia etched surface.

4.DISCUSSION

Auger electron spectra of UHV-cleaved InP surfaces reveal that they are P-rich relative to chemically-etched surfaces, which show excess of In (see fig.1). This excessive In is obviously oxidized. Results of SPS , which proves to be a very surface sensitive technique, show that the effect of oxidation is to produce surface states at $E_v + 1.1$ eV (figs. 3a, 3b, 4c). Treatment with $KAg(CN)_2^-$ removes these states and produces two different states (fig.3c). The first state at $E_v + 0.9$ eV can be reproduced by Ag deposition (fig.4a) and is therefore associated with Ag chemisorption. The other surface state at $E_c - 1.25$ eV is attributed to volatile P-oxide (see also fig.1), since it fades under vacuum conditions (9). It is not reproduced by silver deposition. Thus the $KAg(CN)_2^-$ treatment involves more than just Ag chemisorption. Indeed, observation of the AES features produced by this treatment shows a specific shift of the In and 0 peaks. This is strong evidence for oxygen functional groups associated with hydrogen bonding (10), such as $In.(OH)_3$ or $InO.OH$. Thus we conclude that the potassium silver cyanide treatment promotes a unique and stable hydrated indium oxide layer which we estimate to be about 10 Å thick, based on sputter profiling data. This oxide layer prevents chemisorption of ambient impurities which act as recombination centers, removes dangling bonds and strengthens the chemical bonding at the InP surface. Since there are no intrinsic surface states on the clean InP surface (see fig.2), the rapid surface recombination must be induced by chemical adsorption of impurities, which is avoided by the special oxidation treatment.

In conclusion we have used the power of surface analytical techniques to identify a chemically modified surface layer, which is responsible for a dramatic decrease of surface recombination velocity on InP. This opens the way to investigation of other methods of preparing interfaces with improved surface properties on InP and other semiconductors. Such improvements have significant implications on the performance of photoelectrochemical solar cells as well as on the performance of other surface-dependent electronic devices.

REFERENCES

1. B.A. Parkinson, A. Heller and B. Miller, Appl. Phys. Lett., 33,521(1978).

2. A. Heller, B. Miller, H.J. Lewerenz and K.J. Bachman, J. Amer. Chem. Soc. 102 6555 (1980).

3. A. Heller and R.G. Vadimsky, Phys. Rev. Lett. 46, 1153 (1981).

4. A. Heller, B. Miller and F.A. Thiel, Appl. Phys. Lett. 38, 282 (1981).

5. A. Heller, R.G. Vadimsky, W.D. Johnston, K.E. Strege, H.J. Leamy and B. Miller, Proc. 15th IEEE Photovoltaic Spec. Conf. June 1981, p.1422.

6. P.W. Palmberg, J. Vac. Sci. Technol. 9, 160 (1972); 10, 274 (1973).

7. Y.Shapira, L.J. Brillson and A. Heller, J. Vac. Sci. Technol.Al, 766 (1983).

8. R.H. Williams, R.R. Varma and V. Montgomery. J. Vac. Sci. Technol. 16 1418 (1979).

9. L.J. Brillson, Y. Shapira and A. Heller, Appl. Phys. Lett. 43, 174 (1983).

10. D.T. Clark, T. Fok, G.G. Roberts and P.W. Sykes, Thin Solid Films 70, 261 (1980).

Origin of Surface and Metal-Induced Interface States on InP

Y. Shapira[#] & L.J. Brillson

Xerox Research Center, Webster N.Y., 14580

and

A. Heller

Bell Laboratories, Murray Hill N.J., 07974

ABSTRACT

Surface states on p- and n-InP UHV - cleaved (110) surfaces and chemically etched (100) surfaces have been determined using surface photovoltage spectroscopy (SPS). No intrinsic surface states are found on cleaved or ion bombarded surfaces. The origin of extrinsic surface states is attributed to compositional and stoichiometric variations identified by Auger electron spectroscopy (AES). Chemical treatment, metal deposition, oxidation and Ar^{+} bombardment of these surfaces produce a host of changes in the interface states distribution within the InP band gap. Comparison of AES and SPS data from the various interfaces leads to explanation of the origin of the observed states and of their roles in determining interface electronic properties such as Fermi energy pinning positions.

[#] On Sabbatical leave from the School of Engineering, Tel-Aviv University, Ramat Aviv 69978, Israel.

1. INTRODUCTION

Surfaces and metal interfaces of InP have been in the focus of inten-
sive experimental work during the last few years[1-11]. The accumulated data
are vital for understanding the electronic properties of this prototypical
III - V compound semiconductor and such interfacial phenomena as Schottky
barrier formation[2-9], energy states[9] within the semiconductor band gap
and recombination velocity[12-14]. Experimental works on InP surfaces and
metal interfaces have concentrated on electrical measurements[2-4] (current -
voltage, capacitance - voltage) and spectroscopic techniques[5-10]
(ultra-violet or x-ray photoemission and Auger electron spectroscopies).
The data reveal the important role of surface and interface compositions in
determining their electronic behavior. However, previous works provide no
direct observation of surface states in the InP band gap which, in conjunc-
tion with data obtained by other techniques, can point to the origin of
these important features. This type of approach was shown to be successful
for other compound semiconductors such as CdS[15].

In this paper we report on energy levels within the band gap measured
by surface photovoltage spectroscopy[16] (SPS) on a wide variety of InP sur-
faces. The results are correlated with surface characterization data obta-
ined by Auger electron spectroscopy (AES) and electrical data reported by
other workers[2-4]. These correlations are an indication of our ability to
determine the nature of surface and interface states their origin and their
influence on the electronic features of the studied surfaces. These sur-
faces include UHV - cleaved (110) surfaces on n- and p-InP, Ar+ bombarded

surfaces, aqua-regia or Br_2-methanol etched surfaces, Au and Ag covered surfaces and notably InP (100) surfaces treated with $KAg(CN)_2^-$, which have been reported to have significantly reduced surface recombination velocity[13]. The combined use of SPS and AES yields a variety of surface electronic and compositional features which can be identified with corresponding extrinsic surface states originating from various adsorbates or non-stoichiometry. A description of the UHV techniques employed for surface preparation and characterization is given in Section 2. The results obtained from these surfaces and interfaces are presented in Section 3. In Section 4 we discuss the correlations between our results and electronic surface properties, and we present a physical basis for the observed phenomena on the various surfaces and interfaces.

2. EXPERIMENTAL

The InP crystals studied were of both n- and p-types, with either (110) or (100) surface orientation and with several surface chemical treatments. Single crystals of n- and p-InP yielded (110) surfaces upon cleavage in UHV. These were supplied in the form of 5x5x15 mm^3 bars with either p=4.3x10^{15} cm^{-3} (Zn) or n=3.2x10^{15} cm^{-3} (nominally undoped) by MCP Electronic Materials (Alperton, Middlesex, England). Surfaces oriented in the (100) direction with areas of 15x10 mm^2 were obtained on 2 mm thick polished slices of n- and p-InP. These surfaces were investigated after etching with a 0.2% Br_2- methanol solution or by dilute aqua regia (1:2:2 = $H_2O:HCl:HNO_3$). Some of the former surfaces were subsequently treated in a 0.1M solution of $KAg(CN)_2^-$ + KCN for investigation of the reduced

surface recombination velocity brought about by that treatment. All the samples were equipped with ohmic back contacts, prepared by Sn evaporation and subsequent $350^{\circ}C$ annealing, and cemented by "Ohmex" to a stainless steel holder. All the measurements were done under UHV conditions in a system with a base pressure of 5×10^{-11} Torr. The system was equipped with a crystal cleaver, Ar^+ gun, thickness-monitored metal evaporator and controlled Ar and O_2 introduction manifold. A vibrating Kelvin probe provided the facility to measure the contact potential difference (cpd) between a vibrating Au reference electrode (1mm wire boss) and the InP surface. The cpd is a measure of the band bending via the relationship:

$$cpd = \phi_{Au} - \psi - V_F - V_B \qquad (1)$$

where ϕ_{Au} is the gold work function, ψ is the InP electron affinity, E_F, E_C and E_V are the Fermi level, conduction band edge and valence band edge respectively, V_F is the energy difference between E_F and the bulk E_c and V_B is the surface band bending ($=E_c(surface)-E_c(bulk)$). Photovoltage measurements were carried out using monochromatic light from a wide-band Leiss double-prism monochromator (0.5 eV < hν< 6 eV) which was directed through a sapphire viewport and focused onto the InP surface, positioned to within a fraction of a mm of the vibrating Kelvin probe. The cpd between the two could be monitored continuously as a function of incident photon energy h by a detection circuit employing negative feedback from a lock-in amplifier. Experimental details of the SPS arrangement have been published previously[15,16]. Spectra were acquired with 0.5 eV < hν< 2.3 eV and with a monochromator resolution of $\Delta h\nu \approx 0.075$ eV. Gradual changes in cpd slope

could be determined to within 0.1 eV, although in some cases differences in energy positions could be determined to within 50 meV.

Energy positions of changes in cpd slope with energy (Δcpd/Δhν) correspond to onsets of transitions to and from energy levels within the band gap. The direction of the cpd slope determines whether the optical transition removes electrons from a surface state into the conduction band or fills another surface state with valence band electrons. The depopulation of a surface state situated at energy E_o below the conduction band edge E_c is distinguished by a negative Δcpd/Δhν change at photon energy hν = E_o. The population of a surface state situated at energy E_1 above E_v is distinguished by a positive Δcpd/Δhν change at photon energy hν = E_1. Photons of energy hν = E_c - E_v, sufficient for band-to-band optical transition, produces a cpd/h change which is positive if the bands are bent downwards at the surface, which is common for p-type materials (hole depletion). The slope change is negative if the bands are bent upwards at the surface, which is common for n-type semiconductors (electron depletion). Additional details of the SPS technique are given elsewhere[15-17].

AES measurements were performed using a double-pass cylindrical mirror analyzer (CMA) and a grazing incidence electron gun. All spectra were acquired with a 2 keV electron beam energy and 2μeV CMA modulation voltage. Electron gun current was restricted to $\leq$ 2 A focussed on a spot 0.1 mm in diameter in order to minimize electron beam effects. Ar$^+$ bombardment was performed with a 500 eV ion beam energy and a 10μA beam current.

3. RESULTS

The electron structure of the InP band gap and its surface chemical composition were monitored for a variety of conditions by SPS and AES respectively. They are presented according to the type of surface studied. We begin with Ar^+ ion-bombarded surface, continue with UHV - cleaved n- and p- type (110) surfaces and their treatments and finally describe etched n- and p-InP (100) surfaces and their treatments.

3a. Ar^+ ion bombarded InP surfaces.

We studied a large number of Ar^+ bombarded surfaces of InP by aES. Fig. 1 shows a typical spectrum, obtained by Ar^+ bombardment of a UHV-cleaved surface. The relative In and P peak-to-peak intensities shown are typical of a large number of InP surface studied. The In:P intensity ratio increases with sputtering time and gradually reaches a steady value. This is illustrated by the aES sputter-depth profile in Fig. 2. The relative In:P intensity ratio is arbitrarily normalized to 1:1 at extended times. However, the gradual decrease over time (as opposed to the initial In:P change at the surface) suggests a P depletion due to the sputtering process. Thus the characteristic In:P ratio obtained here can be identified with either an In-rich surface or at best a stoichiometric surface.

The surface photovoltage spectrum of a p- type InP Ar^+ ion-bombarded surface is given in Fig. 3. A marked feature appears at 1.25 eV and extends to 1.35 eV. The positive slope agrees with the type of the surface

and we attribute it to transitions from the valence band to the conduction band edge. The other features at 1.5 and 1.7 eV are attributed to transitions from the spin-orbit split valence band maximum to the conduction band at $E_g + \Delta = 1.5$ eV, where $\Delta = 0.2$ eV is the spin-orbit splitting[18]. The sharp transition at 1.3 eV and the total absence of any features at lower photon energies are strong evidence that the ion bombardment removes all gap states, leaving only the band-to-band transitions[19]. These last features correspond to bulk InP transitions and are representative of almost all of the InP spectra studied. It is important to note that the ion bombardment also causes a decrease in the band bending as evidenced by an increase of the cpd (see Eq. 1) measured in the dark.

3.b. UHV - Cleaved InP (110) Surfaces

A typical Auger electron spectrum of a UHV-cleaved InP (110) surface appears in Fig. 4. We obtained similar spectra for n- and p-InP specimens. The spectrum exhibits no evidence for chemical contamination. However, the In:P ratio is reduced by almost 50% from that of the Ar^+ bombarded surface (Fig. 1). The initially fast decay of P with sputtering (below 2 min. in Fig. 2) suggests that the UHV-cleaved surface is P-rich and that a stoichiometric surface exhibits an In:P intensity ratio intermediate between the UHV-cleaved and Ar^+ bombarded values extracted from Figs. 1 and 4 respectively. The nonstiochiometry of the UHV-cleaved surface has consequences for the corresponding SPS measurements, as described in the following subsections.

3.b.I. n-type UHV cleaved (110) surfaces

SPS measurements of n-InP are expected to produce a negative $\Delta cpd/\Delta h\nu$ change at $h\nu = E_g$. This is indeed the response shown in Fig. 5a, which is obtained from a freshly UHV-cleaved n-InP. The slope change starting at · 1.15 eV, indicates a surface state at ~ 0.2 eV above E_v. There are no gap states below $h\nu \gtrsim 1.15$ eV. The gradual slope change is due to the superposition of the surface state response and the free carriers generation at E_g, which are in the same direction. The entire response is suppressed relative to the etched surfaces' response (Sec. 3.c) due to the lower band bending at the cleaved surfaces. Coverage by 1ML (monolayer) of Ag, evaporated in-situ at $p < 5 \times 10^{-9}$ Torr, produces the spectrum shown in Fig. 5b. The light response is attenuated below the detectable level, which is consistent with further lowering of the band bending and with the lower work function observed. This is similar to observations on etched n-InP surfaces.

The curve in Fig. 5c shows the SPS data for 1ML Au covered (110) surface. The higher E_g response is consistent with the increase observed in the InP work function and the higher band bending. Also, the E_g response is sharper and its onset is shifted to $h\nu \gtrsim 1.2$ eV. This confirms the conclusion that the 1.15 eV onset of curve 5a is due to a surface state, $\simeq 0.2$ eV above E_v. The origin of this surface state may lie in the characteristic surface stoichiometry shown in Fig. 4. It is interesting to note that both ion bombardment and Au deposition eliminate this surface state. It is however possible that the latter introduces surface states closer than the

0.5 eV detectability threshold of our apparatus.

3.b.II p-type UHV-cleaved (110) surfaces

The p-InP surfaces are expected to exhibit a positive cpd/h response as discussed in Sec. 2. The p-InP cleaved surfaces studied showed several distinctly different classes of SPS data, which were, in turn, modified differently by metal deposition.

Fig. 6a shows a typical spectrum for a class of cleaved surfaces which we shall denote as type I. It is characterized by a positive slope change at h = 1.15 eV and a sharp negative change at 1.25 eV. These features seem to be superimposed on a low p-type E_g response (as indicated schematically by the dashed curve). The low E_g response is similar to that encountered at n-type surfaces (but with an opposite change in slope). The slope changes suggest surface states at E_c-1.25 eV and E_v + 1.15 eV. The former is close in position to the surface state encountered at n-type cleaved surfaces (Fig. 5).

The effect of 2ML Au deposition on type I p-InP surface is shown by curve 6b. The E_g response and the 1.15 eV feature are almost totally eliminated. The onset is shifted to 1.2 eV (see Fig. 5c) while the 1.25 eV slope change is attenuated. This is compatible with a large (0.7 eV) increase in the InP work function (lower band bending). There is also a change in the subband gap features, the most interesting being a positive change in Δcpd/Δhν around 0.8 eV. This is a significant transition in

view of the observed Schottky barrier of $\simeq$ 0.5 eV at such interfaces[2]. Similar behaviour was observed on etched surfaces.

The deposition of Ag on type I cleaved surfaces caused a decrease of 0.2 eV in the surface work function and produced the spectra shown in Fig. 7. Curves 7a, b and c are for 1/2ML, 1ML and 4ML (+ ~ 150°C anneal) of Ag, respectively. As Ag coverage increases the 1.15 eV onset shifts towards lower energies. In the same trend, the surface work function decreases. Accordingly, the structure appearing at 1.5 and 1.7 eV seems to indicate a strengthening of the p-type surface E_g response.

Fig. 8 shows a different class of p-InP cleavages, denoted as type II. Their surface work function is higher by 0.2 eV than type I. Although they are somewhat shifted in energy, the main features of the cleaved surface (curve 8a) are similar to type I cleavages (Fig. 6a). However, they seem in this case to be superimposed on an n-type-surface-like E_g response, opposite to the dashed line in curve 6a. The 1.3 eV feature may be masked by this band-to-band response. Indeed, mild Ar$^+$ bombardment causes a shift of this feature to ~ 1.2 eV as seen in curve 8b, the surface work function decreases by almost 1 eV and the surface seems to exhibit a p-type band gap response again. In fact, prolonged Ar$^+$ sputtering, shown by curve 8c, tends to eliminate all SPS features. Curve 8d shows the effect of Ag(1ML) deposition on such a bombarded surface. The silver monolayer tends to increase the band bending again (by $\simeq$ 0.4 eV), reproduce the subband gap structure and restore the p-type surface behavior.

Fig. 9 illustrates a third class of cleavages (type III) of p-InP. This type of cleaved surfaces seems to have the largest downward band bending, as seen by the large decrease of the surface photovoltage and the $h\nu \geq E_g$ features (see also Fig. 5a). This is supported by a further increase of the work function by 0.4 eV relative to type II cleavages. The behavior of this apparently inverted surface maybe due to surface states at $\sim E_c - 1.15$ eV (see onset), pinning E_F near E_v.

Curve 9b shows the dramatic effect of Ag (1ML) deposition. It causes the removal of the 1.2 eV peak, forming a slight slope at 1.25 eV. This is followed by a spectral feature typical of a p-type surface, whereas the large decrease in the photovoltage is eliminated. The surface work function is also decreased by 0.1 eV. Consequent Ar^+ bombardment causes all these features to disappear, as seen in curve 9c. The surface work function is further reduced by 0.2 eV.

The variations of SPS patterns with surface treatment point to their surface origin. Although all the cleavage types look visibly similar, they include cleavage – dependent distributions of surface states, whose source may be in different surface stoichiometries. These surface states can cause band bending of various degrees (to the point of inversion), but these features can be removed by different surface treatments. Another illuminating example of the effect of surface treatment on the band bending, as well as on the surface states distribution, is shown by curve 9d. It was produced after exposing the ion – bombarded surface (curve 9c) to 10^{12} Langmuirs of O_2. Clearly oxidation reintroduces states at $E_v + 1.25$ eV and

a p-type band bending emerges[20]. Deposition of Ag on such Ar$^+$ bombarded surface produces a similar effect. The implications of these results are discussed from a more general viewpoint in Sec. 4.

3C. Etched InP (100) Surfaces

As expected, Auger electron spectroscopy shows signs of oxidation and carbon contamination on InP (100) surfaces, polished and etched prior to their introduction into the analysis chamber. This is evident in Fig. 10, which is an AES spectrum taken from a (100) surface etched by 0.2% Br$_2$ - methanol solution. Similar results are obtained on surfaces etched by aqua regia (Fig. 11) and also on (100) surfaces, which were treated with KAg(CN)$_2^-$ - after etching (see Sec. 2), a typical spectrum of which is shown in Fig. 12. The latter spectrum shows traces of adsorbed Ag, as well as C and O.

The striking impression of these surfaces is twofold: i) They all display an In:P ratio much larger than both the ion-bombarded, and obviously the cleaved surfaces. This indicates that these surfaces are rich in indium, which is apparently oxidized. This P deficiency is typical of the etched surfaces and can be removed by sputtering.

Fig. 13 shows an AES sputter depth profile of a (100) surface. The initial P- deficiency is easily observed at the surface. Both In and P increase due to C removal. Similar time dependence of In and O signals points to the existence of indium oxide. Below the top layer (which is esti-

mated to be 10 - 20 Å thick) the P intensity becomes higher, balancing the excess In found at the surface layer. Eventually the In:P ratio increases to the constant value we have found on bombarded surfaces.

ii) Each spectrum shows a unique set of P LMM lineshapes. This may indicate combinations of metallic, In-bonded and oxidized P, which may vary in proportion according to the surface treatment[21]. More importantly, the $KAg(CN)_2^-$ treated surfaces show a significant shift of the In and O lines towards higher binding energies. These shifts are measured relative to the C and P lines which remain unchanged. These shifts are accentuated in Fig. 14, where a composite of integrated Auger electron spectra of the cleaved and etched surfaces are shown compositely. The shifted In and O lines are evidence for In - O functional groups associated with hydrogen[22], such as $In(OH)_3$, $InO \cdot OH$ or $InPO_4 \cdot (H_2O)_x$. The implications of such hydrated In-oxide layers are discussed in Sec. 4.

3C.I. Etched p-InP (100) surfaces

Surface photovoltage spectra taken from etched (100) surfaces are given in Fig. 15. Curve 15a (Br_2-methanol etched surface) shows a positive $\Delta cpd/\Delta h\nu$ slope at $h\nu$ = 1.05 eV, indicating surface states at E_v + 1.05 eV. These states are apparently induced by impurity absorption from the etchant (see Fig. 10). This feature is superimposed on a p-type E_g response, similar to the bulk optical band-to-band transitions observed in Fig. 2.

Etching by dilute aqua-regia produces similar SPS features (curve 15b), even though the surface work function is smaller by about 0.8 eV. The E_v + (1.05÷1.1) eV state may be associated with the P - deficient indium oxide surface layer (Fig. 14). Fig. 15c shows the SPS features of a surface treated with $KAg(CN)_2^-$ after Br_2-methanol etch (see Fig. 12). The treatment apparently produces new surface states at E_v + 0.9 eV and E_c - 1.25 eV. The surface work function decreases by 0.2 eV due to this treatment. The origin of these surface states is discussed later in view of the following results.

Fig. 16 shows the effect of various coverages on aqua-regia etched (100) surfaces. Deposition of 2 ML of Ag (curve a) shifts the onset to 0.9 eV (from 1.1 eV) but does not produce the 1.25 eV feature. Therefore only the former feature should be associated with silver absorption. It is interesting to note that it coincides within experimental error with E_F pinning of Ag-InP junctions[23]. The shift of the E_v + 0.9 eV feature is coverage dependent and may point to a broader distribution of surface states.

An aqua-regia etched surface covered with 1 ML Au produces the SPS features shown by curve 16b. The 1.1 eV onset shifts by 0.3 eV and indicates a surface state 0.8 eV above E_v. As in the case of Ag, this surface state coincides with the reported position of E_F at Au - InP Schottky junctions[2]. As seen by curve 16c, exposure of the latter surface to 10^{12} Langmuirs of oxygen removes this E_v + 0.8 eV Au - induced state and introduces a new surface state at E_v + 1.15 eV. This shift in surface state position is consistent with the E_F movement reported for oxidized p-InP[20].

3C. II <u>Etched</u> <u>n-InP</u> <u>(100)</u> <u>surfaces</u>

Fig. 17 is a composite graph of the SPS features taken from etched n-type (100) surfaces. Etching with Br_2 - methanol solution produces spectrum 17a, which indicates a surface state at E_c - 1.05 eV. Etching with aqua-regia produces a similar spectrum. We notice the similarity to the p-type surfaces, but the latter display surface states which are closer to the conduction band edge. These variations may be due to masking by the absorption edge response. Deposition of silver on the aqua-regia etched surface (curves c and d) produced a gradual shift of the onset until it reaches a position of E_c - 1.25 eV. This is accompanied by a lowering of the band bending, which is consistent with a lower E_g response. It is interesting to note the negative slope change (curved) at $h\nu \leq 0.55$ eV, which may be the complementary transition to the one observed on Ag-covered p-type (100) surfaces (Fig. 16a) and a similar transition to that observed on Ag-covered p-type (110) surfaces (type I), shown in Fig. 7c.

4. <u>DISCUSSION</u>

The extensive study of many different types of InP surfaces and interfaces produced a wide range of results which can be combined in order to highlight the main points.

As with most other III-V compounds, InP exhibits no intrinsic surface states. This is illustrated by the ion-bombarded surface (Fig. 2). The fact that such treatment eliminates all sub-band gap SPS features points to

their surface origin. It leaves only the bulk interband optical transition. This coincides with the observation of Williams and others[19] on InP as well as other compound semiconductors[15,17].

On UHV-cleaved InP (110) surface, the main compositional feature seems to be a P-rich surface layer (Figs. 2 and 3). This relatively thin layer may be associated with surface states at about E_c - 1.25 eV (Figs. 6, 8, 9), whose density N_{ss} is dependent on the excess P concentration. The cleaved surfaces are distinguished by a relatively low band bending Figs. 5, 6, 8 and 9), so variations in N_{ss} may easily affect it especially on p-InP surfaces. We find that different p-InP cleavages, although visibly similar, may produce band bending ranging from hole depletion to hole accumulation, depending on the cleavage surface phosphorus concentration. Such variations of several percent in surface stoichiometry by cleavage have been observed on InP[24], GaAs[25] and other compounds.

The surface P excess on UHV-cleaved surfaces and its consequences for the electronic structure have serious implications for related studies and their interpretations. The position and density of the surface states, associated with deviations from surface stoichiometry, may affect E_F pinning positions and defect structure calculations. Cleavage-dependent band bending may affect valence band spectra taken by UV- or soft x-ray-photoemission spectroscopy and consequently have implications on core level positions. Different degrees of excess P on the cleaved surfaces may affect interdiffusion and reaction with subsequently deposited metal layers and obviously any boundary or initial conditions of models and such phe-

nomena. Therefore, such initial conditions must be a priori determined for each suface studied. We find that these stoichiometry-induced surface states and others, can be drastically changed, or even entirely removed, by different surface treatments.

Etched InP (100) surfaces are distinguished by high In:P ratio (Fig. 13). Independent of the type of etchant they all seem to be covered with a thin In-rich surface layer, which appears to be mostly oxidized (Figs. 10 and 11). Generally, these surfaces show a stronger band bending relative to the cleaved (110) surfaces. This is mostly due to surface states around E_v + 1.1 eV (Fig. 15) and E_c-1.1 eV (Fig. 17). It also may depend on the crystallographic plane, as shown by the Ar^+-bombardment effects (Fig. 3 versus Figs. 8b, 9c). The stronger band bending apparently prevents any surface inversion such as found on cleaved (110) surfaces (Figs. 8a and 9a).

Treatment by $KAg(CN)_2^-$ following the etching of (100) surfaces produces a unique surface layer, apparently comprising hydrated indium oxide[26] (Fig. 14). It also shows creation of surface state (Fig. 12) at Ev + 0.9 eV (which can be reproduced by Ag deposition (as shown in Fig. 16a) and at E_c-1.25 eV (which are not related to Ag absorption but may point to a reversal of surface stoichiometry by this treatment). We believe that, as a result of these effects, and in particular the special oxide layer formation, there is a large decrease in the concentration of absorbed ambient-originating species and dangling bonds, which act as surface recombination centers.[27,28] These chemical features provide an explanation for

the reduced surface recombination velocity reported on such surfaces.[12-14]

Metal deposition on the various InP surfaces shows dramatic changes in their electronic sub-bandgap structure. Notably, we have for the first time observed direct optical transitions to and from Au-induced surface states at E_v + 0.8 eV (Figs. 5 and 16) and Ag-induced states at E_v + 0.9 eV (Figs. 15 and 16) and possibly at E_c-0.55 eV (Figs. 7 and 17). These interfacial states positions have never been directly measured before but have been deduced from indirect Schottky barrier measurements of photoemission, J-V and C-V curves. There is good agreement between our values, within experimental error, and the reported E_F positions at the corresponding interfaces. An exact correspondence between surface photovoltage thresholds and surface state positions has to be established by comparison with photoluminescence measurements.

The observation that monolayers of deposited atoms on InP produce considerable changes in SPS features and that these features are removed by ion bombardment point to the surface character of these changes. The direct observation of surface states, their type and position, as well as the type and changes in band bending determined by the $h\nu > E_g$ features and surface work function measurements, shows the unique capabilities of SPS as a tool for surface and interface studies. The technique shows that different chemical treatments have profound effects on the compositional and electronic state of the InP surface. Besides introducing new surface states, such treatments can cause changes in band bending and surface work function. A strong example can be found in the effect of oxidation on

cleaved surfaces (Fig. 9d). Different metals may also affect the degree of band bending depending on their interfacial reactivity and information on such trends may shed more light on semiconductor surface phenomena. Efforts in this direction are presently under way.

5. Conclusion

An extensive study of a number of InP surfaces and interfaces by SPS and AES produced a variety of electronic and chemical features which can be associated with surface states and their compositional origin. The results highlight the power of the spectroscopies used to determine chemical-composition-induced surface states by direct observation. Correlating the results provides a spectroscopic basis for electronic features, such as band bending, surface recombination velocity and Fermi level pinning, reported on differently treated sufaces.

Acknowledgements

References

1. See for example, H.H. Wieder, J.Vac. Sci. Technol. 17 (1980) 1009.

2. R.H. Williams, R.R. Varma and A. McKinley, J. Phys. C11 (1978) 735.

3. R.H. Williams, J. Vac. Sci. Technol. 18 (1981) 929.

4. R.H. Williams, A. McKinley, G.J. Hughes, V. Montgomery, and I.T. McGovern, J. Vac. Sci. Technol. 21 (1982) 594.

5. L.J. Brillson, C.F. Brucker, A.D. Katnani, N.G. Stoffel and G. Margaritondo, J. Vac. Sci. Technol. 19 (1981) 661.

6. L.J. Brillson, C.F. Brucker, N.G. Stoffel, A.D. Katnani and G. Margaritondo, Phys. Rev. Lett. 46 (1981) 838.

7. L.J. Brillson, C.F. Brucker, A.D. Katnani, N.G. Stoffel, R. Daniels and G. Margaritondo, J. Vac. Sci. Technol. 21 (1982) 569.

8. Y. Shapira and L.J. Brillson, J. Vac. Sci. Technol., in Press.

9. W.E. Spicer, P.W. Chye, P.R. Skeath, C.Y. Su, and I Lindau, J. Vac. Sci. Technol, 16 (1979) 1422.

10. J.A. Babalola, W.G. Petro, T. Kendelewicz, J. Lindau and W.E. Spicer, J. Vac. Sci. Technol. A1 (1983). 762; W.E. Spicer and T. Kendelewicz, J.Vac. Sci. Technol., in press.

11. E. Hokelek and G.Y. Robinson, Appl. Phys. Lett. 40 (1982) 426.

12. A. Heller, R.G. Vadimsky, W.D. Johnston, Jr., K.E. Strege, H.J. Leamy, and B. Miller, in Proceedings of the 15th IEEE Photovoltaic Specialists Conference (IEEE, New York 1981), p. 1422.

13. A. Heller, B. Miller, and F.A. Thiel, Appl. Phys. Lett. 38 (1981), 282; A. Heller and R.G. Vadimsky, Phys. Rev. Lett. 46 (1981) 1153.

14. A. Heller, J. Vac. Sci. Technol. 21 (1982) 559.

15. H.C. Gatos and J. Lagowski, J. Vac. Sci. Technol. 10 (1973) 130.

16. L.J. Brillson, Surf. Sci. 51 (1975) 45.

17. L.J. Brillson, Surf. Sci. 69 (1977) 62.

18. W. Richter, in Springer Tracts in Modern Physics 78 (1976) 174.

19. R.H. Williams, R.R. Varma, and A. McKinley, J. Phys. C: Solid State Phys. 10 (1977) 4545.

20. P.W. Chye, C.Y. Su, I. Lindau, C.M. Garner, P. Pianetta and W.E. Spicer, Surf. Sci. 88 (1979) 439.

21. Y. Shapira, L.J. Brillson, and A. Heller, J. Vac. Sci. Technol. A1 (1983) 766. L.J. Brillson, Y. Shapira and A. Heller, Appl. Phys. Lett. 43 (1983) 174.

22. D.T. Clark, T. Fok, G.G. Roberts and R.W. Sykes, Thin Solid Films. 70 (1980) 261.

23. A. McKinley, A.W. Parke and R.H. Williams, J. Phys. C13 (1980) 6723.

24. S. Singh, R.S. Williams, L.G. Van Uitert, A. Schlierr, I. Camlibel and W.A. Bonner, J.E. Electrochem. Soc. (1982) 447.

25. W. Mönch and H. Gant, Surf. Sci., in press.

26. H.J. Lewerenz, D.E. Aspnes, B. Miller, D.L.Malm and A. Heller, J. Amer. Chem. Soc. 104 (1982) 3325.

27. H.C. Casey, Jr., and E. Buehler, J. Electron, Mater. 3 (1974) 279.

28. T. Suzuki and M. Ogawa, Appl. Phys. Lett. 34 (1979) 447.

Figure Captions

Fig. 1   AES features of a UHV-cleaved p-InP (110) surface after 40 minutes of 500 eV Ar^+ ion bombardment (i.e. after a constant In:P peak-to-peak ratio was achieved).

Fig. 2 · Normalized AES intensities of P (solid curve) and In (dashed curve) as a function of sputtering time taken from an initially UHV cleaved p-InP (110) surface.

Fig. 3   SPS features of an ion bombarded p-InP surface under similar conditions as shown in Fig. 1.

Fig. 4   AES features of a UHV-cleaved p-InP (100) surface. The spectrum was taken under the same AES parameters as Fig. 1 (i.e. electron beam at 2 keV, $\leq$ 2 µA/0.1 mm diameter spot and 2 eV CMA modulation).

Fig. 5   SPS features of n-InP (110) surfaces after (a) UHV cleavage, (b) 1 ML Ag deposition on a UHV cleaved surface and (c) 1 ML Au deposition on a UHV cleaved surface.

Fig. 6   SPS features of p-InP (110) surfaces after (a) UHV cleavage (type I) and (b) 2 ML Au deposition on the cleaved surface. Dashed line schematically indicates the cpd change associated with absorption edge alone.

Fig. 7   SPS features of UHV cleaved p-InP (110) surface (Type I) after deposition of (a) 1/2 ML, (b) 1 ML and (c) 4 ML Ag + annealing at 150° C.

Fig. 8   SPS features of p-InP (110) surfaces after (a) UHV-cleavage (type II), (b) mild Ar$^+$ ion bombardment of the cleaved surface, (c) prolonged ion bombardment and (d) 1 ML Ag deposition on the ion bombarded surface.

Fig. 9   SPS features of p-InP (110) surfaces after (a) UHV cleavage (type III), (b) 1 ML Ag deposition on the cleaved surface, (c) Ar$^+$ ion bombardment of the Ag-covered surface shown by curve b and (d) after exposing the Ar$^+$ bombarded surface to 10^{12} Langmuirs O_2.

Fig. 10   AES features of a 0.2% Br_2-methanol etched p-InP (100) surface. AES parameters are the same as given in Fig. 3.

Fig. 11   AES features of an aqua-regia etched p-InP (100) surface.

Fig. 12   AES features of a p-InP (100) surface treated by $KAg(CN)_2^-$ after a Br_2-methanol etch.

Fig. 13   Normalized AES intensities of P (solid curve) and In (dashed curve) as a function of sputtering time, taken from an initially etched p-InP (100) surface.

Fig. 14   Integrated AES features of various p-InP surfaces shown composi-
           sitely for comparison of line positions end shapes.

Fig. 15   SPS features of p-InP (100) surfaces after (a) Br_2-methanol etch,
           (b) Aqua regia etch and (c) Br_2-methanol etch followed by
           $KAg(CN)_2$ treatment.

Fig. 16   SPS features of an aqua-regia etched p-InP (100) surface after
           (a) 2 ML Ag deposition (b) 1 ML Au deposition and (c) exposing
           the Au-covered surface (curve b) to 10^{12} Langmuirs O_2.

Fig. 17   SPS features of p-InP (100) surfaces after (a) 0.2% Br_2-methonal
           etch, (b) aqua regia etch followed by (c) 1 ML Ag and (d) 2 ML Ag
           deposition.

UHV - CLEAVED InP(110)
After 40 min. Ar⁺ Bombardment

FIG. 1

UHV-CLEAVED p-type InP (110)

P ——
In ----

FIG.2

FIG. 3

CLEAVED InP(110)

FIG. 4

FIG. 5

TYPE I $E_C - 1.25\,eV$ CLEAVED p-type InP(110)

SPV

a. $E_V + 1.1\,eV$ CLEAVED

20mV

b. $E_V + 0.8\,eV$

CLEAVED + 2 ML Au

0.5 0.7 0.9 1.1 1.3 0.5 1.7 1.9 2.1 2.3 2.5

$h\nu\,(eV)$

FIG. 6

TYPE I   20mV   CLEAVED p-type InP(110)

a. E_V+1.15 eV ↓   CLEAVED + ½ ML Ag

SPV

b.   +1ML Ag

↑E_C- 0.55 eV   + 4 ML Ag$^+$
c. E_V+1.1 eV↓   ANNEALING

0.5   0.7   0.9   1.1   1.3   1.5   1.7   1.9   2.1
hν (eV)

FIG. 7

FIG. 8

CLEAVED p-type InP

TYPE III

20mV

CLEAVED   a.

CLEAVED + IML Ag   b.

Ar⁺ BOMBARDED   c.

Ar⁺ BOMBARDED + 10¹² LO₂   d.

SPV

hν (eV)

FIG. 9

FIG. 10

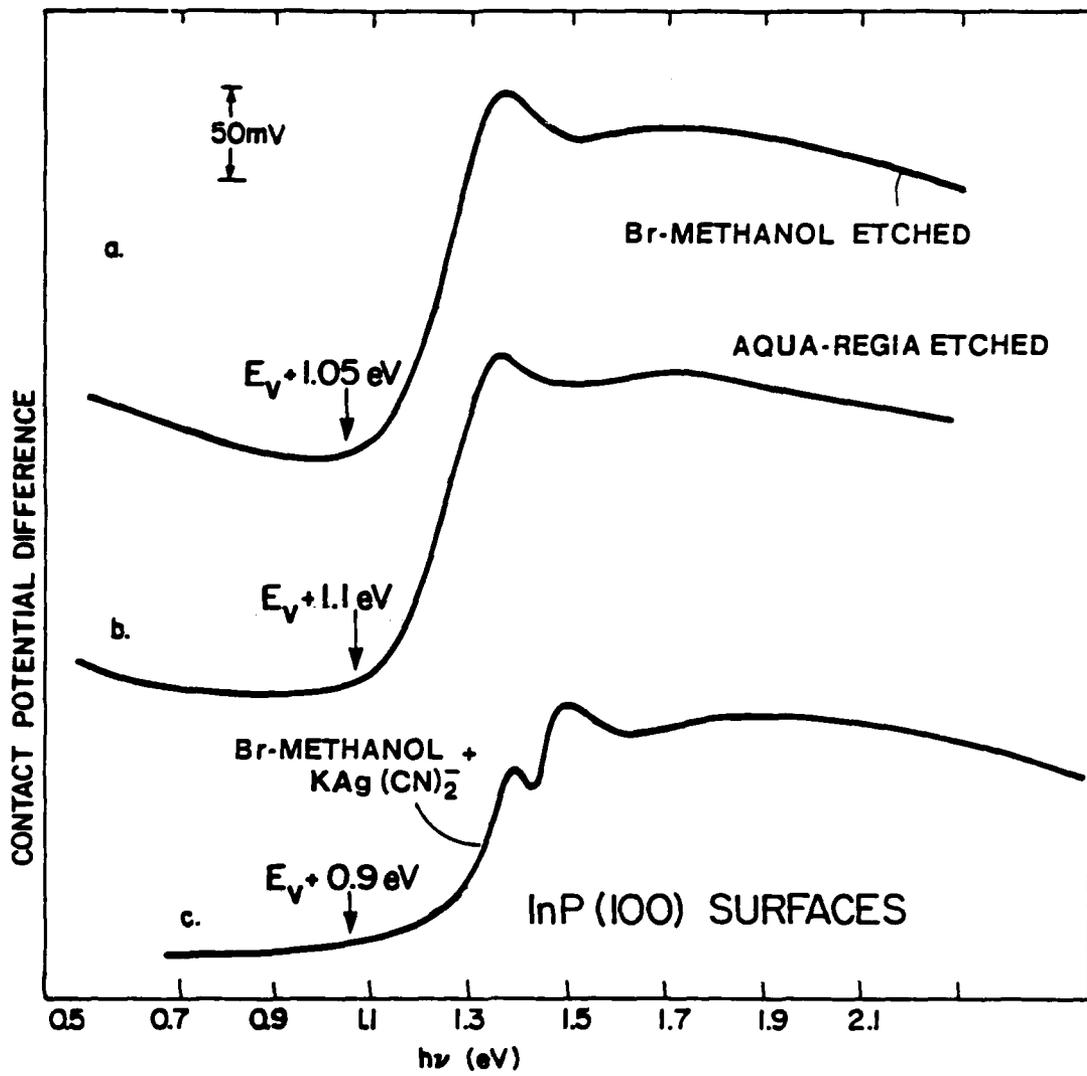AQUA REGIA ETCHED InP(100)

FIG. 11

KAg (CN)$_2$ TREATED InP (100)

FIG. 12

FIG. 13

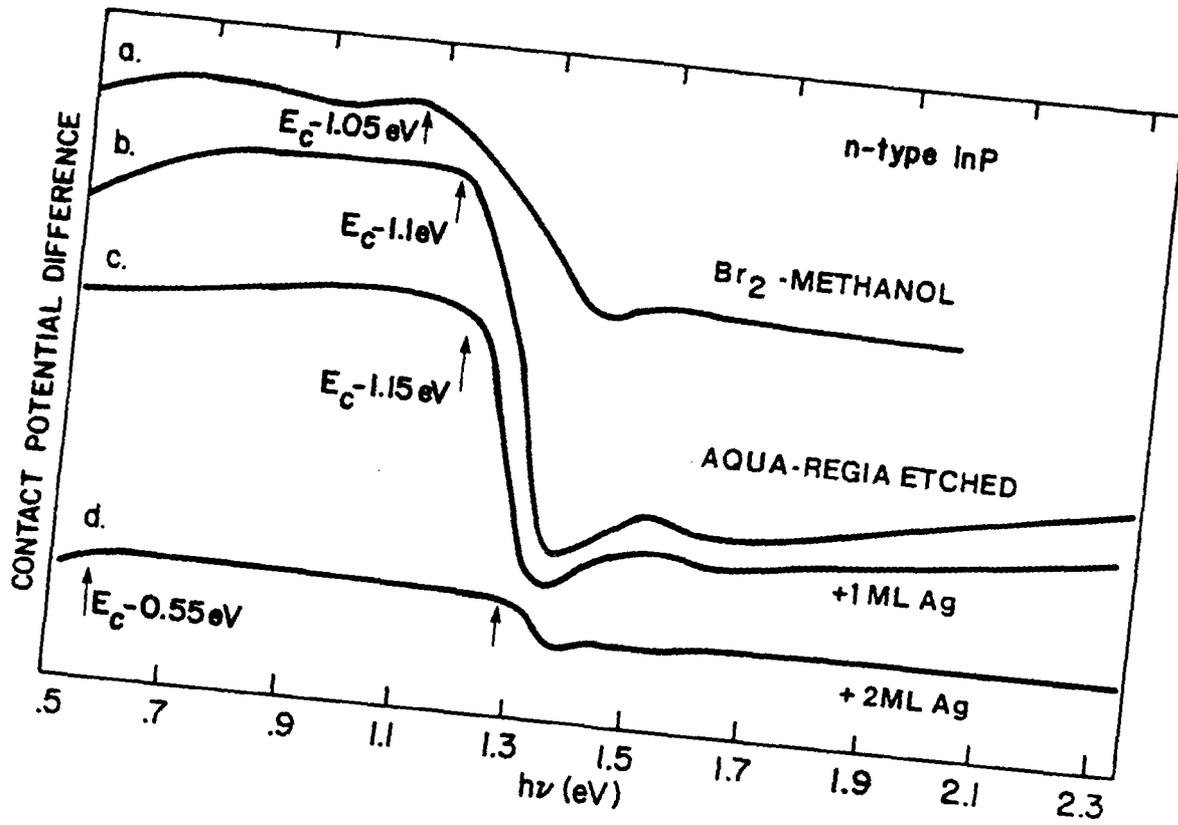FIG. 14

FIG. 15

FIG. 16

FIG. 17

AUGER DEPTH PROFILING STUDIES OF INTERDIFFUSION AND CHEMICAL TRAPPING AT METAL-INP INTERFACES

Y. Shapira† & L. J. Brillson

Xerox Webster Research Center
800 Phillips Rd.   W-114
Webster, NY 14580

ABSTRACT

We have used Auger electron spectroscopy (AES) combined with Art sputtering to profile the chemical composition of UHV-cleaved InP (110) interfaces with Au, Al, Cu, Ni, Ti, and Ag films. We observe pronounced anion and cation segregation to the free metal surface which depend sensitively on the metal-InP reactivity. Reactive metal (e.g. Al, Ti, or Ni) interlayers at Au-InP interfaces decrease anion diffusion and surface segregation monotonically with increasing interlayer thickness and AES depth profiles indicate a P accumulation at or just below the intimate metal-InP interface. These and other sputter–AES studies suggest that the lower higher Schottky barriers of unreactive (reactive) metals are associated with cation (anion) depletion within the InP bulk and on anion accumulation at the intimate InP-metal interfaces.

Introduction

Studies of the InP-metal interface have provided considerable information in understanding Schottky barrier-formation of III-V compound semiconductors. Photoemission studies have revealed evidence for chemical reaction and interdiffusion[1-7] which can lead to the formation of electrically-active sites within the semiconductor (e.g. defects)[8-10] and local band bending effects. While effective in demonstrating new chemical and electronic phenomena on an atomic scale, soft x-ray photoemission spectroscopy (SXPS) is too surface-sensitive to determine the chemical structure of the interface after deposition of relatively thick metallic

coverages. In this paper, we report on the use of auger electron spectroscopy (AES) combined with sputter depth-profiling to probe elemental distributions after interface formation in order to obtain spatial variations in semiconductor stoichiometry. These spatial variations can provide a basis for identifying defects formed by interdiffusion.

Unlike SXPS, AES sputter-profiling is disruptive, particularly for the nanometer thicknesses relevant to Schottky barrier formation. Ion beam effects which can distort the chemical distribution with depth include spatial broadening due to atomic mixing ("cascade" or "recoil"), preferential removal of species, enhanced diffusion, nonuniform sputter rate, surface roughening, segregation, structural changes, and chemical reactions.[11,12] In order to identify chemical effects associated with particular metal-InP interfaces despite these complications, we performed sets of depth profile measurements in which only a single parameter - e.g. the thickness or the reactivity of the metal films - was varied.

We observed several regular trends in the In/P stoichiometry near the InP-metal interface and at the free metal surface which can be correlated with SXPS results . These include: a) surface segregation of anion and cation which depend sensitively on the particular metal at the InP interface and b) chemical trapping of anions by reactive metal interlayers which reduce anion segregation to the free metal surface.[13] Thus we associate the lower Schottky barrier heights ϕ_{SB} of reactive metals (such as Al, Ti, and Ni) with In depletion within the InP bulk and a P accumulation at the intimate InP interface. Correspondingly, higher ϕ_{SB} of unreactive metals (such as Au and Cu) are associated with a bulk P depletion. Comparison of these results with energy levels calculated for particular defects within InP[14,15] suggest that simple defects alone do not account for the Schottky barrier formation.

Experimental

We cleaved InP bars of dimension SXSX15mm^3 in an ultrahigh vacuum chamber (base pressure $p \leq 4\mathrm{x}10^{-11}$ torr) to expose clean, visually-smooth (110) surfaces. These surfaces were coated with metals evaporated at pressures rising into the 10⁻

$10 - 10^{-9}$ torr ranges. Depositions were monitored with a quartz crystal oscillator. AES spectra were obtained using a double-pass beam currents were 1-5uA with a 2eV peak-to-peak CMA modulation. The PHI Ar^+ ion gun operated at a $3x10^{-8}$ torr background Ar pressure with 25ma emission current, glancing incidence, and 1kV beam voltage to minimize sputter damage and to improve spatial resolution. Each spectrum was acquired by signal averaging for 100 sec.

.Results

Fig. 1 shows typical dN(E)/dE AES spectra for a metal-InP interface at various stages of the depth-profiling procedure. For 30A Au on InP(110), the AES spectrum before sputtering exhibits characteristic dN(E)/dE features of Au, P, and In, the major features of which are labelled. Minor features due to Au also appear. No features due to C or O are evident. After an 8 min. sputtering, the P signal within the Au overlayer has declined substantially, while the In features have increased in strength. A spectrum obtained after 92 min of sputtering exhibits features of only P and In, since the Au overlayer has been completely eroded away.

To obtain depth profiles, we recorded the AES peak-to-peak intensities as a function of sputtering time. Fig. 2 displays Au, In, and P depth profiles for different Au overlayer thicknesses on UHV-cleaved InP (110). For example, the middle panel incorporates the data in Fig. 1. Sputtering conditions were identical throughout the profiles for all fine interfaces. Unless otherwise stated, ion beam dimensions were 4 x $4mm^2$. The family of depth profiles in Fig. 2 reveals several regular characteristics of In, P, and Au interdiffusion at the Au-InP interface. First, there is a pronounced segregation of In and P to the free metal surface which is evident for Au thicknesses of 30Å or larger. With increasing Au thickness, both In and P concentrations within the Au decreases, although P signals decrease more rapidly. This effect reflects the limited bulk solubility of In and the absence of solubility of P in Au.[16] At Au coverages below 30Å, P segregation is no longer apparent, due in part to the broadening effect of the sputtering process and to the characteristic P profile above the bulk InP which dominates any segregated P signal. In segregation is not apparent for coverages below 50Å Au (not shown).

Based on the known metal thicknesses deposited and the changes in P concentration resolved in, for example, the 30Å Au panel of Fig. 2, we estimate that sputter-induced broadening amounted to between 10 to 20Å. This means that the P outdiffusion in the 30Å Au panel of Fig. 2 has a characteristic width of at least 10Å. This conclusion is consistent with the SXPS measurements of anion outdiffusion from III-V compound semiconductors which reveal decreases to plateau values at Au coverages of 10-20Å[17].

We normalized the In and P signal intensities to each other using AES sputter profiles of UHV-cleaved InP (110) obtained under identical conditions but with no metal overlayers. Such profiles exhibit a P decrease relative to In with respect to the stoichiometric free surface. This decrease is due to preferential sputtering of P and reaches a characteristic value after 10-20 min. of Ar^+ sputtering. We used a single In/P normalization factor for all sputter profiles which produced the same relative P/In decrease after prolonged Ar^+ sputtering of bulk InP. As a result, most (but not all) of the profiles in Figs. 2-4 display a similar In excess after prolonged Ar^t sputtering of the bulk InP. Furthermore, this normalization should produce P and In signals of equal intensity at the InP surface - unless perturbed by the presence of the metal overlayer.

All five panels in Fig. 2 demontrate an In excess at or above the apparent Au-InP interface. At the free Au surface, more In than P is detected up to coverages of 30-50Å. This is in opposition to SXPS measurements, for which roughly equal In and P concentrations are evident below 20Å coverages and more P than In is observed for coverages above. This effect may be due partly to the preferential sputtering of P from the surface. For 70Å Au on InP (110), Fig. 2 shows a P excess on the surface but an apparent excess of In within the Au film. Such effects are potentially misleading for an SXPS analysis which samples only the surface layer, but they are not significant at coverages of 10-20Å for which anion and cation out diffusion dominate any segregation . By probing below the Au surface with different photon energies, one observes SXPS intensity increases rather than decreases at these low coverages.[18] SXPS analyses of outdiffusion stoichioimetry are based on data at these lower coverages.[4,6,7]

In order to determine how the relative In/P concentration changes with reactive vs. unreactive metals, we performed similar AES profiles on Au-InP interfaces containing an additional reactive metal interlayer. Reactive interlayers were thin (5-20Å) relative to the Au (70Å) overlayer. With this approach, changes in relative In vs. P sputter rates in different metal environments were minimized.

Fig. 3 illustrates the effect of "reactive"[19] metal interlayers on the In and P outdiffusion. In Fig. 3a, a 20Å Ni interlayer leads to a pronounced increase in P near the Ni-InP interface. In contrast to 70Å Au only on InP, there is now more P than In at the metal-InP interface. The 70Å Au-InP profiles with and without the Ni use the same AES normalization factor and, as shown, exhibit the same P and In variation within the bulk InP. Furthermore, with the Ni interlayer, the P intensity decreases to zero within the Au overlayer and no segregated P appears at the free au surface. Thus the Ni interlayer traps P atoms which would otherwise diffuse through the au overlayer to the free Au surface. The P signal reaches a maximum within the Ni film, which exhibits an asymmetric broadening due to a slower sputter rate.

Fig. 3b reveals similar effect for a 10Å Ti interlayer. Again, P is completely attenuated within the Au layer and at the free Au surface. Likewise, the P intensity exceeds that of In within the Ti film. Analogous behavior occurs for other Ni and Ti interlayer thicknesses as well as for Al interlayers.

Overlayers of reactive metals alone produce preferential decreases of P relative to In as well in comparison with unreactive metals such as Au, Cu, or Ag.[18] These experiments are complicated, however, by different sputter rates of In and P within each new metal.

Discussion

By probing below the free metal surface at a metal-InP interface, the AES depth-profiling technique revelas significant new information about the diffusion and segregation of In and P in the metal. Even taking effects of sputtering into account, a contrast in redistribution of In and P is apparent at the reactive vs.

unreactive metal-InP interfaces in Figs. 2 and 3. This contrast demonstrates the importance of local chemical interactions in determining the chemical structure of the metal-InP interface over thicknesses of many tens of Å. These studies show that reactive metals trap P atoms as they diffuse out of the InP, whereas unreactive metals promote higher levels of anion outdiffusion throughout the metal. The chemical trapping by reactive metals appears to produce an accumulation of P at the metal-InP interface which extends into the InP. Thus we associate the lower $\emptyset_{SB}$'s of reactive metals such as Ni, Ti, and Al[1,19] with an anion accumulation at the intimate metal-InP interface and a cation depletion within the InP. Conversely, we associate the higher $\emptyset_{SB}$'s of unreactive metals such as Au, Cu, and Ag with an anion depletion within the InP bulk. (Because of the preferential sputtering of P, it is difficult to establish an In accumulation at the unreactive metal-InP interface unambiguously).

While considerable effort has been devoted to understanding Schottky barrier formation of III-V compounds in terms of defects, no identification of particular defects or other electrically - active sites formed by metal deposition on the III-V compound surface has yet been made.[20] Recently, Dow and Allen[14] and Daw et al[15,21,22] have calculated energy levels for various defects in InP. Dow and Allen determine a P vacancy V_P level in the conduction band, antisite P_{In} and In_P levels deep in the InP band gap, and an In vacancy V_{In} below midgap which can pin the Fermi level of n-type InP. Daw et al. calculate a V_P level near the conduction band edge and a V_{In} near midgap. Since unreactive metals produce large n-type $\emptyset_{SB}$'s, the AES depth-profiling as well as previous SXPS results are not consistent with the shallow donor levels of a V_P defect. Such levels should yield low n-type $\emptyset_{SB}$'s which are produced by reactive metals and which AES results demonstrate cause an accumulation of P at the intimate InP-metal interface. Similarly, a V_{In} level producing a large n-type $\emptyset_{SB}$ does not agree with the P depletion apparent for unreactive metals. Only the In_P level appears consistent with both electrical and spectroscopic measurements.

The AES and SXPS results are consistent with photoluminescence measurements of Tempkin *et al.*[23] Based on the photoluminescence spectra of InP wafers grown and annealed under P-deficient conditions, Tempkin *et al.* identify a donor level 0.99eV above the valence band edge with V_P. This energy level can account for the ~0..5eV $\emptyset_{SB}$'s reported for unreactive metals, since the InP band gap at the 6°K measurement temperature is 1.42eV. Levels lower in the gap were identified with V_{In} and donor-acceptor complexes. These identifications neglect the presence of residual impurities and their interactions.[23]

Since the highest-lying energy levels in the vacancy and antisite calculations of both Dow and Allen and Daw *et al.* are V_P levels and since this defect alone is unlikely to produce the low $\emptyset_{SB}$'s associated with a P accumulation at the interface, other defect complexes are more likely to determine the Schottky barrier for reactive metals. These could include P interstitials as well as combinations of interstitial, antisite, and vacancy defects.

Conclusion

AES sputter-profile experiments provide new information on atomic redistribution at the metal-InP interface. Complementing SXPS measurements, this data demonstrates that qualitative differences in interdiffusion occur over many tens of Å for reactive vs. unreactive metals on the InP (110) surface. Unreactive metals such as Au, Cu, and Ag permit diffusion of both In and P through the metal film and segregation at the free metal surface. Reactive metals attenuate P outdiffusion, producing an accumulation of P at the intimate metal-InP interface. These effects depend monotonically on the thickness of the reactive metal layer. Therefore we associate low $\emptyset_{SB}$'s of reactive metals with a P excess at the metal-InP interface and within the InP bulk and high $\emptyset_{SB}$'s with a P deficiency at the interface. The results for reactive metals are inconsistent with Fermi level pinning by simple native defects and suggest that more complex defects may dominate the metal-InP Schottky barrier formation.

!On sabbatical leave from Tel Aviv University, Dept. of Engineering, Tel Aviv, Israel.

Figure Captions

1. Auger electron spectra for 30Å Au deposited on UHV-cleaved InP (110) after 0, 8 and 92 min of Ar^t sputtering. The major Au, In, and P dN(E)dE features are labelled. Note the different behavior of In and P signals with sputtering time.

2. AES Au, In, and P depth profiles for different Au overlayer thicknesses on UHV-cleaved InP (110). Sputtering conditions were identical throghout the profiles for all five interfaces. Ion beam raster dimensions were 4 by 4 mm^2.

3. AES Au, In, P, and interlayer metal depth profiles for a 70Å Au - 20Å Ni-InP (110) and b) 70Å-10Å Ti-InP (110) interfaces. Raster area in b) was twice that in Fig. 2 so that sputter rate was 1/2 as large.

References

1. R. H. Williams, R. R. Varma, and A. McKinley, J. Phys. C 11, 735 (1978).

2. R. H. Williams, A. McKinley, G. J. Hughes, V. Montgomery, and I. T. McGovern, J. Vac. Sci. Technol. 21, 594 (1982).

3. R. H. Williams, J. Vac. Sci. Technol. 18, 929 (1981).

4. L. J. Brillson, C. F. Brucker, A. D. Katnani, N. G. Stoffel, and G. Margaritondo, J. Vac. Sci. Technol. 19, 661 (1981).

5. L. J. Brillson, C. F. Brucker, A. D. Katnani, N. G. Stoffel, R. Daniels, and G. Margaritondo, J. Vac. Sci. Technol. 21, 569 (1982).

6. L. J. Brillson, C. F. Brucker, A. D. Katnani, N. G. Stoffel, and G. Margaritondo, Appl. Phys. Lett. 38, 784 (1981).

7. L. J. Brillson, C. F. Brucker, N. G. Stoffel, A. D. Katnani, and G. Margaritondo, Phys. Rev. Lett. 46, 838 (1981).

8. W. E. spicer, P. W. Chye, P. R. Skeath, C. Y. Su, and I. Lindau, J. Vac. Sci. Technol. 16, 1422 (1979).

9. W. E. Spicer, I. Lindau, P. Skeath, C. Y. Su, and P. Chye, Phys. Rev. Lett. 44, 420 (1980).

10. R. H. Williams, R. R. Varma, and V. Montgomery, J. Vac. Sci. Technol. 16, 1418 (1979).

11. G. K. Wehner, in: Methods of Surface Analysis, edited by A. W. Czanderna (Elsevier, Amsterdam, 1975).

12. E. Zinner, J. Electrochem. Soc., in press.

13. L. J. Brillson, G. Margaritondo, and N. G. Stoffel, Phys. Rev. Lett. **44**, 667 (1980).

14. J. D. Dow and R. E. Allen, J.Vac. Sci. Technol. **20**, 659 (1982).

15. M. S. Daw and D. L. Smith, Appl. Phys. Lett. **36**, 690 (1979).

16. M. Hansen and K. Anderko, Constitution of Binary Alloys (McGraw-Hill Co., New York 1958).

17. L. J. Brillson, Appl. Surface Sci. **11/12**, 249 (1982).

18. Y. Shapira, L. J. Brillson, A. Katnani, and G. Margaritondo, unpublished.

19. L. J. Brillson, Phys. Rev. Lett. **40**, 260 (1978).

20. For a review of interface defect models and current results bearing on their identification, see L. J. Brillson, Surface Sci. Repts. **2**, 123 (1982).

21. M. S. Daw and D. L. Smith, Phys. Rev. **B 20**, 5150 (1979).

22. M. S. Daw, D. L. Smith, C. A. Swarts, and T. C. McGill, J. Vac. Sci. Technol6. **19**, 508 (1981).

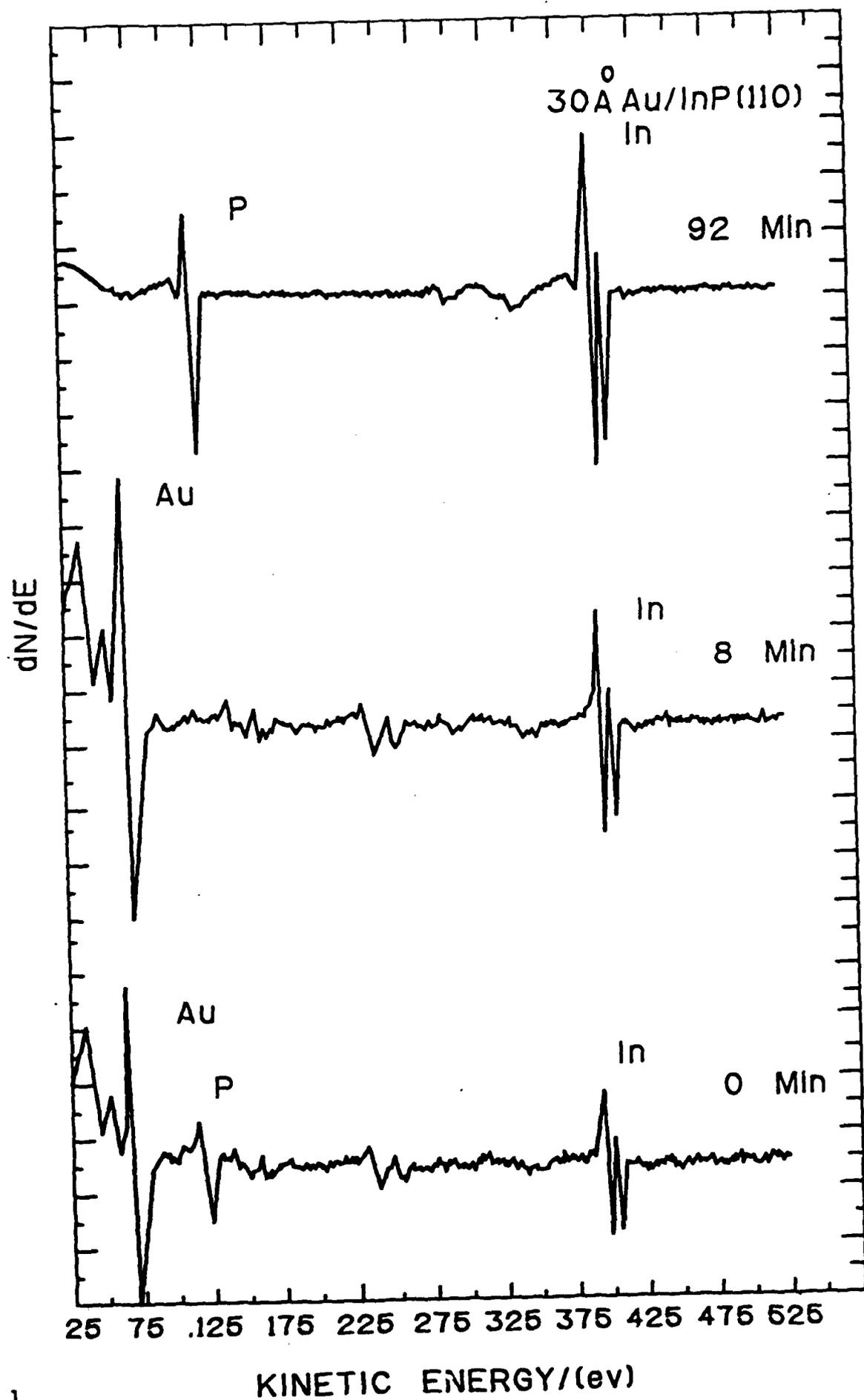23. H. Tempkin, B. V. Duff, W. A. Bonner, and V. G. Keramidas, J. Appl. Phys. **53**, 7526 (1982).
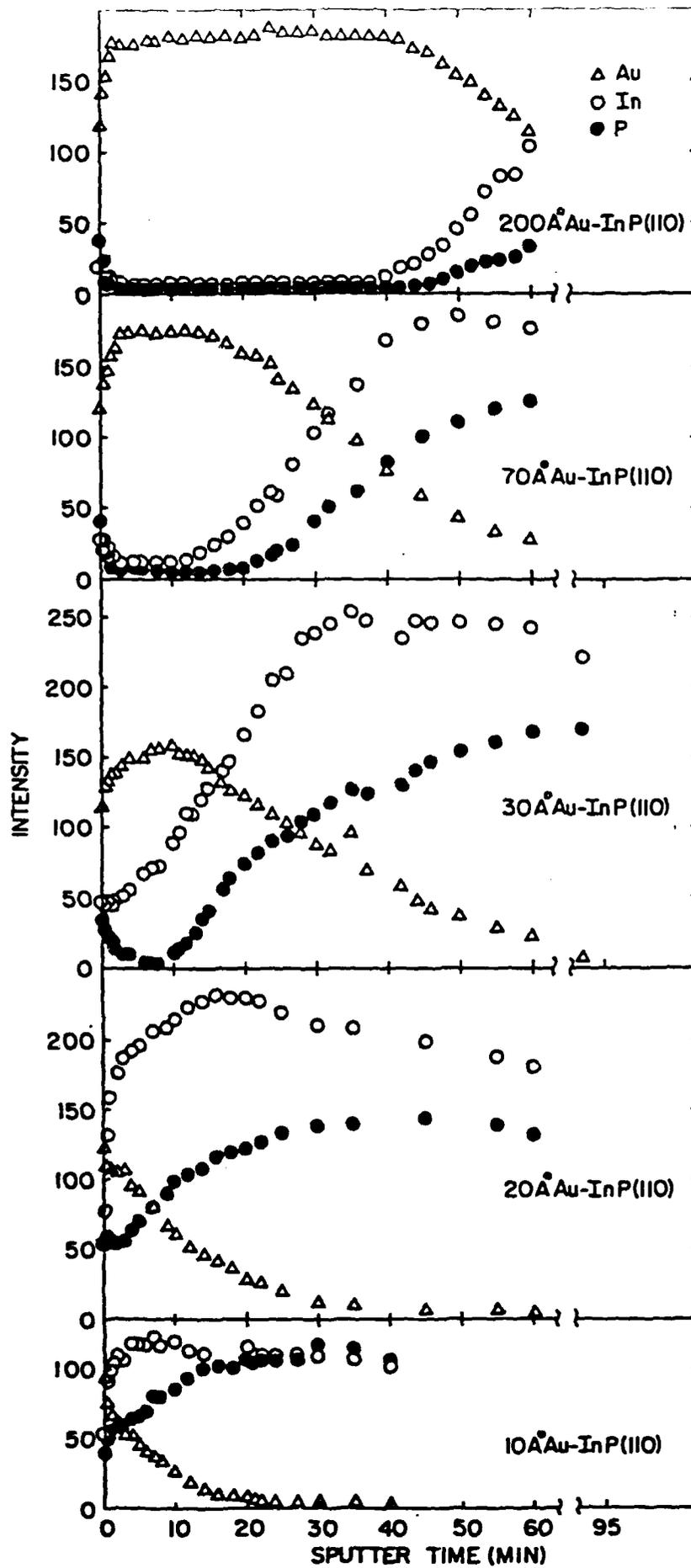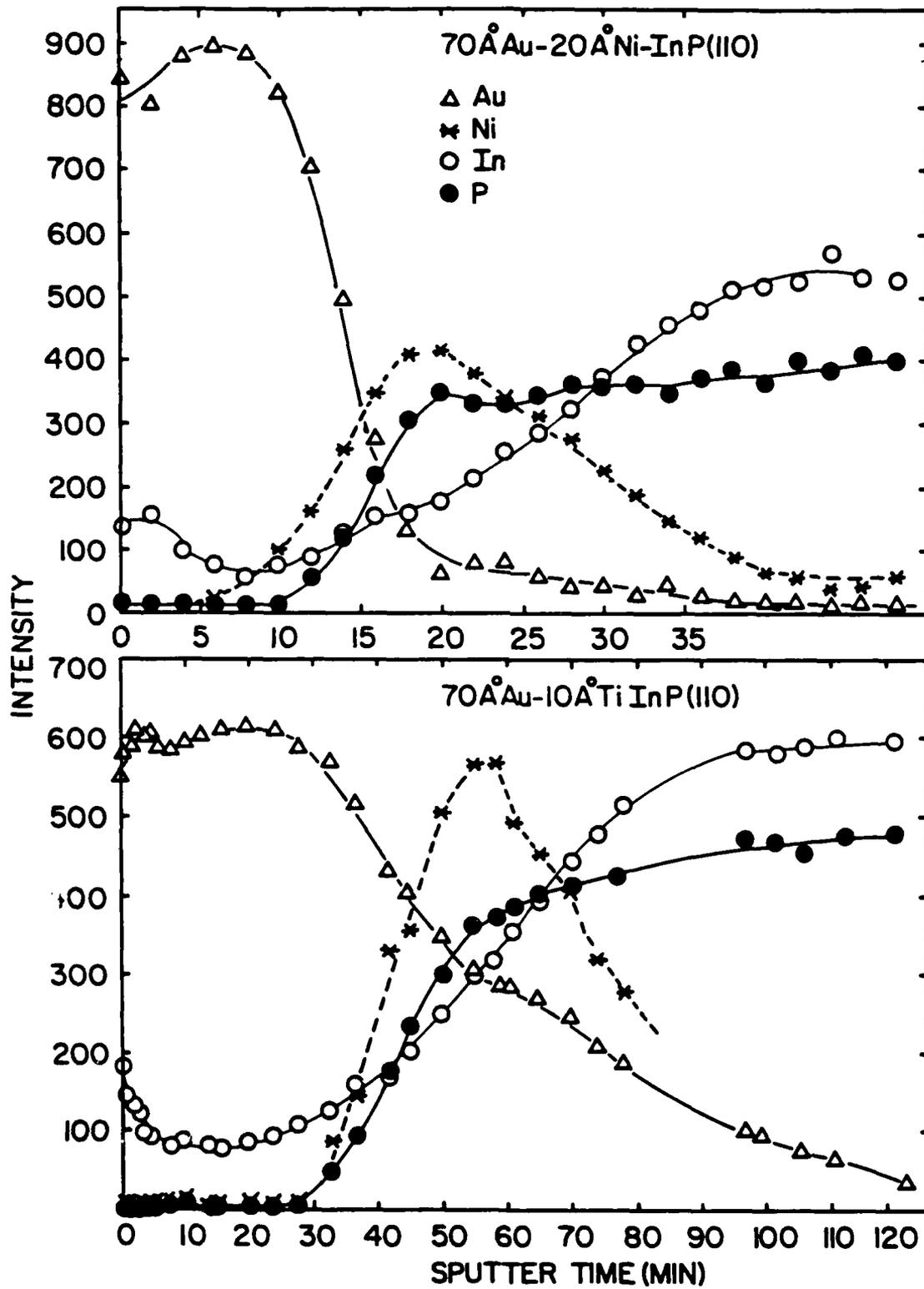
Fig. 1

Fig. 2

Fig. 3

Reduction of Silicon-Aluminum Interdiffusion by Improved Semiconductor Surface Ordering

L.J. Brillson and M.L. Slade
Xerox Webster Research Center, 800 Phillips Road W114, Webster, NY 14580

and

A.D. Katnani, M. Kelly, and G. Margaritondo
Dept. of Physics, University of Wisconsin, Madison, WI 53706

Abstract

Aluminum overlayers on highly-ordered single-crystal silicon (100) and (111) surfaces in ultrahigh vacuum are found to exhibit characteristic interface widths less than tens of Å at room temperature and hundreds of Å at 400°C - orders of magnitude more abrupt than conventionally reported for Al-Si contacts. We demonstrate that surface disorder plays a critical role in promoting Si diffusion into the Al overlayer.

The Si-Al interface is of high technological interest in large part because of the widespread use of Al as interconnects in integrated-circuit structures.[1] Considerable work over the past decade has focussed on the Si-Al interdiffusion, in which Si from a single-crystal substrate diffuses into an Al metallization layer and Al penetrates to the dissociated interface.[2] Such diffusion at temperatures of 400-500°C reportedly extends tens of microns or more into both the Si[2,3] and the Al[4], promoting Al "spikes" extending into the Si as well as recrystallized Si layers doped with Al at the metal-semiconductor interface.[5] It is desirable to minimize such diffusion in the fabrication of ultrasmall devices, where the semiconductor thickness may be only a fraction of a micron. To date, the most effective approach to this problem has been the use of barrier layers, such as Ti, V, and W.[1,6] It is also known that thin layers of Si oxide retard diffusion and reaction.[7,8] However, the latter are insulating and thus undesirable for reproducible, low resistance electrical contacts.

Despite the massive diffusion reported for the Al-Si interface at temperatures of 400-450°C,[2] the bulk Al-Si phase diagram indicates no solubility for Si in Al up to temperatures of ~ 430°C and no solubility of Al in Si up to 577°C, the eutectic temperature.[9] We have carried out soft x-ray photoemission spectroscopy (SXPS) and Auger electron spectroscopy (AES)-depth profiling studies of Al-Si interfaces prepared by depositing Al on to clean, ordered Si (111) or Si (100) surfaces in ultrahigh vacuum (UHV). The experimental results demonstrate that the Al-Si interface is much more abrupt than previously believed, even when annealed at 400°C for ½ hour. The reduced interdiffusion is believed due to higher crystal perfection and lower strain near the Si surface than is conventionally realized with conventional Si wafers. By intentionally disordering such surfaces, we confirm the critical role of surface disorder in promoting Si diffusion into the Al overlayer.

In order to prepare clean, ordered Si surfaces, we cleaved Si bars of dimension 3x3x15 mm^3 and n = 3-6x10^{15} B cm^{-3} in UHV to obtain (111) faces, and annealed

1/4" x 3/4" rectangles cut from Si wafers (p-type, uncompensated, resistivity $\rho = 20$ Ω cm^{-1}) to obtain (100) faces. The latter were annealed first at 1250°C for 1 minute then at 950°C anneal for 10 minutes, in accordance with a recipe used for low energy electron diffraction studies.[10] AES and low energy electron diffraction (LEED) revealed an atomically-clean, ordered (1x1) surfaces. SXPS valence band spectra exhibited a characteristic shoulder above the valence band edge associated with intrinsic surface states of the clean Si surface. For this high temperature annealing, we passed current (10-15 A) through wafers held by tantalum clips. We monitored surface temperature with an Optitherm radiometer (Barnes Eng.) focussed through a sapphire viewport and using emissivity ϵ = .49 at 1250°C, ϵ = .52 at 950°C, and ϵ = .59 at 400°C for clean Si and ϵ = .37 for Si overcoated with 200 Å Al. Al was deposited by evaporation from a W coil and monitored by a quartz crystal oscillator. During evaporation, pressure rose from p < 10^{-10} torr to the high 10^{-9} torr range. Equipment for AES depth profiling included a differentially-pumped PHI Ar^{+} gun operated with 25ma emission current and 1kV beam energy (to minimize surface damage), a glancing incidence electron gun operated at 10 μA current and 2kV beam energy, and a cylindrical mirror analyzer (also used for SXPS) for electron energy analysis. We performed the SXPS experiments at the University of Wisconsin storage ring facility at the Stoughton Physical Sciences Laboratory, using a "grasshopper" monochromator.

Figure 1 illustrates Si 2p core level spectra taken as a function of a) deposited Al thickness at constant photon energy hν (130 eV) and b) hν at constant thickness (20Å). At hν = 130 eV, photoelectrons excited from Si 2p core levels have a scattering length λe of only 4-6 Å[11] and therefore yield highly surface-sensitive core level spectra. For hν = 120, 110, and 107 eV, λe = 6-10 Å, 10-20 Å, and 20-50 Å respectively, representing a variable depth sensitivity. In Fig. 1a, the initial deposition of 1 Å Al (1 monolayer = 9.27 x 10^{14} cm^{-2} = 1.54 Å Al) produces a core level shift to lower binding energy, consistent with an increase in n-type band

bending. Further deposition attenuates the Si intensity and produces a shoulder at lower binding energy due to Si segregated at the free Al surface. Figure 1b confirms this relatively small segregation for the case of 20 Å Al on Si (111). As hν decreases, the escape depth increases, the surface contribution becomes a small portion of the sampled volume, and the shoulder almost completely disappears. For metals such as Au, for which Si diffuses throughout the metal overlayer, spectral features due to the diffused Si (not shown) do not change appreciably with probe depth. Furthermore, when the 20 Å Al Si interface was annealed at ~ 200°C for 45 minutes using a focussed projection lamp, the same spectral features as in Fig. 1 were observed, albeit with increased Si segregation to the free Al surface. Indeed, massive Si-Al interdiffusion (as gauged by the Si:Al ratio of core level intensities) did not occur until the interface was annealed at 600°C or higher. No significant differences in diffusion behavior were manifest between SXPS data for UHV-cleaved Si (111) surfaces and Si (100) faces subjected to the 1250°C/950°C annealing procedure. All these results indicated that, except for a relatively small amount of Si segregation at the free Al surface, the Si-Al interfaces were abrupt to within tens of Å and laterally uniform across the Si surface. Consistent with the low (0.25 wt% at 400°C) solubility of Si in Al,[9] SXPS data indicated negligible Si mixing within the Al overlayer, even at temperatures of 200-400°C.

To confirm these observations, we obtained depth profiles of chemical composition normal to the interface plane using AES with thickner Al overlayers on the Si (100) wafer surfaces. Figure 2 shows depth profiles for 200Å Al deposited in UHV on Si (100) after a) the 1250/950°C preanneal and a 400°C, 30 minute post anneal versus b) a 5kV, 30 minute post anneal. Carbon and oxygen contamination appeared only for initial sputtering times, i.e., at the free Al surface. Figure 2a demonstrates that the Al-Si interface width (here taken between 10% - 90% Si and Al limits) is 200-400 Å, based on the time required to sputter through the crossover point (i.e., 150 minutes). Without a post anneal, the same interface is ten times more abrupt (not

shown). For the latter case, the measured interface width (20-40 Å) is due in large part to sputter-induced broadening and the escape depths of Auger electrons.[12] Figure 2a is consistent with sputter-profiling results of Hwang et al.[13] who used the same Al thickness, ion beam energy and post anneal temperature on polycrystalline Si layers. However, their interfaces exhibited sufficient oxygen contamination to produce a significant barrier to Si outdiffusion.[8] Indeed, we obtain similar results for air-exposed, Si (100) surfaces with no preanneal. For 100 Å Al on Si (100) faces with a 1250/950°C preanneal and the 400°C, 30 minute post anneal, we measure a profile analogous to Fig. 2a with a top surface concentration of 80% Al and 20% Si - equal to the composition after ~ 75 minutes of sputtering or halfway through the 200 Å Al overlayer. Thus any dependence of Si outdiffusion on Al thickness must be secondary.

Figure 2b demonstrates the effect of intentionally disordering the Si surface prior to Al deposition. As shown, Si diffuses through the Al overlayer with no evident attenuation. If C and O data are factored out, the Si and Al intensities exhibit some Si segregation near the free Al surface but are otherwise roughly constant out to the free Al surface. Interestingly enough, there appears to be no enhancement of Al extending into the Si over the preannealed case. This is consistent with Si movement into Al as the primary diffusion process. SXPS marker experiments confirm this result, showing only Si movement into Al during the initial stages of interface formation.[14] Such results are understandable since Al is not soluble in Si below 577°C but Si is slightly soluble in Al.[9] The large Si outdiffusion is not due to any gross surface roughening since reannealing the sputtered Si prior to Al deposition leads to a profile similar to Fig. 2a.

Figure 2b reveals that lattice disorder, strain, and/or Ar interstitials promote a massive outdiffusion into Al, and they agree with analogous ion bombardment studies carried out at much higher beam energies and Al film thickness.[15] Lattice

disorder may also account for the high interdiffusion of Al with amorphous Si.[16] The reduction of lattice defects and stress by high temperature annealing can also account for the extreme uniformity in the interface plane - for example, the attenuation of Si with only 20 Å of Al over a ~ 1 mm^2 analysis region in Fig. 1. Since Si wafers are polished, etched, and in many cases ion-implanted, it is reasonable to expect some degree of residual crystal imperfection and stress near the semiconductor surface. To our knowledge, the only other report of high temperature Si annealing to reduce Al-Si interdiffusion was accomplished by laser annealing polycrystalline Si[18] and in this case, the reduction was attributed to lower grain-boundary diffusion between enlarged grains. Our results highlight the importance of high temperature preannealing for single crystal Si. Furthermore, such annealing must be carried out in UHV to prevent the deleterious effects of oxide formation.

In conclusion, surface science techniques performed in UHV reveal that atomically-clean Al-Si interfaces can be prepared which are two to three orders of magnitude more abrupt than conventionally reported, even after annealing at device-processing temperatures. To achieve such interfaces, one must remove surface disorder by high temperature annealing in UHV. These observations suggest that contact penetration of the semiconductor, one of the limiting factors in preparing submicron devices, may be overcome by relatively straightforward procedures.

References

1. See, for example, D. Pramanik and A.N. Saxena, Solid State Electron. January 1983, p. 127.

2. R. Rosenberg, M.J. Sullivan, and J.R. Howard, in Thin Films - Interdiffusion and Reaction, Eds. J.M. Poate, K.N. Tu, and J.W. Mayer (Wiley-Interscience, New York, 1978) p. 13 and references therein.

3. R.J. Anstead, IEEE Trans. Electron. Devices ED-16, 38 (1969).

4. J.O. McCaldin and H. Sankur, Appl. Phys. Lett. 19, 524 (1971).

5. J.O. McCaldin and H. Sankur, Appl. Phys. Lett. 20, 171 (1972).

6. K. Nakamura, S.S. Lau, M.-A. Nicolet, and J. Mayer, Appl. Phys. Lett. 28, 277 (1976).

7. R.W. Bower and J.W. Mayer, Appl. Phys. Lett. 20, 359 (1972).

8. S.M. Goodnick, M. Fathipour, D.L. Ellsworth, and C.W. Wilmsen, J. Vac. Sci. Technol. 18, 949 (1981).

9. M. Hansen, Constitution of Binary Alloys (McGraw-Hill, New York, 1958).

10. B. Webb, private communication.

11. M.P. Seah and W.A. Dench, Surface Interface Analysis 1, 2 (1979).

12. C.R. Helms, N.M. Johnson, S.A. Schwarz and W.E. Spicer, J. Appl. Phys. 50, 7007 (1979).

13. J.C.M. Hwang, P.S. Ho, J.E. Lewis, and D.R. Campbell, J. Appl. Phys. 51, 1576 (1980).

14. L.J. Brillson, A.D. Katnani, M. Kelly, and G. Margaritondo, unpublished.

15. M. Nakajima, K. Kusao, T. Hirao, K. Inoue, and S. Takayanagi, Jpn. J. Appl. Phys. 18, 1869 (1979).

16. S. Ishihara, T. Hirao, K. Mori, M. Kitagawa, M. Ohno and S. Kohiki, J. Appl. Phys. 53, 3909 (1982).

17. H. Sankur, J.O. McCaldin, and J. Devaney, Appl. Phys. Lett. 22, 64 (1973).

18. A.J. Learn and R.S. Nowicki, Appl. Phys. Lett. 35, 611 (1979).

Figure Captions

1. SXPS Si 2p core level spectra for Al deposited on UHV-cleaved Si (111) surfaces as a function of a) deposited Al thickness at constant photon energy hν (130 eV) and b) hν at constant thickness (20Å).

2. AES depth profiles for 200 Å Al deposited on Si (100) in UHV after a) high temperature preanneal and a 400°C, 30 minute post anneal and b) a 5kV Ar$^+$ bombardment prior to Al deposition and a 400°C, 30 minute post anneal. Data points (not shown) are spaced every 2 minutes.
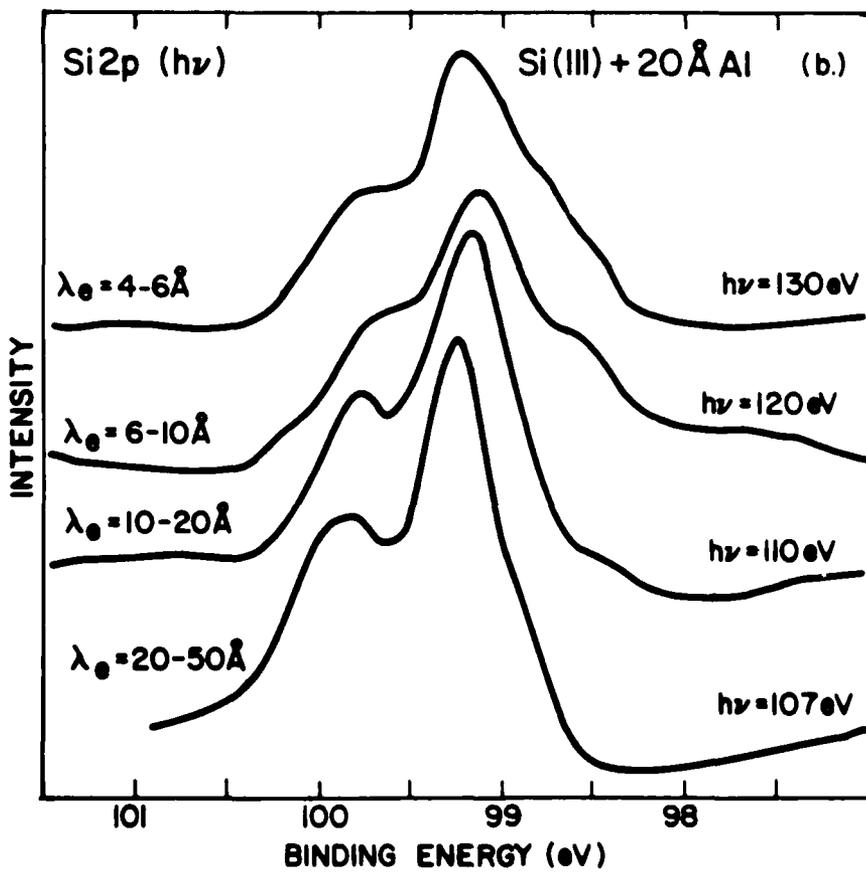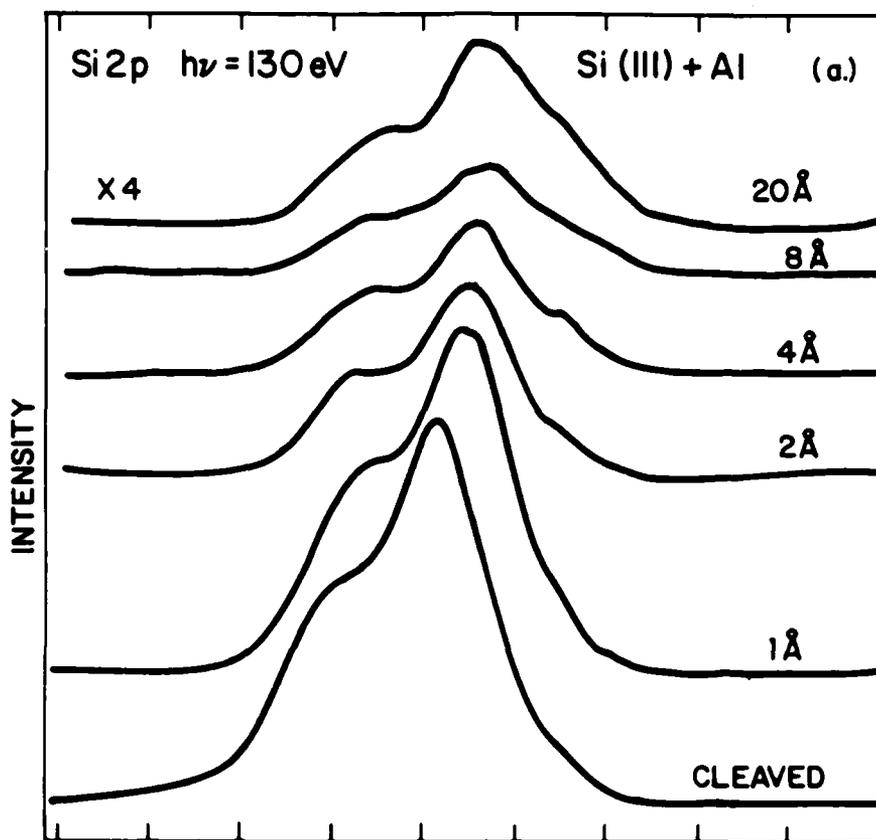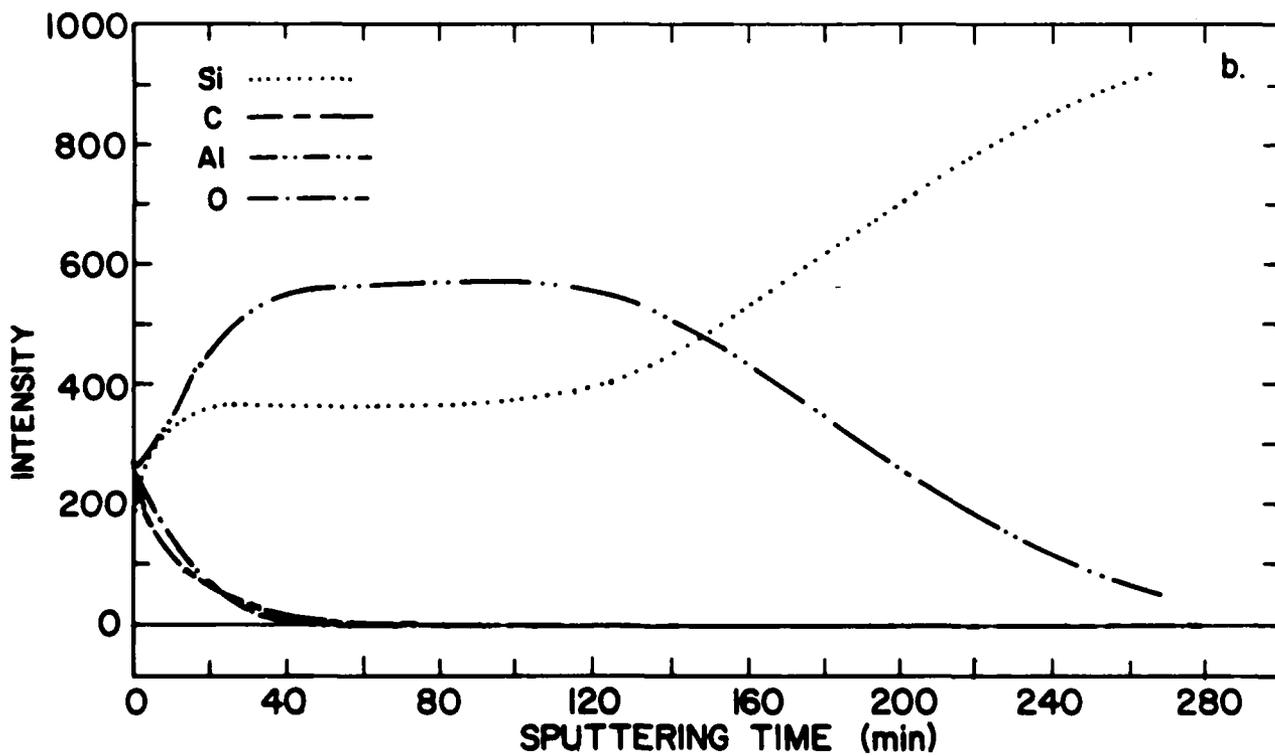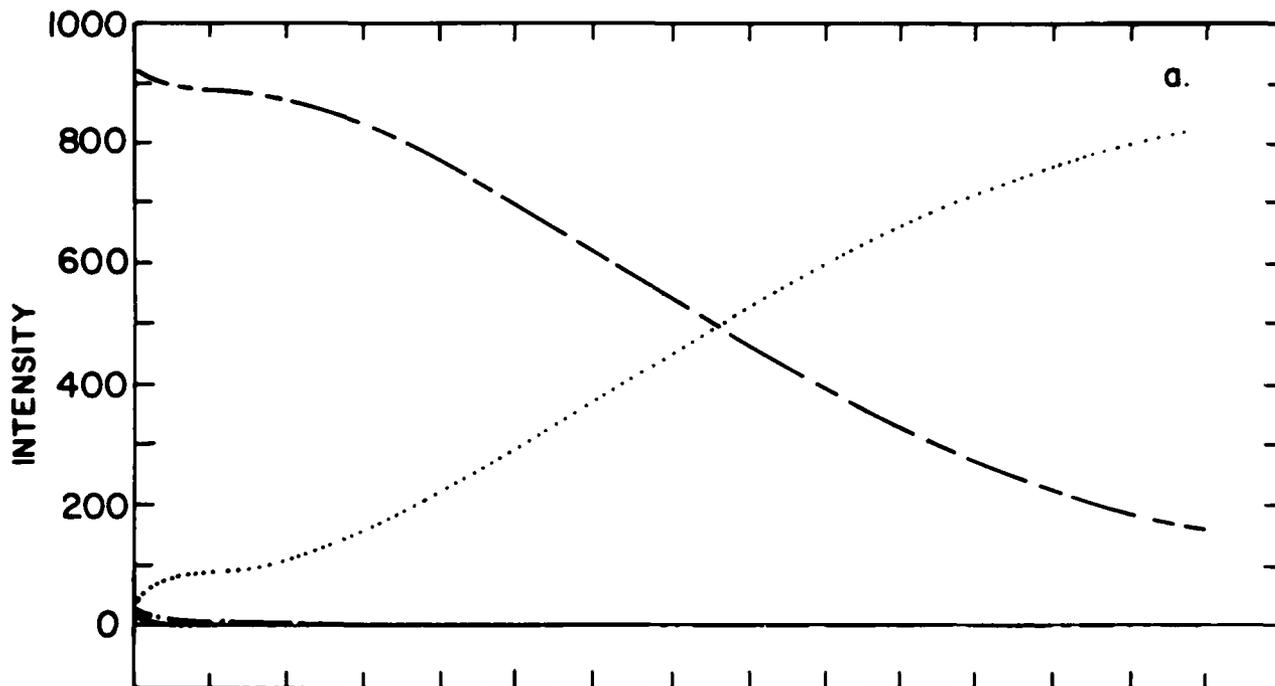
Si 2p hν = 130 eV   Si (III) + Al   (a.)

X 4

20 Å
8 Å
4 Å
2 Å

1 Å

CLEAVED

INTENSITY

Si 2p (hν)   Si (III) + 20 Å Al   (b.)

λ_e = 4-6 Å   hν = 130 eV

λ_e = 6-10 Å   hν = 120 eV

λ_e = 10-20 Å   hν = 110 eV

λ_e = 20-50 Å   hν = 107 eV

INTENSITY

101   100   99   98

BINDING ENERGY (eV)

Fig. 1

Fig. 2

Photoemission Studies of Atomic Redistribution at Gold-Silicon and Aluminum-Silicon Interfaces

L.J. Brillson
Xerox Webster Research Center
Webster, New York 14580

and

A.D. Katnani, M. Kelly, and G. Margaritondo
Dept. of Physics, University of Wisconsin
Madison, WI 53706

Abstract

We have used soft x-ray photoemission spectroscopy (SXPS) to monitor the rearrangement of Si and metal atoms during the initial stages of Au or Al interface formation with UHV-cleaved (111) or (100) Si surfaces. From Si 2p core level spectra as a function of metal overlayer thickness and as a function of incident photon energy, we obtain evidence for strong Si bond changes at submonolayer Au coverages but only weak Al-Si interactions. Marker experiments reveal that Au diffuses into Si (Si diffuses into Al) with the first few deposited metal overlayers. We examine our new information on the interface evolution at room and elevated temperatures in relation to the corresponding bulk phase diagrams.

I. Introduction

A wide range of surface science investigations have now established that metal-semiconductor interfaces are far from the atomically-abrupt junctions commonly envisioned.[1,2] Instead, interdiffusion and chemical reactions appear to dominate the chemical as well as the electronic interface structure. Strong chemical interactions are certainly evident for Si interfaces with metals.[3] Two of these - the Au-Si and Al-Si interfaces - have been studied extensively[4-6] in part because Au and Al are common metals which are employed extensively in Si devices. Nevertheless, the detailed rearrangement of Si with Au and Al atoms during the initial stages of interface formation is only now beginning to be explored on an monolayer scale.[3,6-9] Such experiments provide new clues to the forces which drive the observed diffusion on a macroscopic scale.

In this paper we report soft x-ray photoemission spectroscopy (SXPS) results which provide detailed new information on the evolution of these common interfaces at room and elevated temperatures. In addition we show that, in contrast to the Au-Si interface, initial movements of metal vs. Si atoms at the Al-Si interface are quite consistent with expectations based upon the Al-Si bulk phase diagram.

Our approach is to monitor Si-metal interdiffusion and chemical bonding via changes in the intensity and energy of electrons photoemitted from the Si 2p core level by soft x-ray radiation. We performed SXPS experiments on clean Si (111) surfaces obtained by cleavage in ultrahigh vacuum (UHV) with metal overlayers deposited by *in-situ* evaporation. Si (100) surfaces cleaned by resistive heating to 1250°C were also examined. Five types of SXPS features were examined. Si 2p core level intensities vs. metal coverage provided a test for Si-metal interdiffusion. Si 2p core level energies vs. metal coverage yielded information on the Si-metal chemical bonding. Si 2p core level spectra taken as a function of incident photon energy (i.e., variable photoelectron escape depth[10]) reveal spatial variations in

chemical bonding and Si-metal concentrations near the interfaces. Thus Si 2p core level intensities vs. photon energy indicated variations in atomic concentration while Si 2p core level energies vs. photon energy gave evidence for spatial variations in chemcial bonding. Finally, marker layer experiments[4,11,12] using submonolayers of Ni revealed the order in which Si and metal atoms diffused into each other. Following a description of the experimental apparatus in Sec. 2, we present SXPS results in Sec. 3. The significance of these findings in relation to previous studies is discussed in Sec. 4.

II. Experimental

Angle-integrated SXPS experiments were performed at the Stoughton Synchrotron Radiation Laboratory of the University of Wisconsin, Madison, using a "grasshopper" monochromator[13] and a double-pass cylindrical mirror analyzer (CMA). Si bars of dimension $3 \times 3 \times 5$ mm^3 and $N_A = 3 - 6 \times 10^{15}$ B cm^{-3} were cleaved in UHV (base pressure $p = 5 \times 10^{-11}$ torr) to expose clean, ordered surfaces. Au and Al were deposited by evaporation from a W coil and monitored by a quartz crystal oscillator. During evaporation, pressure increased from $p < 10^{-10}$ torr to the high 10^{-9} torr range for Al and to the high 10^{-10} torr range for Au.

III. Results

Figure 1 illustrates Si 2p core level spectra obtained as a function of Au coverage on the UHV-cleaved Si (111) surface. The clean Si surface exhibits a spin-orbit split Si 2p feature which changes substantially with the initial deposition of 1 Å Au ($= 5.77 \times 10^{14}$ atoms/cm$^2 = 0.74$ monolayer). As shown, a second Si 2p component appears which is shifted to higher binding energy. This shift is consistent with a charge transfer from Si to Au due to the higher electronegativity of Au (2.4) vs. Si (1.8).[14] With increasing Au coverage the Si 2p component at higher binding energy dominates the lower binding energy (substrate) component. At a coverage of 20 Å

Au, the spectrum consists almost entirely of the higher binding energy component, and its spin-orbit splitting is now clearly resolved. These features were not reported in previous studies, presumably because they were unresolved in these lower resolution experiments.[6]

The slow decrease in the integrated Si 2p peak intensity I_{Si}^{2p} with Au coverage indicates that substantial diffusion takes place. While the intensity decrease for the first 8 Å Au deposit is consistent with a photoelectron escape depth of 4-6 Å, no significant I_{Si}^{2p} attenuation occurs for higher coverages. It is noteworthy that the substrate component of the Si 2p spectral features *does* decrease exponentially at all coverages studied (corresponding to a 3-4 Å escape depth), suggesting that Au on Si forms a uniform overlayer rather than islands. This laterally uniform overlayer must contain Si in a bonding environment different from that of the substrate.

Figure 2 demonstrates that Si within the Au overlayer is distributed throughout the film. Here we studied a 20 Å deposit of Au on Si (111) with three different photon energies corresponding to three different escape depths, ranging from 4-6 Å to 10-20 Å. Despite the difference in escape depth, Fig. 2 shows that only the Si 2p component at higher binding energy is present. Only spectra with the most bulk-sensitive photoemission (hν = 110 eV) shows any evidence for the lower binding energy, substrate feature. Note that the Si 2p spectra taken with hν = 110 eV are just above the Si 2p core level threshold energy. As a result, the baseline at higher binding energy is distorted somewhat. Figure 2 demonstrates that Si diffuses throughout the Au overlayer. If the Si were predominatly near the free Au surface, an entirely different hν dependence would appear - as will be seen in the case of Al on Si.

We have also tested our ability to probe below the top few monolayers with hν near the core level threshold. By varying hν with only a 4 Å Au overlayer on Si (111) we have observed a clear separation of Si phases with depth. Figure 3 shows that at hν

= 130 eV, the surface Au-Si phase dominates the Si 2p spectrum, while at hν = 107 eV, only the bulk Si phase appears to be present. Significantly, at hν = 107 eV, the spin-orbit splitting appears clearly resolved, due to the absence of contributions from chemically-shifted surface core levels.[15] The latter produce an effective broadening which is evident in the cleaved spectrum of Fig. 1. In addition, the Si 2p peak feature at hν = 107 eV is not severely distorted by the core level threshold, despite the low photon energy, in part because the surface work function for 4 Å Au on Si is significantly less than that for 20 Å Au on Si.

SXPS studies of Al on UHV-cleaved Si (111) provide a clear contrast to the Au-Si experiments. Figure 4 illustrates Si 2p core level spectra as a function of Al overlayer thickness. In contrast to Fig. 1, the integrated I_{Si}^{2p} intensity decreases rapidly at all coverages, corresponding to an escape depth of 4-6 Å for coverages up to 8 Å and somewhat higher for 20 Å. The I_{Si}^{2p} intensity is dominated by the substrate photoemission and if the Si 2p component shifted to lower binding energy in the 20 Å spectrum is subtracted away, the attenuation is also consistent with a 6 Å photoelectron escape depth. The decrease of the total Si 2p core level intensity with up to 20 Å Al coverage demonstrates that no strong Al-Si interdiffusion occurs near room temperature. The only evidence for diffusion is the lower binding energy shoulder at 20 Å Al coverage which corresponds to a small accumulation ($\sim$ 6% of the UHV-cleaved surface intensity) of dissociated Si at the free Al surface.

Figure 5 demonstrates that the lower binding energy shoulder is due to dissociated Si at the free Al surface. This shoulder is most prominent for hν = 130 eV, the most surface-sensitive excitation energy for photoemission. This feature disappears almost completely at more bulk-sensitive energies, in constrast to the Si 2p behavior in Fig. 2. Again, one can observe the enhanced spin-orbit splitting at the more bulk-sensitive energies. Furthermore, spectra at hν = 107 eV appear undistorted by the core level threshold, due in part to the lower surface work function of Al on Si

vs. metallic Au on Si (Fig. 2). SXPS features analogous to those of Fig. 5 are obtained for 4 Å Al on Si (111) as well, although the amount of dissociated Si is significantly less than for the 20 Å Al case. Thus Figs. 4 and 5 provide evidence for only a weak Al-Si interaction with considerably less diffusion than for Au on Si.

We have performed marker experiments to identify the diffusing species during the initial stages of Au-Si and Al-Si interface formation. The marker layer between the metal and semiconductor was a 1 Å ($=9.0 \times 10^{14}$ atoms/cm^2 = 1.15 monolayer) layer of Ni, chosen for its strong bonding to Si.[4] Only a monolayer was used in order to minimize any effects on the interdiffusion process itself.[16] These experiments are analogous to marker studies carried out via Rutherford backscattering and Auger electron spectroscopy,[4] except that movement on a monolayer scale rather than on a micron scale is being probed.[11,12] The Ni 3d core level at $h\nu = 110$ eV (for Al-Si) or $h\nu = 130$ eV (for Au-Si) provided a spectral feature with sufficiently high signal-to-noise intensity for our purposes, despite the small amount of Ni used and the intensity attenuation caused by Al or Au overlayers. The movement of Si into the Al or Au overlayer vs. the movement of Al or Au into the Si was monitored by the intensity ratios I_{Si}^{2p} (130 eV)/I_{Ni}^{3d} (110 eV) for Al and I_{Si}^{2p} (130 eV)/I_{Ni}^{3d} (130 eV) for Au as a function of overlayer thickness. An increase in these ratios corresponds to Si diffusion past the Ni into the metal overlayer, while a decrease corresponds to diffusion of metal atoms past the Ni marker layer into the Si lattice. As shown in Fig. 6, the deposition of Al and Au leads to opposite changes in the I_{Si}^{2p}/I_{Ni}^{3d} ratio. In the case of Al, the overall increase indicates only Si outdiffusion. For Au on Si, the decrease followed by an increase suggests that Au first diffuses into Si with the initial deposition of several monolayers with Si diffusion into the Au overlayer dominating at higher Au coverages. Similar results but with more scatter were obtained using Si (111) rather than Si (100) surfaces.

Discussion

The SXPS core level studies provide evidence that Au and Al interact with Si in substantially different ways. These differences are illustrated schematically in Fig. 7. From left to right, the diagrams show atomic movement with initial monolayer deposition, multilayer metal deposition, 20 Å metal overlayer and 20 A metal overlayer plus 200°C, 45 min anneal. For Au on Si near room temperature, Si 2p core level features reveal a strong change in bonding upon initial monolayer (and submonolayer) Au deposition. Coupled with the marker results demonstrating Au diffusion into Si for Au coverages up to at least 4 Å, the spectral changes are consistent with a disruption of the Si lattice at monolayer or submonolayer coverages of Au. Such a disruption of the Si lattice is consistent with results obtained by Narusawa et al.[7] using 1 MeV He^{+} scattering of Si (100) and Si (111) surfaces. They found that the number of displaced Si atoms per row displaced from a normal lattice positions begins to increase from its minimum value with a deposition of ~ 1 monolayer at room temperature. In addition, the medium-energy electron diffraction pattern of the surface changes. A more pronounced increase in the number of displaced Si species takes place at ~ 4 monolayers for both Si (111) and Si (100). UV photoelectron spectroscopy (UPS) and SXPS measurements of Braicovich et al.[6] suggest Au dispersion in and on the Si (111) surface below 2 monolayers as well - from the removal of intrinsic surface states and production of new states in the band gap. Experiments of Derrien et al.[8] and Cros et al.[9] confirm such interdiffusion effects at multilayer coverages. The SXPS features illustrated in Fig. 1 at monolayer coverage does not support the proposal[17,18] that bonding of Au to Si atoms leads to metallic bonding and screening which reduces the activation energy of Si dissociation. Lattice disruption is observed for Au coverages well below the appearance of bulk Au spectral features, such as the characteristic Au 5d valence band splitting.[19,20] Rather, our results appear consistent with the reaction mechanism proposed by Tu[21], in which Au atoms diffuse into the Si as interstitials,

which then weaken the Si-Si bonds. The partially dissociated Si atoms are then available for reaction with the Au at lower temperatures than otherwise required. Such a mechanism accounts for the substantial interdiffusion of Au with Si at temperatures well below the Au-Si eutectic temperature of 370°C.[22] The I_{Si}^{2p} (hν) variations for 20 Å Au on Si in Fig. 3 normalized to I_{Si}^{2p} (hν) dependence of the clean Si surface[23] reveal that some segregation of Si to the free Au surface occurs with thicker Au deposits, consistent with earlier conclusions of Braicovitch et al.[6] A 200°C, 45 min anneal of the 20 Å Au - Si (111) interface produces a richer Si diffusion throughout the Au overlayer.

Our SXPS results demonstrate that only a weak interaction occurs between Al and Si near room temperature. With initial Al deposition, a fraction of a Si monolayer diffuses into the metal overlayer and segregates to the free metal surface. The marker experiment indicates no evidence for Al diffusion into the Si lattice. As shown schematically in Fig. 7, no substantial increase in diffused and/or segregated Si occurs for Al deposits up to 20 Å. Annealing the 20 Å Al-Si interface at 200°C for 45 min increases the amount of segregated Si somewhat without increasing Si mixing within the Al. Only when the 20 Å Al-Si interface is annealed at 600°C or higher does massive interdiffusion occur.[23]

Each of these SXPS results is consistent with the bulk phase diagram for the Al-Si system.[22] This diagram shows very low (< 1%) solubility for Si in Al at temperatures below 400°C and no solubility whatever for Al in Si. Furthermore, the solubility of Al and Si with each other increases abruptly at the eutectic temperature of 577°C.[22] This correspondence betwen the bulk phase diagram and the observed atomic behavior is an encouraging sign that macroscopic thermodynamic behavior is relevant to microscopic interface phenomena. On the other hand, the pronounced interdiffusion of Au and Si at temperatures well below the Au-Si eutectic emphasizes the need to take into account particular atomic processes - e.g., formation of rapidly

diffusing, dissociated species vis lattice disruption. Application of these findings to the corresponding Si device interfaces could have useful implications.

Summarizing, SXPS core level studies reveal that the Au-Si interface exhibits a strong interaction, even at monolayer coverages or less. In contrast, the Al-Si interface is only weakly interactive, with interdiffusion characteristics consistent with the bulk thermodynamic predictions.

Figure Captions

Fig. 1   SXPS Si 2p core level spectra as a function of increasing metal coverage for Au on Si (111) with incident photon energy $h\nu$ = 130 eV.

Fig. 2   SXPS Si 2p core level spectra as a function of incident photon energy $h\nu$ for 20 Å Au on Si (111). The photoelectron escape depth λ_e corresponding to the incident $h\nu$ appears for each curve.

Fig. 3   SXPS Si 2p core level spectra as a function of incident photon energy $h\nu$ for 4Å Au on Si (111).   The photoelectronic escape depth λ_e corresponding to the incident $h\nu$ appears for each curve.

Fig. 4   SXPS Si 2p core level spectra as a function of increasing metal coverage for Al on Si (111) with incident photon energy $h\nu$ = 130 eV.

Fig. 5   SXPS Si 2p core level spectra as a function of incident photon energy $h\nu$ for 20 Å Al on Si (111). The photoelectron escape depth λ_e corresponding to the incident $h\nu$ appears for each curve.

Fig. 6   SXPS intensity ratios of $I_{Si}{}^{2p}$ (130 eV)/$I_{Ni}{}^{3d}$ (130 eV) for Au and $I_{Si}{}^{2p}$ (130 eV)/$I_{Ni}{}^{3d}$ (110 eV) for Al overlayers on Si (100). Intensity ratios are arbitrarily normalized to unity at zero overlayer coverage.

Fig. 7   Schematic illustration of Si and metal interdiffusion in the sequence, from left to right: initial monolayer deposition multilayer metal deposition, 20 Å metal overlayer, 20 Å metal overlayer plus 200°C anneal.

References

1. L.J. Brillson, Surf. Sci. Repts. 2, 123 (1982); J. Phys. Chem. Solids 44, 703 (1983).

2. G. Margaritondo, Solid State Electron. 26, 499 (1983).

3. For recent reviews, see P. Ho, J. Vac. Sci. Technol. A1, 745 (1983); P. Ho and G.W. Rubloff, Thin Solid Films 89, 433 (1982); G.W. Rubloff and P. Ho, Thin Solid Films, 93, 21 (1982).

4. K.N. Tu and J.W. Mayer, in Thin Films - Interdiffusion and Reactions, edited by J.M. Poate, K.N. Tu and J.W. Mayer (Wiley-Interscience, New York, 1978), p. 359, and references therein.

5. A. Hiraki, M.A. Nicolet, and J.W. Mayer, Appl. Phys. Lett. 18, 178 (1971); A. Hiraki, K. Shuto, F. Kim, W. Kammura, and W. Iwami, Appl. Phys. Lett. 31, 611 (1977), and references therein.

6. L. Braicovitch, C.M. Garner, P.R. Skeath, C.Y. Su, P.W. Chye, I. Lindau, and W.E. Spicer, Phys. Rev. B20, 5131 (1979); L. Braicovitch, I. Abbati, J.N. Miller, I. Lindau, S. Schwarz, P.R. Skeath, and W.E. Spicer, J. Vac. Sci. Technol. 17, 1005 (1980) and references therein.

7. T. Narusawa, K. Kinoshita, W.M. Gibson, and A. Hiraki, J. Vac. Sci. Technol. 18, 872 (1981).

8. J. Derrien, C. Cohen, A. Cros, J.M. Layet, F. Salvan, F. Abel, J.C. Bouillard, J.L. Domange, and M. Sotto, Appl. Phys. Lett. 39, 915 (1981).

9. A. Cros, J. Derrien, and F. Salvan, Surface Sci. 110, 471 (1981); A. Cros, F. Salvan and J. Derrien, J. Appl. Phys. 52, 4757 (1981).

10. M.P. Seah and W.A. Dench, Surf. Int. Analysis 1, 2 (1979).

11. L.J. Brillson, R.S. Bauer, R.Z. Bachrach, and G. Hansson, Appl. Phys. Lett. 44, 667 (1980).

12. L.J. Brillson, R.S. Bauer, R.Z. Bachrach, and G. Hansson, Phys. Rev. B23, 6204 (1981).

13. F.C. Brown, R.Z. Bachrach, R.B.M. Hagstrom, N. Lien, and C.H. Pruett, in Vacuum Ultraviolet Radiation Physics, edited by E. Koch, R. Haensel, and C. Kurz (Pergamon, Elmsford, NY, 1975) p. 785.

14. L. Pauling, The Nature of the Chemical Bond, 3rd Ed. (Cornell Univ. Press, Ithaca, NY, 1960).

15. W. Eberhardt, G. Kalkoffen, C. Kunz, D. Aspres and M. Cardona, Phys. Stat. Solidi B88, 135 (1978); F.J. Himpsel, P. Heimann, T.C. Chiang and D.E. Eastman, Phys. Rev. Lett. 45, 1112 (1980).

16. L.J. Brillson, G. Margaritondo, and N.G. Stoffel, Phys. Rev. Lett. 44, 667 (1980).

17. A. Hiraki, in Points Defects (Univ. Tokyo Press, 1977) p. 393.

18. K. Okuno, T. Ito, M. Iwani, and A. Hiraki, Solid State Commun. 34, 881 (1980).

19. K.S. Liang, W.R. Salaneck, and I.A. Aksay, Solid State Commun. 19, 329 (1976).

20. P.W. Chye, I. Lindau, P. Pianetta, C.M. Garner, C.Y. Su, and W.E. Spicer, Phys. Rev. B18, 5545 (1978).

21. K.N. Tu, Appl. Phys. Lett. 27, 221 (1975).

22. M. Hansen and K. Anderko, _Constitution of Binary Alloys_ (McGraw-Hill, New York, 1958).

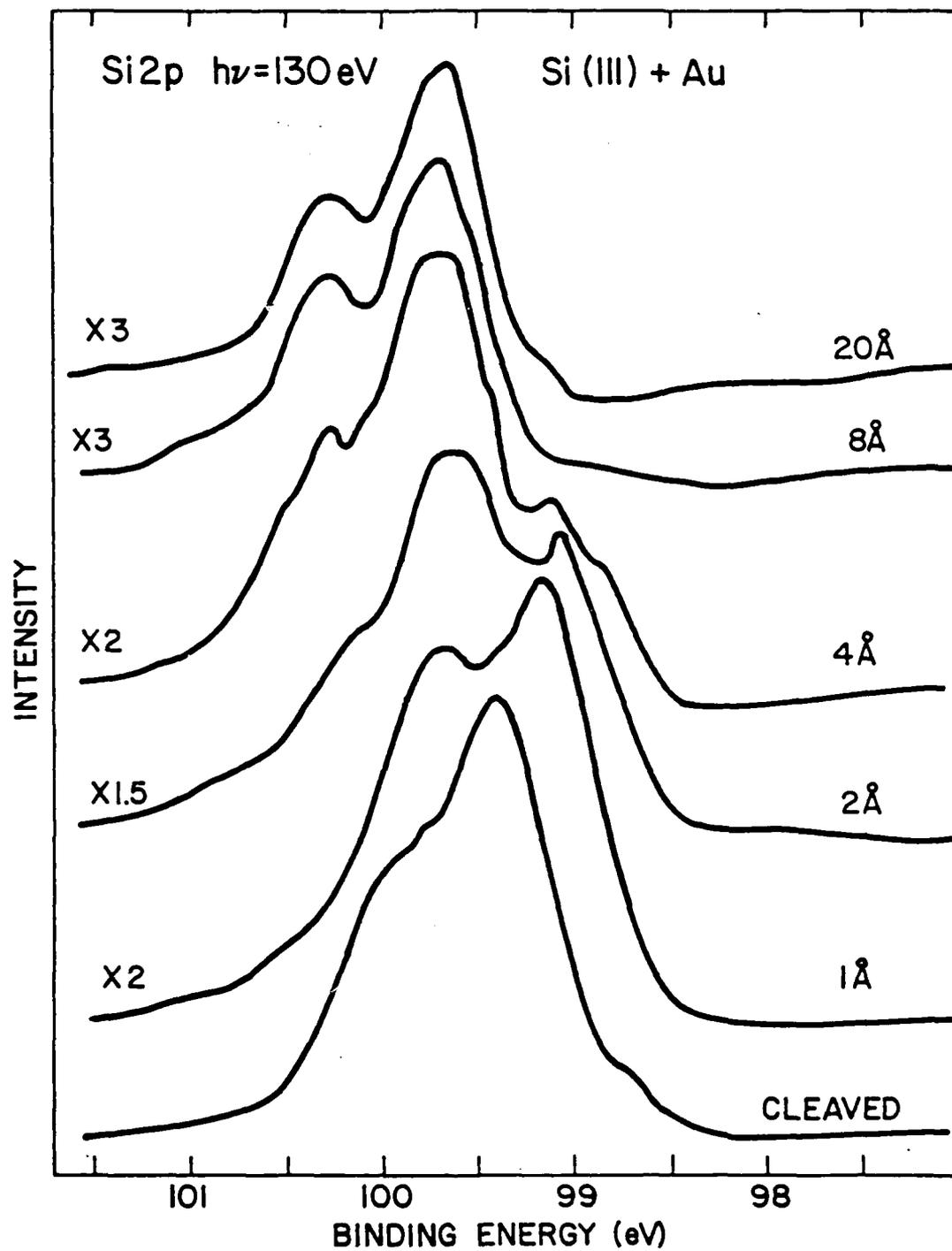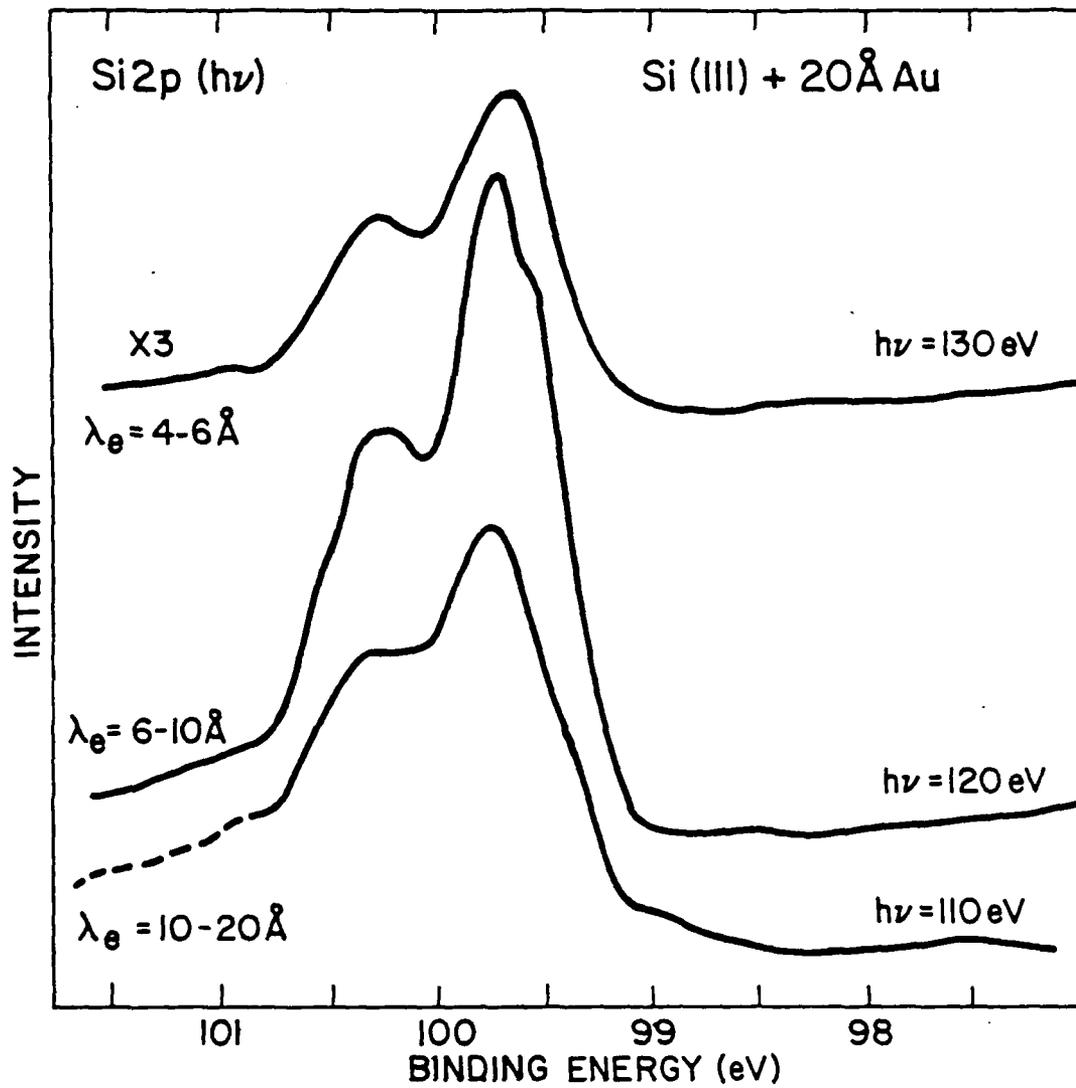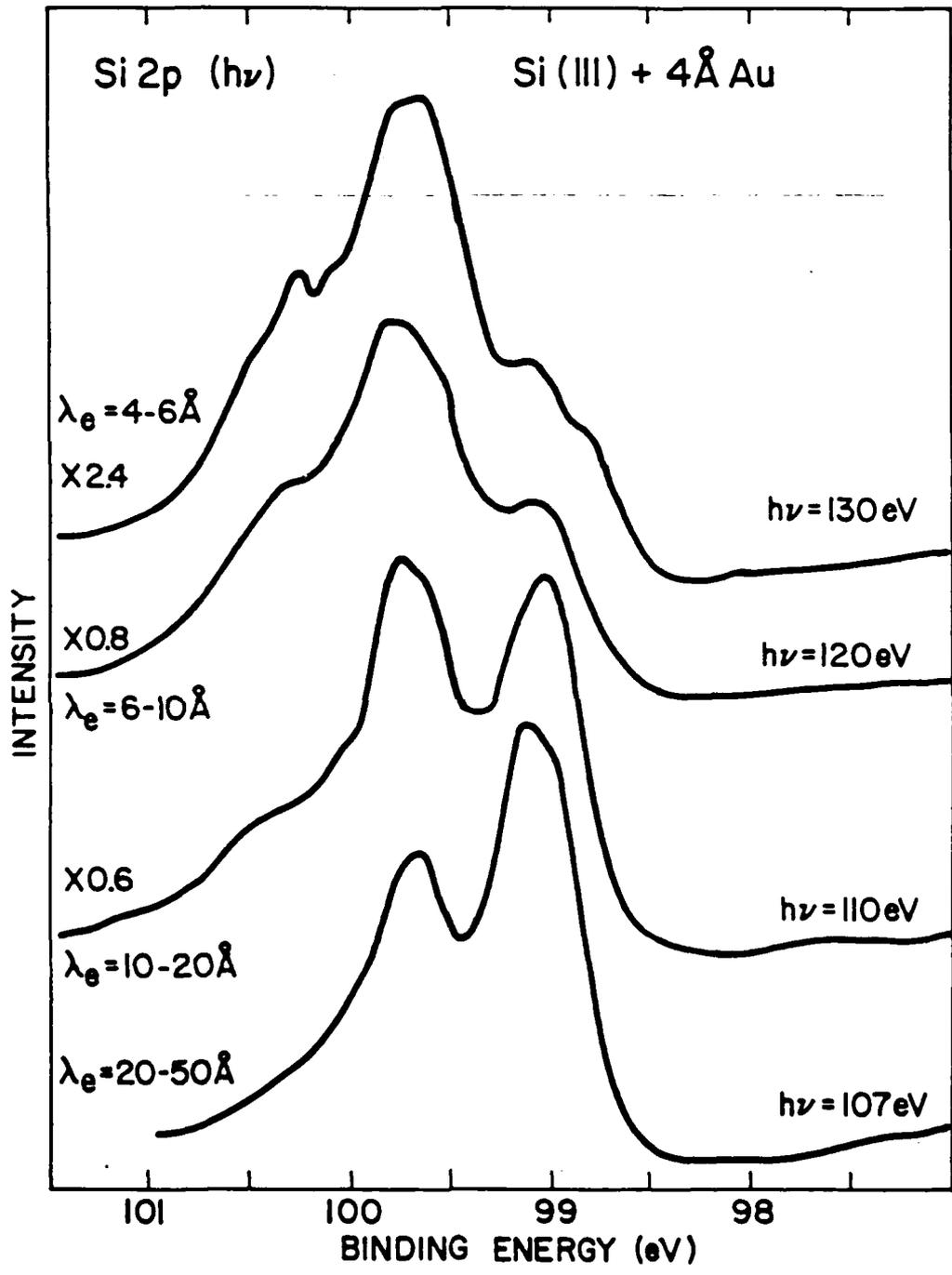23. L.J. Brillson, A.D. Katnani, M. Kelly, and G. Margaritondo, unpublished.

FIG. 1

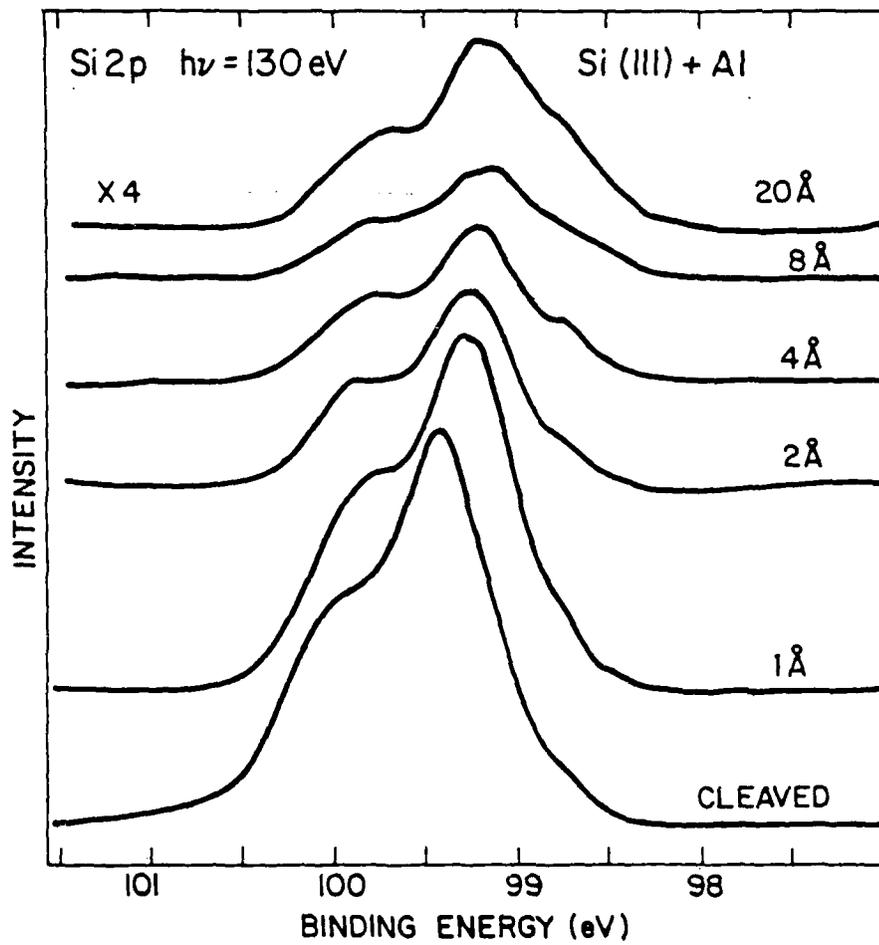Si2p (hν)   Si (III) + 20Å Au

X3   hν = 130 eV

λ_e = 4-6Å

λ_e = 6-10Å   hν = 120 eV

λ_e = 10-20Å   hν = 110 eV

INTENSITY

BINDING ENERGY (eV)

FIG. 2

FIG. 3

Si 2p hν = 130 eV   Si (III) + Al

X 4

20 Å

8 Å

4 Å

2 Å

1 Å

CLEAVED

INTENSITY

101   100   99   98

BINDING ENERGY (eV)

FIG. 4

MICROCOPY RESOLUTION TEST CHART

NATIONAL BUREAU OF STANDARDS-1963-A

Si2p (hν)   Si(III) + 20Å Al

λ_e = 4-6Å   hν = 130 eV

λ_e = 6-10Å   hν = 120 eV

λ_e = 10-20Å   hν = 110 eV

λ_e = 20-50Å   hν = 107 eV

INTENSITY

101   100   99   98
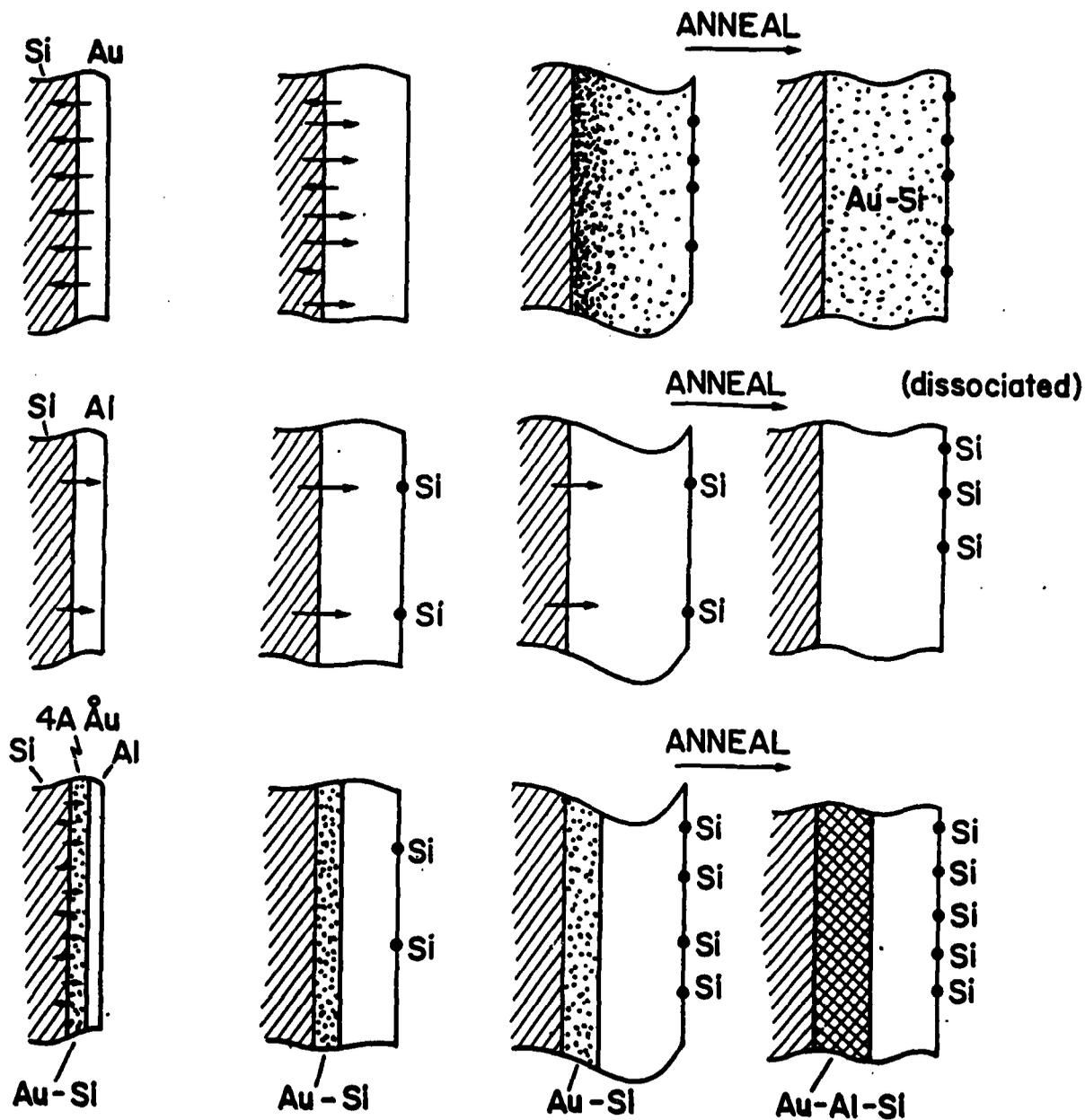BINDING ENERGY (eV)
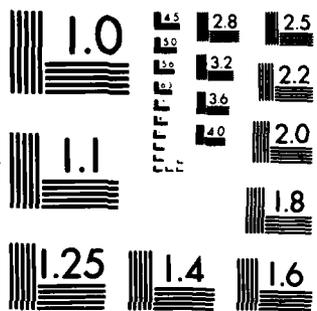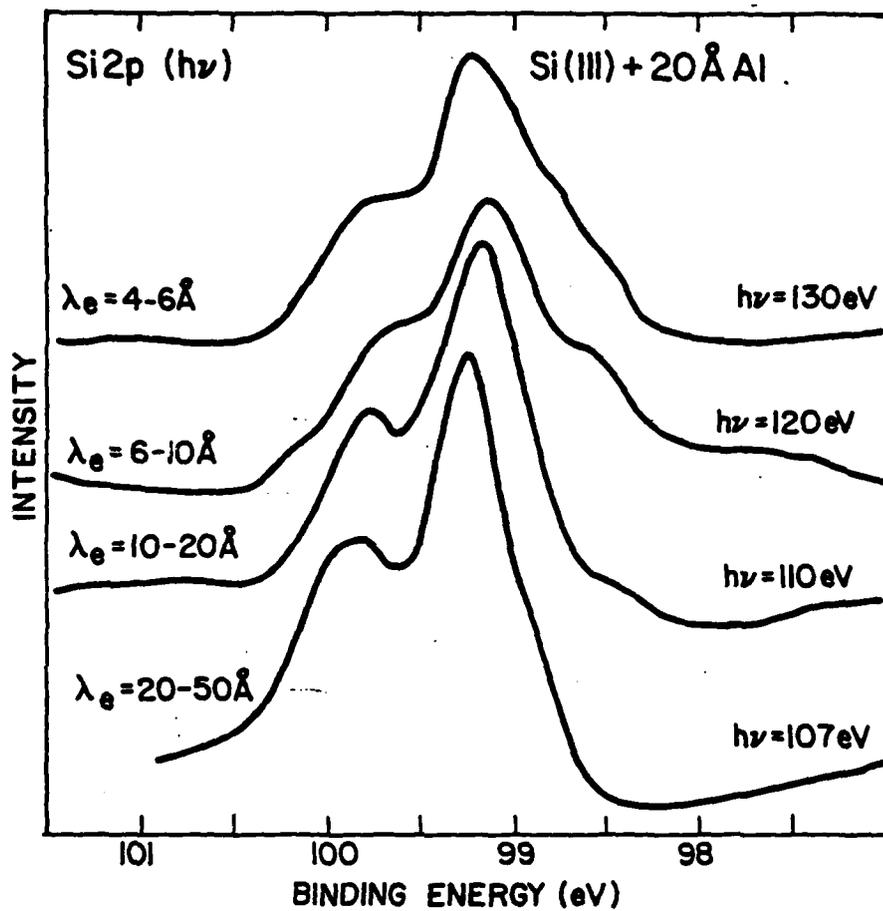
FIG. 5
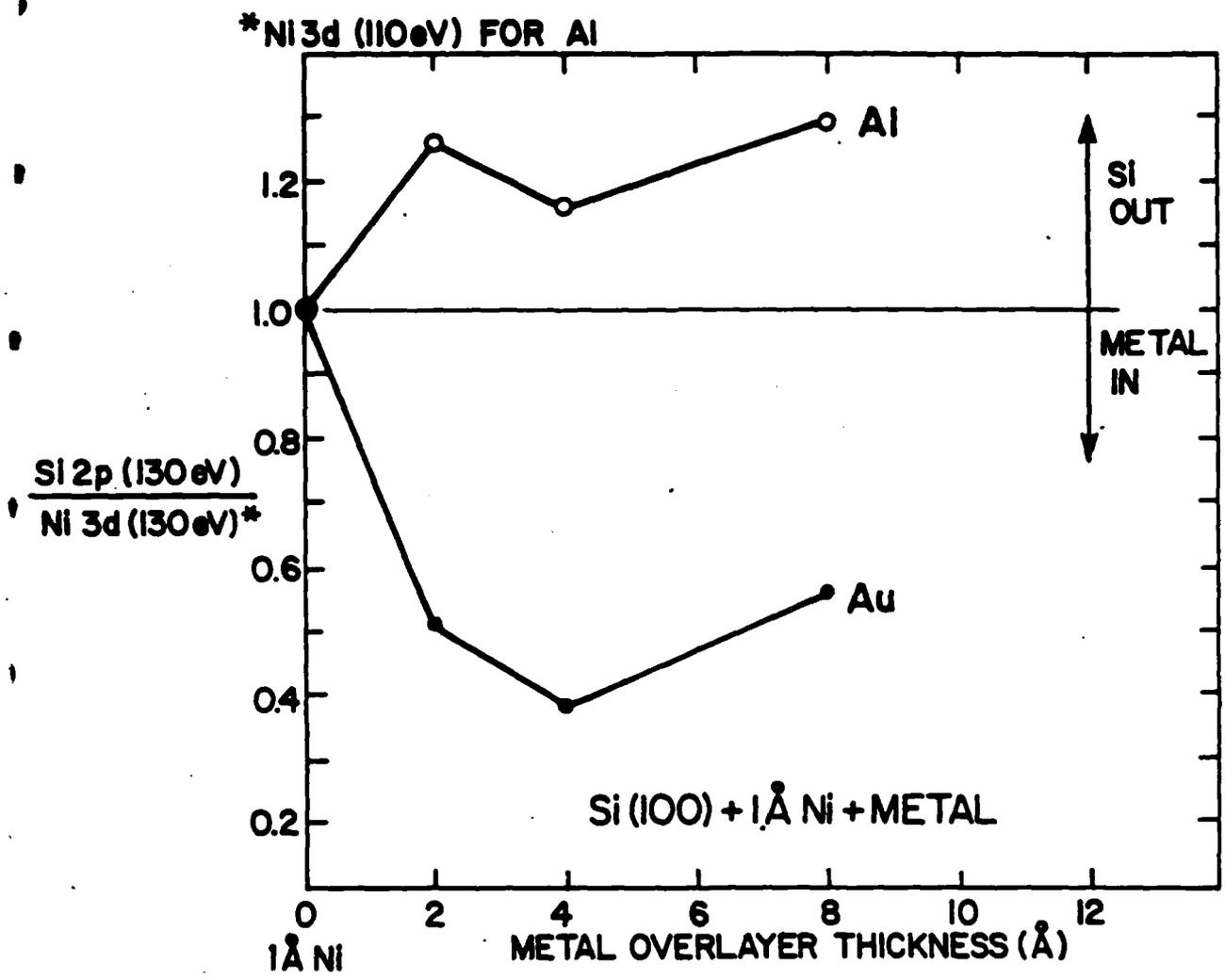
FIG. 6

Si-METAL INTERDIFFUSION

FIG. 7

Ultrafast UV-Laser Induced Oxidation of Silicon

T.E. ORLOWSKI AND H. RICHTER
Xerox Webster Research Center
Rochester, NY 14644

ABSTRACT

A new low temperature method of forming high quality patterned silicon dioxide (SiO_2) layers up to a thickness of 1 μm on silicon substrates is presented. UV pulsed laser excitation in an oxygen environment is utilized. IR absorption spectroscopy, CV and IV measurements are employed to characterize the oxide films and the Si-SiO$_2$ interface. No shift but a significant broadening of the Si-O stretching mode compared with thermally grown oxides is found indicating that the laser grown oxide is stoichiometric but with a higher degree of disorder. From CV measurements we deduce a fixed oxide charge near the Si-SiO$_2$ interface of $6 \times 10^{10}/cm^2$ for oxides that have been thermally annealed in O_2 following the laser induced growth making this material a candidate for applications in semiconductor devices.

INTRODUCTION

There has been considerable activity in the search for efficient low temperature techniques for depositing thin dielectric films in semiconductor device fabrication processes to eliminate problems such as substrate warpage, dopant redistribution and defect generation and propagation [1] associated with conventional high temperature processing steps. Much progress has been made in rapid low temperature deposition of Si_3N_4 and SiO_2 using laser-initiated CVD techniques [2,3] utilizing UV lasers to photolyze gas phase reactants which combine at the substrate surface to form the insulating film. Other studies have shown that oxygen trapped in laser-induced amorphous silicon layers during pulsed laser annealing of silicon wafers rapidly forms SiO_2 [4]. The work reported here is concerned with a new low temperature method of rapidly forming high quality patterned silicon dioxide layers on silicon substrates involving pulsed UV laser excitation and characterizing the electrical properties of the resulting insulating films.

EXPERIMENTAL

Shown in Figure 1 is the apparatus developed for laser induced oxidation of silicon. The technique involves electronic excitation and subsequent rapid heating of a silicon substrate (p-type, 10-20 Ωcm, (100) surface) to near or above its melting point in an oxygen environment using a XeCl excimer laser which provides 5 nsec pulses with up to 5mJ energy at 308 nm. Focusing the beam to 1.0 x 0.5 mm spot on the sample results in energy densities up to 1.0 J/cm^2. The laser penetration depth at 308 nm in silicon is less than 100 Å and with a laser pulse duration of 5 nsec there is no residual substrate heating (i.e., the sample cools within 1 μsec of excitation). In order to reduce the strain in the substrate during the rapid heating and cooling, the substrate was resistively heated to 400°C. Sample temperature was measured using an optical pyrometer. Repetitive pulses (100Hz) combined with scanning the focused laser beam over the sample surface produced patterned oxide layers large enough to perform IR and electrical measurements.

Growth Kinetics

Figure 2 shows the thickness of laser-grown oxides (L-SiO$_2$) as a function of laser exposure time. For oxides between 300 and 1800 Å thick the growth rate is linear (~ 100 Å/sec) and comparable to that found for deposition of SiO_2 by laser assisted CVD techniques [2,3]. For thicker oxides the growth kinetics appear to follow a quadratic behavior (i.e., X_{SiO_2} (Å) $\propto$ (Bt)$^{1/2}$ where B is a time-averaged parabolic rate constant)

indicating that the diffusion of oxygen across the SiO_2 layer toward the Si-SiO_2 interface is influencing the overall oxide formation rate. From the fit in Figure 2 (dotted line) we obtain a value of B ~ 8.5 μm^2/hr which is ~ 30X larger than that found for the thermal oxidation process at 1000°C and 1 atm. O_2 pressure [5]. These considerations do not take into account that the SiO_2 and the surface of the Si wafer stay at elevated temperatures for less than 1 μsec after each laser pulse. Taking this time as an upper limit, and with a laser repetition rate of 100 Hz, the effective parabolic rate constant would be 8.5 x 10^4 μm^2/hr or 3x10^5 times larger than in conventional thermal oxidation processes!
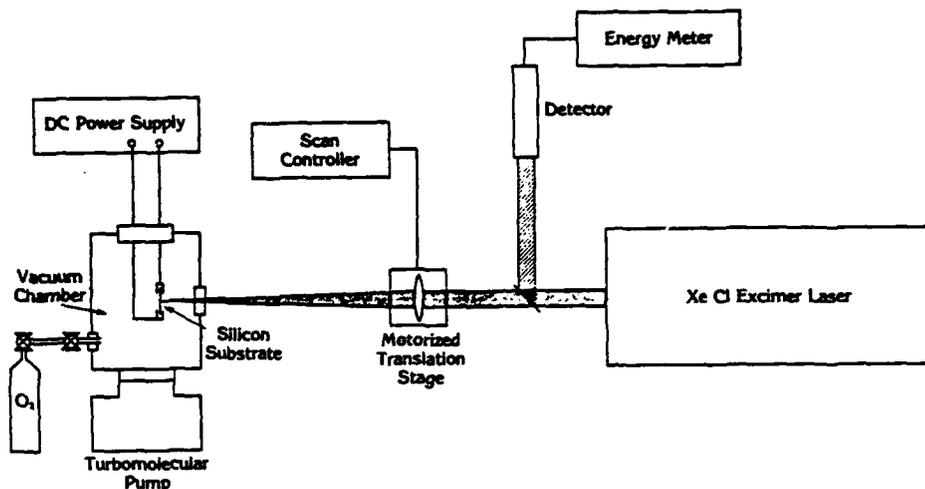

Fig. 1 Schematic diagram of the apparatus: the XeCl excimer laser operates at 308 nm producing 5mJ pulses of 5 nsec duration (FWHM) at 100 Hz. The laser spot size at the sample was 1.0 x 0.5 mm. SiO_2 patterns were made by lens translation. The Si substrate was resistively heated to 400°C. In all experiments the O_2 pressure was 1 atm. and the Si(100) surface was exposed.
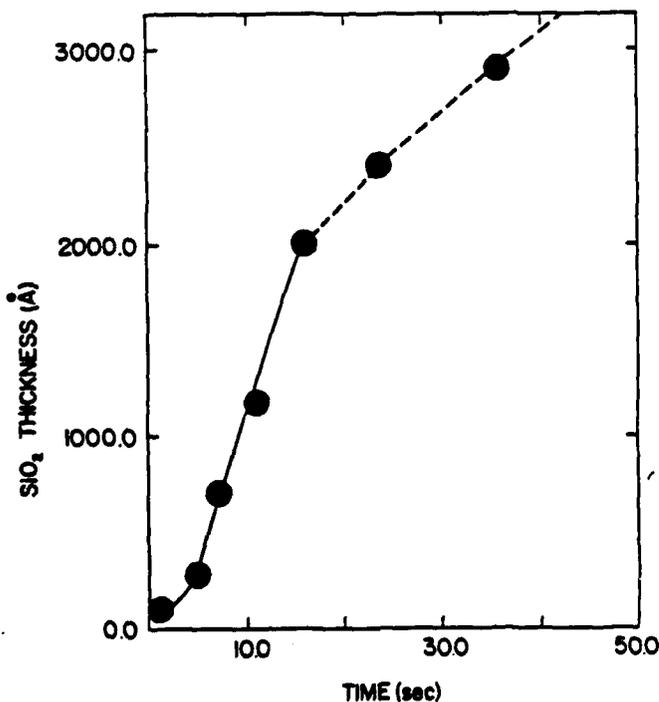

Fig. 2 Plot of SiO_2 thickness (from IR absorption data) as a function of laser exposure time. The observed growth rate is linear from 300 - 1800 A SiO_2 thickness becoming quadratic (i.e. X_{SiO_2} (A) $\propto$ (Bt)$^{1/2}$ dotted line fit with B~8.5μm^2/hr) at greater SiO_2 thicknesses.

Several possible explanations exist concerning these results. The concentration of dissolved O_2 in the oxide layer may be larger for the laser induced oxidation process and the diffusion of oxygen through the SiO_2 layer toward the $Si-SiO_2$ interface may be promoted by the UV photodissociation of O_2 into oxygen atoms. In addition, the effect of Si electronic excitation upon the formation of Si-0 bonds is not clearly understood. We observe a rather sharp onset to oxide formation at a laser pulse energy near 2mJ which we attribute to the onset of melting of the Si surface but more detailed experimental effort is needed to explain the catalytic effect of the laser upon the growth process and is in progress. In any event, very thick oxides can be grown using this method. With longer exposure times and tighter laser focusing oxide layers up to a thickness of 1μm have been made. Considerable effort has been expended to characterize the quality of the oxide formed by this laser induced process as discussed in the following sections.

Infrared Spectroscopy

Silicon dioxide shows three prominent absorption bands in the IR, namely at 1070 cm^{-1} (Si-0 stretching), 850 cm^{-1} (0-Si-0 bending) and 450 cm^{-1} (Si-0-Si rocking). It has been shown [6] that these bands obey a Lambert-Bouguer law and can therefore be used to determine the thickness of SiO_2 films on an IR transparent substrate, if the absorption coefficient is known. The frequency width and relative intensities also reveal information about stoichiometry and structure of SiO_2 films.

The IR-spectra were recorded on a double beam Perkin-Elmer 283 IR-spectrometer with a bare silicon substrate (covered with native oxide $\approx$ 20-30 A on both sides) in the reference beam. The measurements cover the range from 4000 cm^{-1} to 200 cm^{-1}. Besides the above mentioned SiO_2-bands, no other absorption bands (like that of hydroxyl-groups) were detected. Figure 3 shows a typical Si-0 stretching band of a 2830 A-thick $L-SiO_2$ film in comparison with a 2800 A thermal oxide layer, grown at 1000°C in dry O_2. This figure shows that the position of the absorption band in both spectra is the same, but the $L-SiO_2$ shows a much broader width (133 cm^{-1}) compared to the thermal oxide (90 cm^{-1}). A similar but larger broadening is found in CVD-deposited SiO_2-films [7].
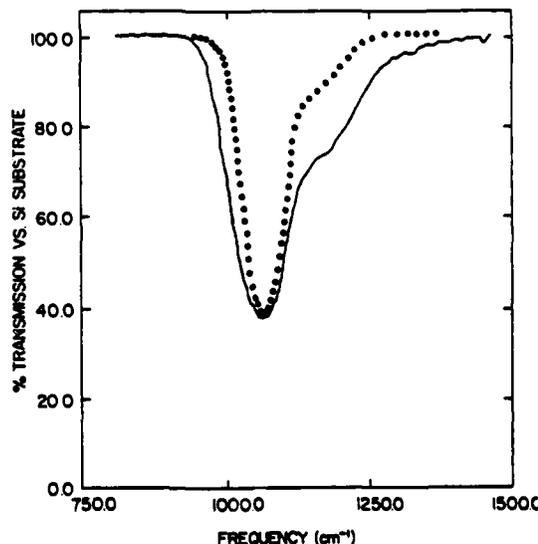

Fig. 3 IR absorption spectra: Laser-grown SiO_2 (solid line) and thermally-grown (1000°C) SiO_2 (dotted line). From the SiO_2 absorption coefficient at 1070 cm^{-1} (3.4 x 10^4 cm^{-1}) we obtain an oxide thickness of ~2800 A. The observed broadening of the Si-0 stretching mode with no shift in the peak absorption frequency indicate that the laser-grown oxide is stoichiometric but with a higher degree of disorder than the thermal oxide.

It has been shown earlier [8] that the Si-O stretching frequency in SiO_x is linearly related to the oxygen concentration x, whereas the band width is mainly determined by the O-Si-O bond-angle variation. We therefore interpret our IR-data in the following way: The $L-SiO_2$ is stoichiometric within the accuracy of the measurement and shows no oxygen deficiency. The broadening of the bands on the other hand shows an additional degree of structural disorder like large variations in bond angle.

The strength of the 1070 cm^{-1} absorption band was used as the standard way of determining the thickness of the $L-SiO_2$ films (Figure 2) using the absorption coefficient of 3.4×10^4 cm^{-1} given in [9]. The thicknesses determined in this way are in good agreement with standard color charts and the oxide thickness determined from capacitance measurements of MOS-capacitors using the standard SiO_2 dielectric constant $\varepsilon_i = 3.5 \times 10^{-13}$ F/cm.

Electrical Measurements

Two critical parameters for the application of an insulating layer in metal-insulator-semiconductor (MIS)-devices are the fixed oxide charge density, D_f, and the interface state density, D_{it}. We have studied both parameters in the $L-SiO_2$ films using the combined high- and low-frequency capacitance, voltage (CV-) technique reviewed in [10]. Al-contacts of .0033 cm^2 area were evaporated onto the $L-SiO_2$ layers with no post metallization annealling. For these capacitors, the CV-plots reveal fixed oxide charge densities in the range of $3\times10^{11} - 1\times10^{12}$ cm^{-2} and surface state densities of the same magnitude, showing a large spread even within nominally identical capacitors on the same substrate. The capacitors also show high leakage currents of typically 10^{-6} A at 3×10^5 V/cm. This poor electrical quality can be improved significantly, as shown in Fig. 4. A short, 20 min. anneal at 900°C in 1 atm. O_2 prior to metallization, reduces both fixed oxide charge and interface states significantly. Characteristic values of 6×10^{10} cm^{-2} fixed charge and 2×10^{11} cm^{-2} eV^{-1} surface states near midgap are achieved with a narrow distribution within the number of samples. Leakage is also reduced dramatically. Up to a field of 5×10^5 V/cm, leakage currents are less than our detection limit of 10^{-10} A.
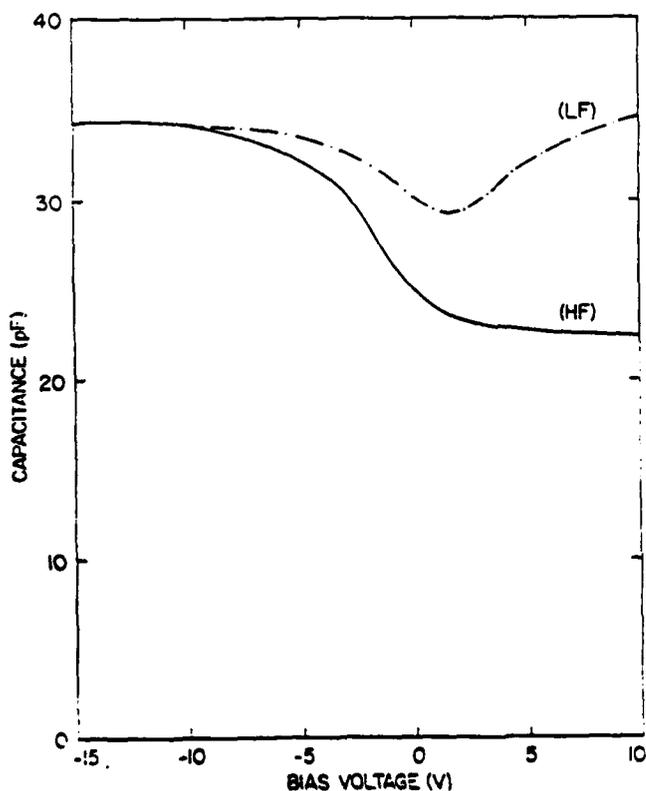

Fig. 4 Typical high-frequency (HF) and low-frequency (LF) CV-plot of an Al-L- SiO_2-Si MOS capacitor. The HF-curve was taken at 1 MHz, the LF-curve at 1 kHz (no changes were observed at lower frequencies). From the HF data one obtains a fixed oxide charge density, D_f, of 6×10^{10} cm^{-2} and from the LF data, an interface state density, D_{it}, of 2×10^{11} cm^{-2}.

These values are in the same range as the ones of plasma oxide [11] or CVD-oxides [12] after post-anneal. Further studies on the annealing behavior are in progress in a variety of ambients (H_2, N_2) and temperatures in order to determine the mimimum requirements for achieving "good" oxide electrical properties. It should be noted that all results reported here were obtained without preoxidation cleaning of the silicon substrate which has proven to be important for achieving good electrical properties in thermally-grown oxides [10].

CONCLUDING REMARKS

We have presented a new, fast, essentially low temperature technique for growing high quality SiO_2. An important advantage of this technique is the use of a focussed laser beam which makes it possible to grow a patterned oxide without using a mask and thus eliminating two steps in the fabrication of IC's (masking and subsequent etching to remove insulation layer for contacts). Since the oxidation process is very strongly temperature dependent, the oxide profile is usually much steeper than the laser beam profile. By varying the energy density it is also possible to modulate the oxide thickness during the growth process as we have shown.

This laser-assisted low temperature oxidation process should result in an Si-SiO_2 interface suitable for application in certain TFT devices. It allows for depositing oxide with great precision and control over geometry in selected areas of circuitry without using masking techniques and in addition provides precise control over gate oxide thickness.

ACKNOWLEDGEMENTS

REFERENCES

1.   S. Su, Solid State Technol. 24, 72 (1981).
2.   T.F. Deutsch, D.J. Silversmith and R.W. Mountain, Mat. Res. Soc. Symp. Proc. 17, 129 (1983).
3.   P.K. Boyer, G.A. Rocke, W.H. Ritchie and G.J. Collins, Appl. Phys. Lett. 40, 716 (1982).
4.   Y.S. Liu, S.W. Chiang and F. Bacon, Appl. Phys. Lett. 38, 1005 (1981).
5.   B.E. Deal and A.S. Grove, J. Appl. Phys. 36, 3770 (1965).
6.   J.E. Dial, R.E. Gong and J.N. Fordemwalt, J. of Electrochem. Soc. 115, 326 (1967).
7.   W.A. Pliskin and H.S. Lehman, J. of Electrochem. Soc. 112, 1013 (1965).
8.   L. Schumann, A. Lehmann, H. Sobotta, V. Riede, U. Teschner and K. Hübner, Phys. Stat. Sol. B110, K69 (1982).
9.   J. Wong, J. Appl. Phys. 44, 5629 (1973).
10.   E.H. Nicollian and J.R. Brews, MOS (Metal Oxide Semiconductor) Physics and Technology (Wiley, NY, 1982).
11.   J.R. Ligenza and M. Kuhn, Solid State Technol. 13, 33 (1970).
12.   G. Pananakakis, G. Kamarinos, M. El-Sayed and V. LeGoascoy, Solid State Electron. 26, 415 (1983).